

Polymorphism of acetaminophen under nanoconfinement

DISSERTATION

zur Erlangung des akademischen Grades

doctor rerum naturalium
(Dr. rer. nat.)
genehmigt durch

die Naturwissenschaftliche Fakultät II
Institut für Physik
der Martin-Luther-Universität
Halle-Wittenberg

vorgelegt von

Herr M. Sc. Gopalakrishnan Trichy Rengarajan
geboren am 19.09.1978 in Tiruchirapalli, India

Gutachterin / Gutachter:

1. PD. Dr. Mario Beiner
2. Prof. Dr. Gyan P. Johari
3. Prof. Dr. Joachim Ulrich

Halle (Saale), Oktober 2009

*This thesis is dedicated to my mother
for her sacrifice, love, endless support
and encouragement.*

Contents

1	Introduction	1
2	Basic Concepts	5
2.1	Fundamentals of crystallisation	5
2.1.1	Thermodynamic description	5
2.1.2	Nucleation and growth	8
2.2	Polymorphism	13
2.2.1	Classification of polymorphic systems	14
2.2.2	Thermodynamics and nucleation of polymorphs	15
2.2.3	Rules to predict thermodynamic relationship between polymorphs	17
2.3	Crystals under confinement	18
3	Experimental Techniques	23
3.1	Differential Scanning Calorimetry	23
3.1.1	Power Compensated DSC	23
3.1.2	Evaluating the DSC Data	25
3.2	Dielectric Spectroscopy as a linear response method	27
3.2.1	Basic principles of dielectric spectroscopy	27
3.2.2	Data evaluation	30
4	Guest - Host system	33
4.1	Guest System	33
4.2	Host Media	34
4.2.1	Controlled Porous Glass (CPG)	35
4.2.2	Porous alumina	35
4.3	Infiltration of guest molecule in host system	37

5	Amorphous acetaminophen	39
5.1	Bulk acetaminophen	40
5.2	Acetaminophen in nanopores	48
6	Polymorphic acetaminophen under Nano-confinement	55
6.1	Melting of form III acetaminophen in CPGs	56
6.2	Phase transition form III \rightleftharpoons II of acetaminophen	62
6.3	Crystallisation of form I in CPGs	71
7	Discussion	75
7.1	Amorphous acetaminophen in bulk and in CPGs	75
7.2	Melting of form III acetaminophen in CPGs	78
7.3	Transitions among three forms of acetaminophen in CPGs	80
7.4	Thermodynamic modeling and free energy simulations	82
8	Conclusions	93
A	Free energy changes between two different crystalline forms (I and II)	97
	Bibliography	103

Chapter 1

Introduction

A polymorph is defined as "a solid crystalline phase of a given compound resulting from the possibility of at least two crystalline arrangements of the molecules of that compound in the solid state" [1]. Mitscherlich was the first one to observe the phenomenon of polymorphism [2]. Early in his scientific career he discovered that certain salts of phosphates and arsenates can appear in different crystalline structures [3]. Ostwald summarised the main findings in his step rules of stages [4] predicting that, "a polymorphic substance passes metastable states during the crystallisation process before the stable polymorph form is formed finally." Groth [5] meticulously compiled a huge data consisting of refractive index, melting point and other physical properties of substances exhibiting polymorphism. Polymorphic behaviour is a common finding for different classes of materials such as pharmaceuticals [2, 6, 7], synthetic macromolecules [8, 9], pigments [10, 11], fat based food such as chocolates and ice creams [12], high energy materials (which reacts rapidly to produce light, heat and gas) [13, 14], and proteins [15–17].

Stabilisation of a particular crystalline form over a period of time is an important issue in the case of a pharmaceutical industry, since each form has its individual properties. Often metastable crystalline forms of a drug are chosen for the end application by the pharmaceutical industry for the following reasons [18]

- Higher solubility and bioavailability when compared to a stable crystalline form.
- Higher dissolution rate necessary for the quick - relief formulations.
- Manufacturing advantages owing to differences in the mechanical properties of the stable and the metastable polymorphs.

- Chemical instabilities of the stable form due to topochemical (orientation of molecules in the crystal) factors.

Apart from the chemical and physical properties of the polymorphs, legal issue concerns the pharmaceutical industry when a new polymorph is accidentally discovered and whose intellectual property is threatened [2, 19]. Several approaches like utilising a polymeric nuclei [20], soluble additives [21], epitaxial growth [22, 23], laser induced nucleation [24], and confined in porous media [25] have been employed to produce polymorphs.

The influence of nanoconfinement on the behaviour of very simple crystallisable liquids has been investigated systematically. Melting point depression of systems showing only a single crystalline form is a well known phenomenon and has been investigated extensively [26]. The investigation of polymorphic systems in nanopores has gained interest only recently. Nanoconfinement effects have been exploited to produce metastable polymorphs of pharmaceuticals [25], which cannot be accessed easily in the bulk. The stabilisation of a particular crystalline form under confinement can be achieved by fine tuning the size of the confining medium. Based on thermodynamic considerations [27] one can expect that the stability of different crystalline forms will also depend on pore diameter.

Amorphous solids are another class of materials which is important for the pharmaceutical industry. Amorphous solids in the glassy state are characterised by non existence of three - dimensional long range order, unlike in a crystalline material, and the position of molecules with respect to one another is disordered. A glassy system shows only a short - range order like liquids which normally extends only to few molecular dimensions and have completely different physical properties compared with its crystalline counterparts. Thermodynamically, glassy solids and supercooled liquids below the melting temperature are commonly defined as out of equilibrium states, since they possess excess of Gibbs free energy (G) with respect to the crystalline state. Achievement of amorphous state is important for the pharmaceutical industry, since its high internal energy leads to systems having enhanced mobility, dissolution, and bioavailability [28–32]. However, stability of amorphous drugs is a significant issue, since amorphous systems have some tendency to crystallise both above and below the glass transition temperature [33].

Variety of approaches [18] such as quenching [34, 35], rapid precipitation from solution [36, 37], freeze drying also know as lyophilization [38], spray drying [39], mechanical grinding or milling [40] and desolvation or dehydration [41] are employed in the pharmaceutical industry to produce amorphous drugs. Lyophilization is the most widely used technique in

the case of drugs and is a common method in the food industry, since it leads to light weight and also preserves the smell and taste. All these methods have both advantages and disadvantages considering the cost of the equipment employed, stability of the final product, purity of the final drug, etc. Although several approaches are known to produce drugs in the amorphous state or their metastable crystalline form, the life time of these states is normally rather limited. In many cases they do not have the required stability and typical shelf times are not reached.

The idea of this work is to make progress with the amorphization of drugs and contribute to a better understanding of polymorphism based on experiments under nanoconfinement. Significant changes in the crystallisation behaviour are expected since (i) there are large surface energy contributions in the total free energy for nanosize crystals and (ii) commonly known changes of nucleation behaviour in nanopores. The influence of pore size on crystallisation kinetics and phase behaviour of the widely used drug acetaminophen (paracetamol) as polymorphic model system will be investigated systematically. A series of controlled porous glasses (CPGs) and nanoporous anodized alumina templates with average pore diameters in the range 4 - 400 nm is used as host systems. Molten acetaminophen is infiltrated into these nanoporous templates. Amorphous state and the crystallisation of acetaminophen in CPGs are investigated by employing experimental techniques such as differential scanning calorimetry and X - ray scattering. Crystallisation kinetics, relaxation behaviour and calorimetric properties of bulk acetaminophen are investigated for comparison by differential scanning calorimetry and dielectric spectroscopy.

Chapter 2

Basic Concepts

This chapter will be dedicated to fundamental concepts describing crystallisation and polymorphism. The thermodynamic parameters and kinetics quantities used in these concepts will be introduced and the underlying assumptions will be explained.

2.1 Fundamentals of crystallisation

In a crystalline solid the atoms or molecules have a periodic arrangement which extends over a long range. It is well known for many substances that upon cooling a liquid, the system solidifies and begins to crystallise. Crystalline solid has higher density due to close packing of its constituents and lower mobility compared to the liquid state. Since the Gibbs free energy (G) of a crystal is lower than that of the liquid below its melting temperature T_m , crystalline state is considered as stable compared to the supercooled liquid in this temperature range.

2.1.1 Thermodynamic description

Free energy of a state (either crystalline or liquid) can be expressed in terms of enthalpy (H) and entropy (S) at a temperature T according to

$$G = H - T S \quad (2.1)$$

The temperature dependence of free energy (G) for both the crystalline and liquid is shown in figure 2.1 (a). Upon increasing the temperature the difference in free energy of liquid and the crystal decreases and becomes zero at a temperature (T_m), known as the melting temperature where the crystals melt. In order to construct the temperature dependence of

free energy for the crystalline and the liquid state basic thermodynamic quantities, enthalpy (H) and entropy (S) have to be estimated. These quantities can be expressed in terms of specific heat. Specific heat is a fundamental thermodynamic property and can be defined as amount of heat required to raise temperature of a gram or mole of substance by 1 Kelvin. It can be measured at constant pressure C_P or at constant volume C_V . Both these quantities can be measured calorimetrically and are defined as follows,

$$C_P = \frac{dH}{dT} \quad (2.2)$$

$$C_V = \frac{dU}{dT} \quad (2.3)$$

where U is the internal energy of the system. The temperature dependence of enthalpy and entropy can be defined as

$$H(T) = \int_0^T C_P d\hat{T} + H^o \quad (2.4)$$

$$S(T) = \int_0^T \frac{C_P}{\hat{T}} d\hat{T} \quad (2.5)$$

The plots containing temperature dependence of internal energy (U) and Helmholtz free energy (A) are known as *Energy Temperature* diagrams. Such diagrams are used to represent phase transformations in crystalline solids. However, widespread use of calorimetric techniques such as Differential Scanning Calorimetry (DSC) has made it easier to construct energy temperature diagrams containing enthalpy (H) vs. temperature and Gibbs free energy (G) vs. temperature. A scheme showing the temperature dependence of free energy, enthalpy and entropy is shown in figure 2.1 (b). The slope of the enthalpy curve yields specific heat and is zero at absolute zero temperature as shown in figure 2.1 (b). Specific heat can be measured experimentally by adding a certain amount of heat and measuring the resulting rise in the temperature. Since both the absolute temperature and enthalpy (H) can take only positive values, the specific heat of a substance increases with the increasing temperature. At absolute zero, liquid has more energy than a crystal hence the enthalpy (H) isobar of liquid is placed above all the isobars of crystals for the same substance. With increasing temperature the heat capacity of the liquid increases more than that of its crystalline modifications. Entropy (S) corresponding to the slope $(-\partial G/\partial T)_p$ always remains positive as a result of third law of thermodynamics, hence the free energy decreases with the increase in temperature. On the

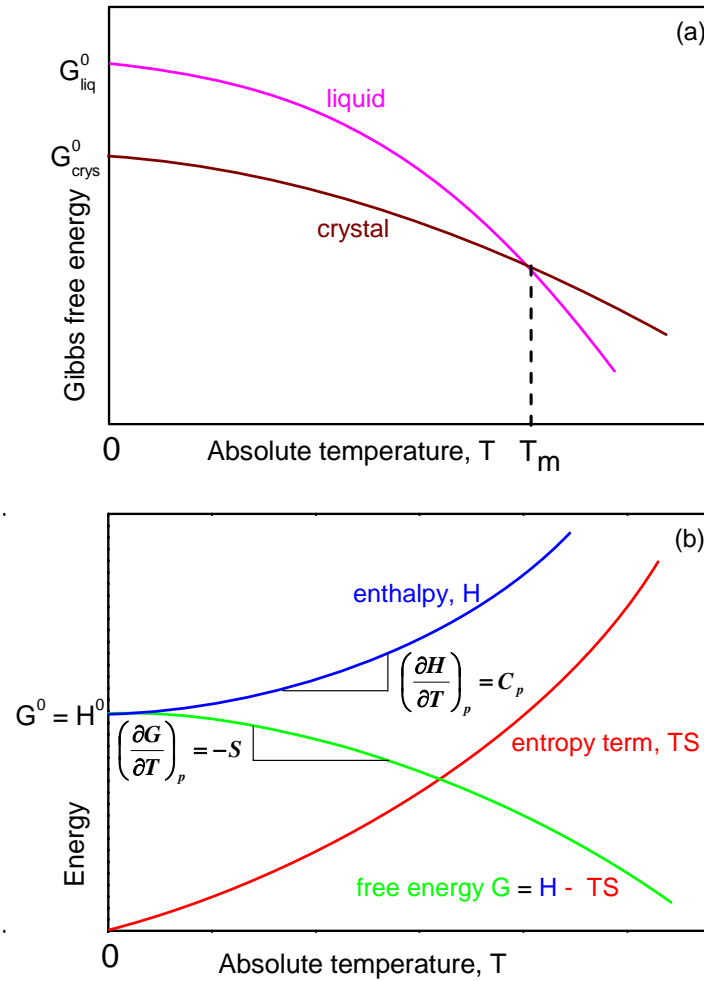


Figure 2.1: (a) Energy vs temperature for a crystallisable solid at constant pressure and (b) Gibbs - free energy plot for a simple crystallisable liquid.

other hand the entropy term (TS) in equation 2.1 increases with the increase in temperature.

Gibbs free energy differences are used to define stability and estimate phase transition temperatures in multi-phase systems. The free energy difference between two states (ΔG) is related to differences in enthalpy and entropy which can be written as

$$\Delta G = \Delta H - T\Delta S \quad (2.6)$$

At the melting temperature

$$\Delta G = \Delta G_{cryst} - \Delta G_{liq} \equiv 0 \quad (2.7)$$

The same condition ($\Delta G = 0$) must be fulfilled at a solid - solid transition temperature defining the stability limits for two different crystalline forms in polymorphic materials.

2.1.2 Nucleation and growth

Crystallisation of a system requires nucleation as the starting point. Nucleation is the formation of minute nuclei (embryos or seeds) in a supercooled liquid below T_m . Nucleation can be classified into two types

- Primary nucleation occurs in a system where no crystals are initially present in the liquid. Primary nucleation can be further classified into homogenous and heterogenous nucleation.
 - Homogenous nucleation happens spontaneously by fluctuative processes in a liquid. The formation of homogenous nuclei is a rare event although the probability increases with the decrease in temperature.
 - Heterogenous nucleation on the other hand occurs at the interface or surfaces and can also be induced by foreign particles. Heterogenous nucleation is the most commonly dominating nucleation process in the bulk systems.
- Secondary nucleation occurs on the surface of the crystal growth front.

Theory of homogenous nucleation will be discussed in the forth coming section. The thermodynamic driving force for a system to crystallise is the reduction in free energy. The homogenous nucleation can be described based on works by Gibbs [42], which was later developed by Volmer and Weber [43], Becker and Döring to a model well know as Classical Nucleation Theory (CNT). Volmer model is based on the stability of the pre-nucleation molecular assemblies also known as clusters having a radius r . The stability of these spherical clusters depends on their size compared to that of the critical nucleus with a mean radius r^* . The total free energy (ΔG_{Total}) is the algebraic sum of volume term (ΔG_{Volume}) and the surface term ($\Delta G_{Surface}$). The volume free energy term favours aggregation of molecules and the surface free energy term favours dissolution of molecular clusters. The total free energy of such a cluster can be written as follows,

$$\Delta G_{Total} = \Delta G_{Volume} + \Delta G_{Surface} \quad (2.8)$$

Due to fluctuations in the system, there exists a distribution of cluster sizes. Only the clusters with size above the critical size ($r > r^*$) can reduce their energy by further growth and can

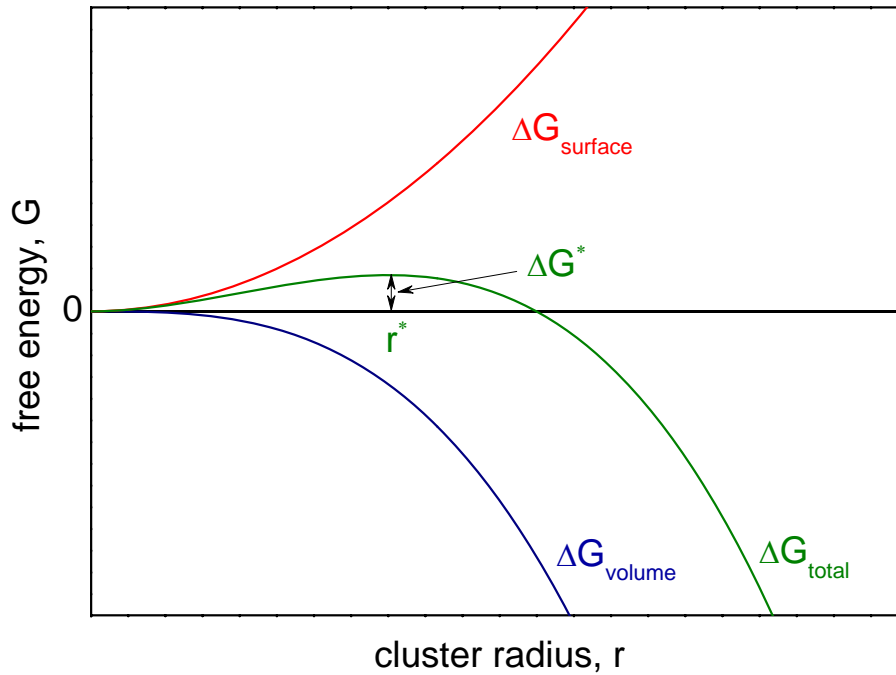


Figure 2.2: Gibbs Free energy change of clusters leading to formation of nucleus.

act as nucleus. For the clusters having critical size ($r = r^*$) the total free energy change of the system attains a maximum, as seen in figure 2.2. This step height (ΔG^*) is the barrier for the nucleation which corresponds to the activation free energy of nucleation. Once the cluster attains the critical size it is termed as nucleus, which then grows into a crystal. If the cluster size is smaller than the critical size the surface term dominates and the cluster dissolves. The total free energy (ΔG_{Total}) can be rewritten as

$$\Delta G_{Total} = V \Delta G_{\nu} + A \sigma \quad (2.9)$$

where, V is the volume of the nucleus, ΔG_{ν} (considered as negative term) the free energy change per unit volume of the system, σ the surface energy, and A the surface area.

If the nucleus is considered to have a spherical geometry then equation 2.9 becomes

$$\Delta G_{Total} = \frac{4}{3} \pi r^3 \Delta G_{\nu} + 4 \pi r^2 \sigma \quad (2.10)$$

Now the critical radius (r^*) and the magnitude of activation barrier step (ΔG^*) can be estimated in the following way from the derivative according to

$$\frac{d\Delta G_{Total}}{dr} \equiv 0 \quad (2.11)$$

$$\text{this gives } r^* = \frac{-2\sigma}{\Delta G_\nu} \quad (2.12)$$

$$\text{and } \Delta G^* = \frac{16\pi}{3} \frac{\sigma^3}{(\Delta G_\nu)^2} \quad (2.13)$$

where ΔG_ν is negative.

The rate of nucleation (J) has a Arrhenius temperature dependence and can be expressed as follows

$$J = A_n \exp\left(\frac{-\Delta G^*}{k_B T}\right) \quad (2.14)$$

substituting equation 2.13 in the above expression

$$J = A_n \exp\left(\frac{-16\pi\sigma^3}{3k_B T(\Delta G_\nu)^2}\right) \quad (2.15)$$

where A_n is a pre exponential constant and, k_B the Boltzmann constant.

The above typical expression is used to describe the rate of homogenous nucleation as a function of temperature. Obviously, the nucleation rate increases with the decrease in the temperature.

In order to approximate temperature dependence of the free energy change ΔG_ν one can make use of the fact that, the total free energy difference ΔG_{Total} becomes zero at the melting point. Then equation 2.9 becomes

$$\Delta G_\nu = \frac{A}{V} \sigma \quad (2.16)$$

The free energy change per unit volume as a function of temperature $\Delta G_\nu(T)$, can be expanded as a Taylor series in the following way

$$\Delta G_\nu(T) = \Delta G_\nu(T_m^\infty) + \frac{d\Delta G_\nu}{dT}(T - T_m^\infty) + \dots \quad (2.17)$$

where T_m^∞ is the melting temperature of the infinitely thick crystal. At the melting point the first term vanishes and by neglecting the higher orders of the equation 2.17 we get

$$\Delta G_\nu(T) = -\Delta S_\nu (T - T_m^\infty) \quad (2.18)$$

$$\text{with } \frac{d\Delta G_\nu}{dT} = -\Delta S_\nu \quad (2.19)$$

and ΔS_ν being the entropy change. Considering again that $\Delta G_\nu = 0$ at the melting point (T_m^∞), the free entropy change can be rewritten as

$$\Delta S_\nu = \frac{\Delta H_m^\infty}{T_m^\infty} \quad (2.20)$$

where ΔH_m^∞ is the enthalpy of melting of infinitely large crystal.

Substituting equation 2.20 in equation 2.18, we get the simple approximation

$$\Delta G_\nu(T) = \Delta H_m^\infty \left(1 - \frac{T}{T_m^\infty}\right) \quad (2.21)$$

Since, ΔG_ν approaches 0 at the T_m^∞ the critical nuclei size diverges at the melting temperature T_m^∞ , i.e, homogenous nucleation will not appear in this temperature range.

Once stable nuclei are formed ($r > r^*$) in a supercooled liquid they begin to grow into crystals of visible size. However the growth of the crystal depends on the viscosity or the mobility of the liquid, since transport of molecules to the growth front is required. The viscosity of liquids increases with decrease in the temperature, however it increases rapidly as it approaches the glass transition temperature (T_g). The temperature dependence of the viscosity is usually well described by the empirical Vogel-Fulcher-Tammann (VFT) equation and is expressed as follows

$$\eta(T) = \eta_o \exp\left(\frac{B}{T - T_v}\right) \quad (2.22)$$

where η_o is a constant, B the curvature of the temperature dependence of viscosity, and T_v is known as the Vogel temperature

If layer by layer growth of crystals is assumed, then nuclei for each new layer have to be formed on the surface of the existing crystal. This process is called as secondary nucleation.

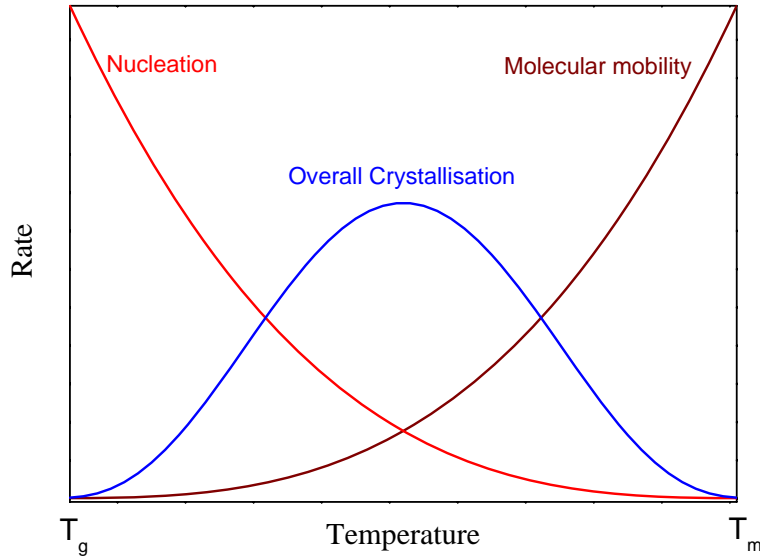


Figure 2.3: Temperature dependence of crystallisation, nucleation rate and, molecular mobility.

The formation of secondary nucleus is then the rate determining step for the crystal growth. Growth along the surface should be much faster than that perpendicular to the overall grow front. Like primary nucleation, the secondary nucleation too is assumed to be a thermally activated process and the rates can be described in a similar way as discussed for primary nucleation. The excess free energy for secondary nucleation can be expressed as a sum of surface and volume contributions according to equation 2.9. If the secondary nucleus is a circular disc with a thickness of h , then the free energy change would be

$$\Delta G_{Total} = \pi r^2 h G_v + 2\pi r h \sigma \quad (2.23)$$

The critical nucleus size (r_{sec}^*) of the secondary nucleus and the activation barrier (ΔG_{sec}^*) can be again derived from the derivative

$$\frac{d\Delta G_{Total}}{dr} \equiv 0 \quad (2.24)$$

$$\text{this gives } r_{sec}^* = \frac{-\sigma}{\Delta G_v} \quad (2.25)$$

$$\text{and } \Delta G_{sec}^* = \frac{\pi h \sigma^2}{\Delta G_v} \quad (2.26)$$

where ΔG_v is negative.

The rate of secondary nucleation which like primary nucleation following a Arrhenius temperature dependence, can be calculated using

$$J_{sec} = A_n \exp\left(\frac{-\pi h \sigma^2}{\Delta G_v k_b T}\right) \quad (2.27)$$

For the overall crystallisation of a system, both the molecular mobility which depends on the viscosity and the nucleation rates are important as depicted in figure 2.3. The nucleation rate increases rapidly with the decreasing temperature due to formation of stable nucleus, since the nucleation barriers in the system at low temperatures are small. On the other hand the mobility becomes small when the glass transition temperature is approached (where the viscosity η reaches 10^{12} Pa.s are reached). In contrary the molecular mobility is high at higher temperatures while the probability of formation of nucleus with a large critical size decreases due to large thermal fluctuations. Due to the competing effects of nucleation rate and molecular mobility the overall crystallisation increases initially with increasing temperature, approaches a maximum and then decreases rapidly as it approaches the melting temperature (T_m). Close to the maximum in the overall crystallisation rate, crystallisation should occur in non - isothermal experiment.

2.2 Polymorphism

According to McCrone "*Polymorphism may be defined as the ability of a element or compound to crystallise as more than one crystal species*".

Frankenheim investigated the polymorphism of potassium nitrate (1839) which was used as a classical example during his time. He showed that conversion of one form of crystal to another can be achieved by solvent mediation and by physical means such as scratching or physical contact with other polymorph. He also studied polymorphsim of mercuric iodide and founded the basic principles of polymorphism which are still widely used. Some of the important principles are listed below:

- each polymorph will have its own melting and boiling point and their vapour densities will differ too.
- transition of polymorph (II) with lower melting to higher-temperature melting form (I) is distinguished by a specific temperature of transition.
- polymorph (II) with lower melting point cannot exist at a temperature above the tran-

sition point to form I. But form I can exist below the transition point where it is a metastable form.

- for temperatures below transition point form I will undergo transition to II upon contact with II, transitions proceeding in all directions, but having different velocities of growth.
- heat is absorbed upon the transition from II to I.

Other authors term "polymorph" more broadly, including both amorphous state and solvates. One has to distinguish polymorphs from *pseudopolymorphs*, also known as solvates, where the solvent molecules are incorporated in stoichiometric and non-stoichiometric ratios. Such as hydrates where water acts as a solvent. If non volatile molecules come into play having the same role as solvent, then the solids are called co-crystals. Solvates and co-crystals too can exist as different polymorphs.

2.2.1 Classification of polymorphic systems

The molecules in the crystal lattice of a polymorph differ in the nature of the non-covalent interactions such as hydrogen bonds, van der waals forces, $\Pi - \Pi$ stacking, and electrostatic interactions. Changes in such non-covalent interactions lead to different crystalline packing in polymorphs. These interactions also influence the way in which heat is dissipated by the molecules in the crystal lattice. Hence each polymorph has its own characteristic enthalpy of fusion (ΔH_m), specific heat (C_p), and Gibbs free energy at a given temperature.

Based on Lehmanns classification, polymorphism can be classified as [2]

- Enantropism
- Monotropism

To illustrate the differences between these two types of polymorphism, a system containing only two polymorphs is considered for the sake of simplicity, with polymorphic form I having higher melting temperature $T_{m,I}$ and form II with lower melting temperature $T_{m,II}$.

Enantiotropism. A pair of polymorphs is said to have enantiotropic relationship (figure 2.4 (a)) if there exists a transition point ($T_{II \rightleftharpoons I}$) at which both the polymorphs can undergo a reversible solid-solid transformation occurring below the melting of both the polymorphic forms. Below this transition temperature ($T_{II \rightleftharpoons I}$) free energy of polymorphic form II is lower

than that of polymorphic form I ($G_{II} < G_I$), hence form II is stable. Polymorphic form I can undergo a transition to form II below this transition temperature ($T_{II=I}$). Above this transition temperature polymorphic form I is stable until it melts. Note that this situation is also considered in Frankenheim's principles discussed above.

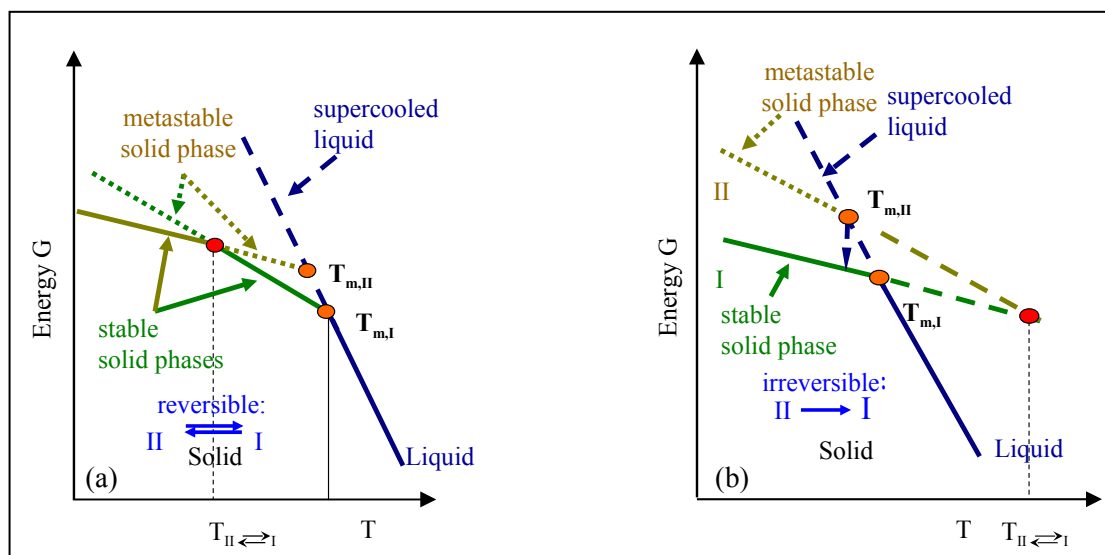


Figure 2.4: Energy - Temperature diagram for a pair of polymorphs exhibiting (a) an enantiotropic relationship and (b) monotropic relationship.

Monotropism. A pair of polymorphs exhibits a monotropic relationship if one of the polymorph is always stable below the melting point of both the polymorphs due to its lower free energy. As shown in figure 2.4 (b) polymorphic form I is always stable ($G_I < G_{II}$) below the melting of both the forms and at all temperatures below the virtual transition point ($T_{II=I}$). For energetic reasons, form II should convert to polymorphic form I at all temperatures. However, such solid - solid transformations are hindered due to the activation barrier. The transition point ($T_{II=I}$) for a monotropic system is called a virtual transition since it lies above the melting of both the polymorphic forms. This notation assumes that the free energy curves converge beyond the melting temperature.

2.2.2 Thermodynamics and nucleation of polymorphs

The Gibbs free energy of a system with a single phase is represented in equation 2.1. Considering a system containing two polymorphs then by using expression 2.1, one can estimate the free energy difference at a temperature T, between crystalline form II (lower melting

polymorph) and form I (higher melting polymorph) based on the general equation

$$G(T)_{II} - G(T)_I = [H(T)_{II} - H(T)_I] - T [S(T)_{II} - S(T)_I] \quad (2.28)$$

$$= \left(\int_0^T (C_{P,II} - C_{P,I}) d\hat{T} + (H_{II}^o - H_I^o) \right) - T \left(\int_0^T \frac{(C_{P,II} - C_{P,I})}{\hat{T}} d\hat{T} \right) \quad (2.29)$$

with H_{II}^o and H_I^o being the enthalpies at 0 K of both the phases respectively.

The above expression is valid only for a system where no phase transition occurs for temperatures between 0 and T. In cases where transitions do occur, the expression will contain additional terms. Mathematical treatment to estimate the free energy differences between two crystalline forms based on experimentally accessible data are dealt in detail in the appendix of this thesis work and by others [44, 45].

To understand influence of kinetics on a system exhibiting polymorphism, consider a system having two crystalline forms (form I and II) with form I being the most stable and II the least stable ($\Delta G_I < \Delta G_{II}$). Individual forms of these crystals have their own free energy barrier (ΔG^*) because of the different surface energy (σ) contribution which then leads to individual critical sizes (r^*). Although form I is favored thermodynamically nucleation of form II may occur if it has the lower free energy barrier compared to form I since it has then a faster nucleation rate. Thus, this metastable form II can appear although it has to finally undergo a transition to form I due to thermodynamic reasons.

Influence of kinetics or thermodynamics on a polymorphic system was discussed by Ostwald [4] in his Rule of stages in 1897 which states that *"When leaving a metastable state, a given chemical system does not seek out the most stable state rather the nearest metastable one that can be reached without loss of free energy"*. The validity of this rule has been shown with different approaches [9, 46, 47]. It was also shown that the presence of the metastable phase can also hinder the formation of stable nucleus [48]. However it can be wrong or does not consider a situation where the crystallisation experiment yields only one polymorphic form. For such a situation one cannot conclude if it contradicts the rule or the system is not polymorphic at all.

2.2.3 Rules to predict thermodynamic relationship between polymorphs

To predict the relative thermodynamic stability of polymorphs and to conclude whether the relationship between different polymorphs is monotropic or enantiotropic several rules were developed by Tamann [18]. Bruger and Ramburger [44] and others [49] further extended its application. These rules are briefly discussed in the following section.

The Heat-of-Transition Rule (HTR) states that if an endothermic transition is observed at some temperature it may be assumed that there is a transition point ($T_{II\rightleftharpoons I}$) below it. This is seen in figure 2.4 (a) and we can conclude that the pair of polymorphs is enantiotropically related. If an exothermic transition is observed at a temperature it may be assumed that there is no thermodynamic phase transition below this temperature. Then the two forms are either monotropically related or they are enantiotropically related and that the transition temperature ($T_{II\rightleftharpoons I}$) is higher than the experimentally observed transition temperature. This rule is based on the assumption that free energy curves of the polymorphs meet only once and that the enthalpy isobars never intersect.

The Heat-of-Fusion Rule (HFR) states that if the higher melting polymorph has lower enthalpy of fusion than the lower melting polymorph then they are enantiotropically related, otherwise have monotropic relationship. This rule is based on the assumption that the heat of transition is approximately equal to the difference in the heats of fusion of the polymorphs. Bruger and Ramburger [44] argued that such approximations are not valid and included correction terms containing the specific heat C_p . The expression for enthalpy of transition from polymorphic form II to form I containing the correction term is

$$\Delta H_{II\rightarrow I} = \Delta H_{m,I} + \int_{T_{m,II}}^{T_{m,I}} (C_{p,l} - C_{p,I})dT - \Delta H_{m,II} \quad (2.30)$$

where ($C_{p,l}$) is the specific heat of supercooled liquid. Exception to this rule may arise when the enthalpy curves of the two polymorphs diverge significantly, or when the difference between the melting points of the two polymorphs is larger than 30 K.

The Entropy-of-Fusion Rule (EFR) states that if the polymorph with higher melting point has a lower entropy of fusion, then the polymorphs are enantiotropically related [18]. On the hand if the polymorph with the higher melting point has higher entropy of fusion then the two polymorphs are monotropically related. The entropy of fusion (ΔS_m) can be obtained

from the enthalpy of fusion at the melting point (T_m), where the Gibbs free energy equals zero. One gets

$$\Delta S_m = \frac{\Delta H_m}{T_m} \quad (2.31)$$

The Heat Capacity Rule (HCR) states that for a pair of polymorphs if the polymorph with higher melting also has higher specific capacity (C_p) at a given temperature they have enantiotropic relationship. Conversely, they have monotropic relationship if the polymorph with higher melting point has lower specific heat. Since the heat capacity of different polymorphs have similar values, high precision measurements are required to estimate the differences. This rule itself has limited application.

Density Rule (DR) is based on closest packing of the molecular crystals and states that for non hydrogen bonded system at absolute zero, the most stable polymorph will have the highest density, because of stronger intramolecular van der Waals interactions. Thus, according to this rule, the crystal structure with most efficient packing will also have the lowest free energy. However exceptions do exist as in the case of acetaminophen [50] where the metastable polymorph has closer packing due to closer molecular packing arising from hydrogen bonding than the stable polymorph.

2.3 Crystals under confinement

When a crystal has a size in the nanometer range then its melting temperature is reduced compared to the bulk melting point. This is because the free energy of the smaller crystals increases due to higher surface to volume ratio when compared to larger crystals. The reduction in melting point of small crystals surrounded by the melt is expressed mathematically by the Gibbs-Thompson relationship

$$T_m(r) = T_m^\infty - \frac{A}{V} \frac{T_m^\infty}{\Delta H_m^\infty} \frac{\sigma}{\rho} \quad (2.32)$$

where $r (= \frac{V}{A})$ is the measure of size, T_m^∞ the melting temperature and ΔH_m^∞ the enthalpy of melting of the infinitely large crystal, σ the surface energy and, ρ the density of the crystal. The Gibbs - Thompson equation can be derived starting from equation 2.9, using the approximation for $\Delta G_\nu(T)$ which is given in equation 2.18 and considering $\Delta G_{\text{Total}} = 0$ at $T_m(r)$. It is assumed that small crystals retain the bulk properties such as melting enthalpy ΔH_m^∞ or

density and that the surface energy is isotropic.

Such an effect can be clearly seen in figure 2.5 for various organic molecules confined in controlled porous glass (CPG). This effect is observed for different class of materials such as organic molecules [25, 51, 52] confined to different porous media, finely dispersed non-porous media [51] and polymer lamella [53, 54] confined to different porous media. Such size effects are also seen in the case of molecular clusters of metal atoms prepared by evaporation techniques [55–57], where reduction in melting point up to 500 K was observed.

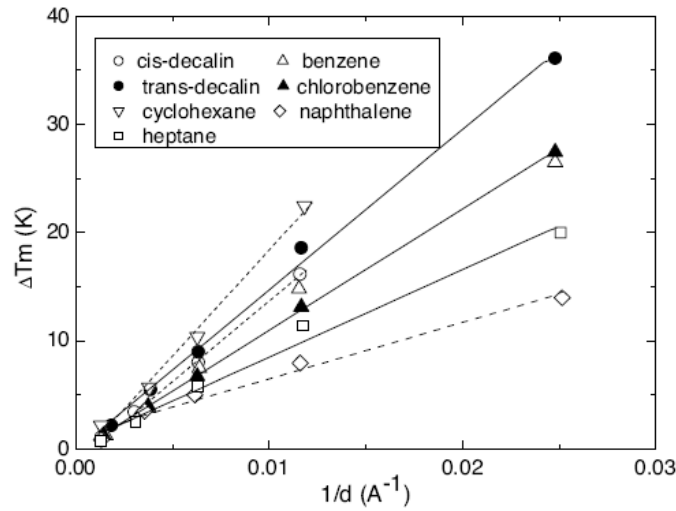


Figure 2.5: Experimental values of reduction in melting point ΔT_m plotted against inverse pore diameter ($1/d$). Taken from reference [51].

Equation 2.32 predicts the linear relationship between the melting point (T_m) and the inverse crystal size $\frac{1}{d}$ of a small crystal surrounded by melt. In the case of crystals confined in nanopores (figure 2.6) surface energies associated with the crystal-substrate (σ_{c-sub}) and the liquid-substrate (σ_{l-sub}) have to be taken into consideration where substrate corresponds to the pore wall. These effects were discussed in reference [25] and the following modified Gibbs - Thompson equation was arrived for cylindrical channels (which is a common approximation for CPGs)

$$T_m(d) = T_m^\infty + \frac{4 T_m^\infty \sigma_{cl}}{\rho_c \Delta H_m^\infty d} \cos \theta \quad (2.33)$$

where ρ_{solid} is the density of the bulk crystal, σ_{cl} the surface energy crystal-liquid and, θ is the contact angle defined as

$$\cos \theta = \frac{\sigma_{l-sub} - \sigma_{c-sub}}{\sigma_{cl}} \quad (2.34)$$

When $0^\circ < \theta < 90^\circ$ reduction in melting point would be negative, which would give rise to increase in the melting point (i.e., solid wets the substrate better than the liquid, thereby inhibiting melting). On the other hand for $90^\circ < \theta < 180^\circ$ the equation 2.33 would yield a positive ΔT_m showing the normal reduction in melting point with the decreasing crystal size (i.e., liquid wets the substrate better than the solid, thereby promoting melting). From equation 2.34 reduction in melting point would occur only when $\sigma_{l-sub} < \sigma_{c-sub}$.

Apart from studies on crystallisable liquids in nanopores there is a large number of stud-

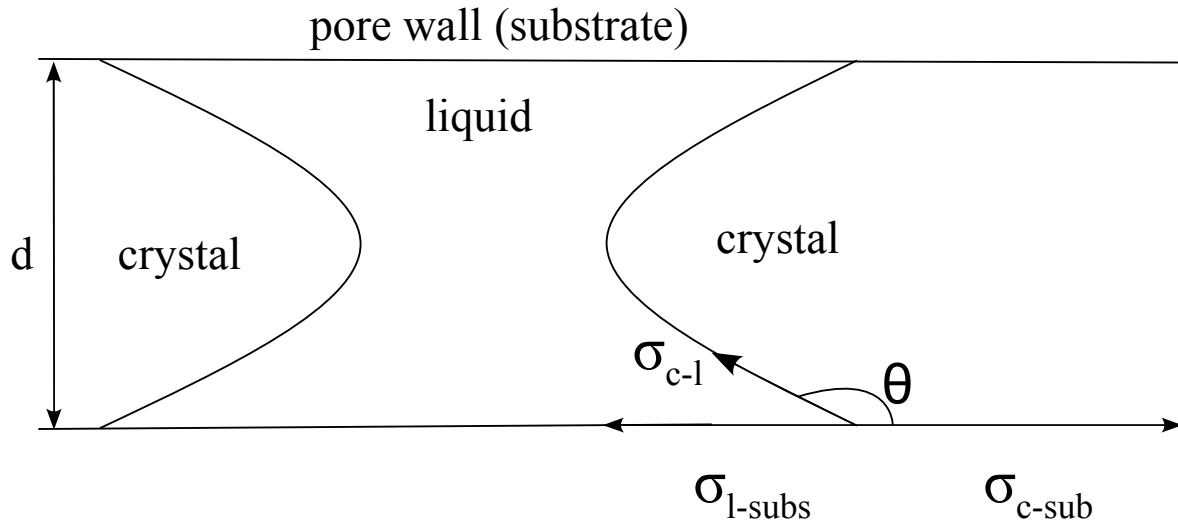


Figure 2.6: Nanocrystal under confinement.

ies focusing on changes in the cooperative dynamics and glass transition behaviour of glass forming liquids in nanopores host systems. This topic is outside the scope of this thesis work and will not be discussed in detail. However one minor aspect of these studies is important for our experiments. It has been shown that the molecules infiltrated in CPGs with untreated pore walls are usually described by a two phase model i.e., molecules close to the surface of the pore walls are distinguishable from the ones in inner core phase. These layers exhibits different dynamics. Arndt et.al. [58] investigated the glass dynamics of the low molecular weight glass forming liquid salol confined in the nanoporous (with diameters in the range 3 - 8 nm) glass substrates. Since salol is known to form intramolecular hydrogen bonds, few

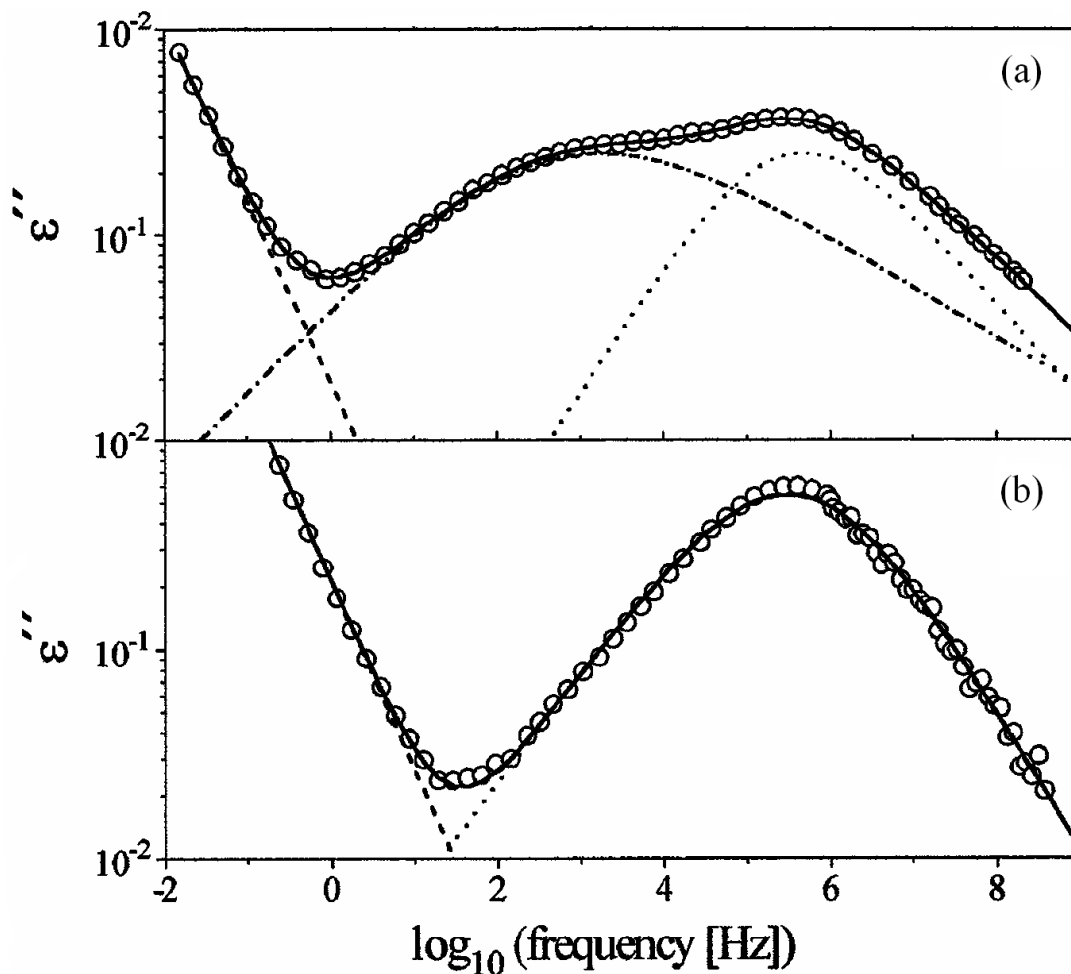


Figure 2.7: Dielectric loss ε'' of salol confined to nanoporous glass having a diameter of 7.3 nm at 253 K for. (a) Confined to untreated pores and (b) to pores with treated walls decorated with trimethylsilyl groups molecules in direct vicinity of the surface (dash-dotted lines) and those of unbound molecules (dotted lines) are indicated. Taken from reference [58].

layers of salol molecules can attach to the untreated pore walls. When such a system was investigated using dielectric spectroscopy, it was revealed that there was an additional loss process apart from the dynamic glass transition, which was slower by two orders of magnitude (figure 2.7 (a)). This additional process was assigned to the motions of molecules which form hydrogen bonds to the surface of the pores as shown in figure 2.7 (a). To conform the effect of the surface layer the salol molecules were filled in CPGs coated with a non interacting hydrophobic silicon layer, which resulted in the complete suppression of the interfacial relaxation process as shown in the figure 2.7 (b). Several other groups [59–62] have reported similar effects for organic molecules infiltrated in CPGs and other porous media with strong interacting pore walls. Calorimetric measurements on propylene glycol confined to porous

media showed indications for two glass transitions (T_g) [63]. It was found that strength of one of the glass transitions increases with decreasing degree of filling, conforming the presence of surface layer. For such a system the thickness of the surface layer was estimated using the following relationship

$$t = \frac{d}{2} \left[1 - \left(\frac{\Delta C_{p,I}}{\Delta C_{p,I} + \Delta C_{p,II}} \right)^{\frac{1}{n}} \right] \quad (2.35)$$

where t is the thickness of the surface layer, n depends on the geometry of the pores (3 for spheres and 2 for cylinders), d the average pore diameter and $\Delta C_{p,I}$, $\Delta C_{p,II}$ are the step height of the first and the second transitions in the heat capacities, as observed in the heating runs respectively.

Chapter 3

Experimental Techniques

Calorimetric and dielectric measurements were performed on both bulk acetaminophen and on nanoporous host systems filled with acetaminophen. The principles of both the experimental techniques and relevant data evaluation methods will be discussed in this chapter.

3.1 Differential Scanning Calorimetry

Differential Scanning Calorimetry is a very widely used characterisation technique to measure thermal and thermodynamic properties. This technique measures heat flow rate to the sample vs temperature, unlike heat flow itself in the case of classical calorimetry. The sample is heated or cooled at preset rates to understand the material behavior. There are two main types of Differential Scanning Calorimeters, namely;

- Power compensation DSC,
- Heat flux DSC

The calorimetry experiments presented in this thesis work were carried out on commercial Perkin Elmer instruments (DSC 7 and Pyris Diamond DSC) which make use of the power compensation DSC principle as discussed in the following section.

3.1.1 Power Compensated DSC

This technique belongs to heat compensating calorimeters. A scheme of a power compensated DSC is shown in figure 3.1. The basic setup of the instrument consists of two identical microfurnaces, which are made up of platinum iridium alloy. One of the furnaces will contain a reference pan with a heat capacity C_3 and the other will hold the sample pan having

a heat capacity C_4 . The sample container holds the sample with a heat capacity (C_s). Since both the microfurnaces contains pans which are identical, their heat capacities are the same ($C_3 = C_4 \equiv C$) at temperatures T_3 and T_4 . The reference and the sample system are connected via the heat resistances of reference furnace (R_1) and the sample furnace (R_2) with ($R_2 = R_1 \equiv R$). The furnaces are separated from each other and are surrounded by aluminium block, which is maintained at a constant temperature. Both the furnaces have sensitive temperature sensors which monitor the temperature (T_1 and T_2) and heaters which supply electrical power (P_1 and P_2) to heat the microfurnaces. Disturbances from outside will affect both the furnaces similarly and will cancel out in ΔP .

During a heating scan both the microfurnaces are supplied with heating power through the power control circuit to achieve a constant heating rate β . The heating power is controlled in such a way that the sensor temperatures T_1 and T_2 , undergo linear change. If both the furnaces are in thermal symmetry, then the temperature of the reference furnace (T_1) and the sample furnace (T_2) would be the same for identical heating power. If there is a thermal imbalance caused by the sample, then there will be a detectable power difference ($\Delta P = P_1 - P_2$) between the both microfurnaces. In particular, when the temperature on the sample furnace increases due to heat produced during crystallisation (exothermic process), then the power supplied to the sample microfurnace (P_2) is reduced to maintain the same temperature on both the microfurnaces. When the sample melts (endothermic process), additional power is supplied to the sample furnace. This change is directly measured as power difference ΔP during the scan.

The whole system can be mathematically described [64] using the following differential equation

$$\Delta P = \left(\frac{dH}{dt} \right) + C_s \beta - (C_4 + C_s) R \left(\frac{d\Delta P}{dt} \right) \quad (3.1)$$

where the ΔP is the difference in the heating power between the sample furnace (P_2) and the reference furnace (P_1), C_s the specific heat of the sample and, $(C_4 + C_s)R$ the time constant τ describing heat transfer.

The measuring system can be well described by the above differential equation. Thus the difference in heating power depends on the enthalpy production ($\frac{dH}{dt}$) of the sample, its heat capacity C_s , the heating rate β , as well as the time constant τ which consists the heat

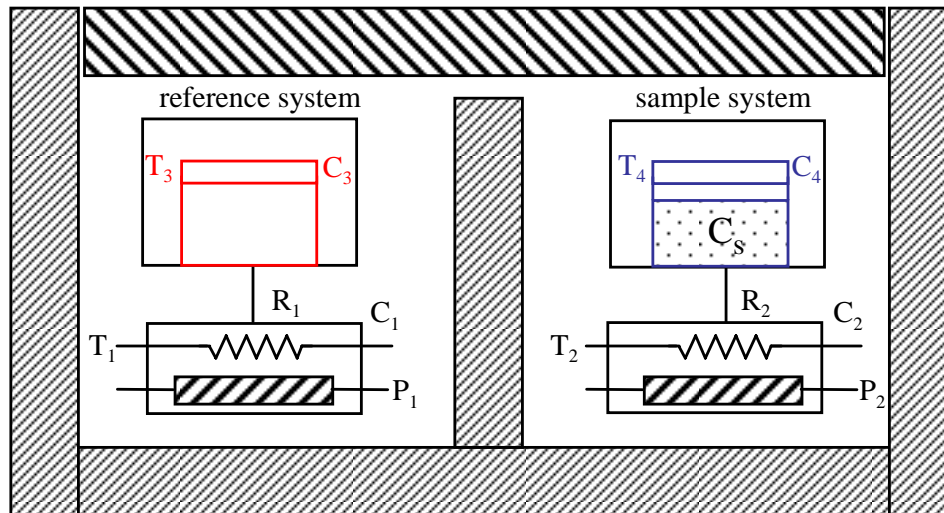


Figure 3.1: A model scheme of a power compensated Differential Scanning Calorimeter.

capacity of sample C_s and container C_4 and, the thermal resistance between heating element and container R . The expression 3.1 describes non steady state conditions during a transition ($\frac{dH}{dt} \neq 0$) and ($C_s \neq \text{const}$) in the sample affecting ($\Delta P(t)$). Hence the term $(C_4 + C_s) R \left(\frac{d\Delta P}{dt}\right)$ appears in the differential equation. Under steady state condition without transitions ($\left(\frac{dH}{dt}\right) = 0$) and $C_s \approx \text{const}$, the difference in power between the sample and reference ($\Delta P = P_2 - P_1$) should be practically constant, and $C_s\beta$ would dominate in equation 3.1.

3.1.2 Evaluating the DSC Data

For evaluating the DSC scans, different transition phenomena to be considered are discussed below.

A **peak** appears when there heat is released (exothermic process like crystallisation) or consumed (endothermic process like melting) by the sample. The peaks in heat flow rate related to endothermic process are assigned positive and plotted upwards, the exothermic peaks are assigned negative and plotted downwards as a convention. Only first order phase transitions associated with a transition enthalpy (e.g. melting, crystallisation) lead to a peak, while the glass transition leads to a step in the measured curve as shown in figure 3.2. The peak itself is affected by the heating rate, the thermal conductivity, mass of the sample and even the position [65] of sample in the microfurnace.

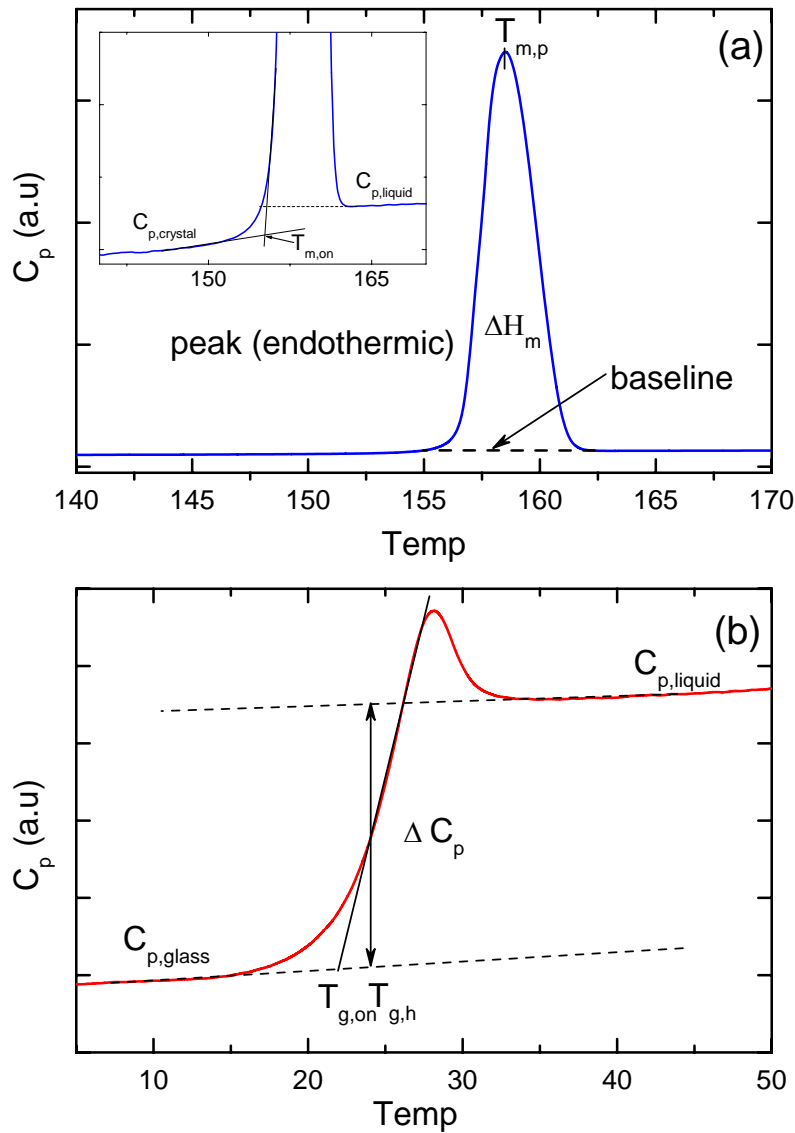


Figure 3.2: DSC curve from a heating scan showing (a) a melting peak and, (b) a glass step.

Some of the characteristic features used to define melting temperature as sketched in figure 3.2 (a) are discussed below

- $T_{m,on}$ - **Extrapolated peak / onset temperature** here the auxiliary line through the ascending peak (eg. melting) slope intersects the baseline. The auxiliary line is drawn through (almost) linear section of the ascending peak slope, either as inflectional tangent or as fitted line.
- $T_{m,p}$ - **Peak maximum temperature** is designated to the maximum value of the difference between the curve of measured values and the interpolated baseline (not neces-

sarily the absolute maximum of the curve of measured values).

- ΔH_m - **Enthalpy of melting** is estimated based on the area under the peak (both exothermic and endothermic). The base line is an extrapolation of the liquid line ($C_{p,liquid}$) to intercept the melting curve on the crystal side (shown as insert in figure 3.2(a)).

Analogously crystallisation temperatures can be defined for a exothermic crystallisation peak.

Typical methods to define the glass temperature T_g based on experimental data in the glass transition region are shown in figure 3.2 (b) and are discussed as follows

- $T_{g,on}$ - **Extrapolated onset temperature** is estimated based on the intersect of tangents drawn in the glassy region and in the transition range.
- $T_{g,h}$ - **Half C_p extrapolated T_g** is the temperature on heating or cooling where the heat capacity change of the system is half of the total glass transition step height ΔC_p .

The estimation of the characteristic temperatures as well as the pros and cons of different methods are described in detail in references [66, 67].

In this thesis work the peak maxima or minima are used to define melting or crystallisation temperatures. T_g values are estimated based on the half step height.

3.2 Dielectric Spectroscopy as a linear response method

3.2.1 Basic principles of dielectric spectroscopy

Relaxation spectroscopy experiments are based on Fluctuation Dissipation Theory (FDT), which relates linear response experiments with spontaneous fluctuations on a microscopic scale. In an isotropic system the time dependent response $y(t)$ which follows a sufficiently small disturbance $x(t)$, can be described using a linear relationship. A good example for this is dielectric spectroscopy, where the disturbance is the time dependent external electrical field $x(t)=E(t)$ and the response of the system is the polarisation $y(t)=P(t)$. For such a system the linear response gives

$$P(t) = P_{\infty} + \varepsilon_0 \int_{-\infty}^t \varepsilon(t-t') \frac{dE(t')}{dt'} dt' \quad (3.2)$$

where, $\varepsilon(t)$ is the time dependent dielectric function and P_∞ which covers all the contributions arising from electronic polarisation.

There are two conditions that are to be satisfied for linear response methods, an outer disturbance $x(t)$ may act on system and cause response $y(t)$ [68],

- linearity - the response of the system on the sum of two disturbances is equal to sum of the two single responses resulting from the individual disturbances
- causality - only the disturbances in the past contribute to a response at a later time

Susceptibilities like the dielectric function ε are closely connected to the molecular motions in the material. FDT connects macroscopically measured properties (susceptibilities) and the microscopic motions in the form of fluctuations. The relation can be described mathematically in the frequency domain as

$$\frac{\varepsilon^*(\omega) - \varepsilon_\infty}{\varepsilon_{Sta} - \varepsilon_\infty} = \int_0^\infty \frac{-d\Phi(t)}{dt} \exp(-i\omega t) dt \quad (3.3)$$

$$\text{with } \Phi(t) = \frac{\langle \Delta P(t) \Delta P(0) \rangle}{\langle \Delta P(0)^2 \rangle}$$

In equation 3.3 the quantities ε_∞ and ε_{Sta} are the permittivities at very high frequency (unrelaxed permittivity) and at low quasistatic frequencies (relaxed) permittivity. ΔP is the fluctuation of the polarisation P around its average value $\langle P \rangle$.

Dielectric spectroscopy is widely used to study the relaxation behaviour of polymeric materials, small molecular glass forming liquids and liquid crystalline materials. It detects dipole fluctuations on different time scales seen in dielectric spectra as relaxation processes and also provides useful information related to mobility of charge carriers [69]. Differences in electronegativity between covalently bonded atoms lead to a permanent electric dipole moment. The dynamics of molecules having significant permanent dipole moments can be studied by dielectric spectroscopy. However, molecules having permanent dipole moment show no macroscopic polarisation in the absence of electric field. When an electric field either alternating or static, is applied to such type of molecules the dipoles can reorient to the applied electric field leading to dipolar polarisation of the entire sample. The ability of dipoles to reorient depending on temperature and frequency or time is detectable by dielectric spectroscopy, which gives information about the relaxation behaviour of the sample.

The basic principle of dielectric measurement in the frequency domain will be shortly described below [70].

Consider a parallel plate capacitor of plate area A , and the distance between the plates d . If the space between the electrodes is vacuum, then the capacitance of the empty cell is given by

$$C_0 = \frac{A \varepsilon_0}{d} \quad (3.4)$$

where $\varepsilon = 8.85 \times 10^{-12} \text{ A s V}^{-1} \text{ m}^{-1}$ is the permittivity of vacuum

If a sample is replaced instead of vacuum the new complex capacitance is given by

$$C^*(\omega) = \varepsilon^*(\omega) C_0 = \frac{A \varepsilon_0 \varepsilon^*(\omega)}{d} \quad (3.5)$$

where $\varepsilon^*(\omega)$ is the complex dielectric function of the sample which depends on the applied frequency and the temperature. The dielectric function is a compliance which has a real and an imaginary part

$$\varepsilon^*(\omega) = \varepsilon'(\omega) - i \varepsilon''(\omega) \quad (3.6)$$

In order to measure $\varepsilon^*(\omega)$ an alternating voltage is applied the sample. The program is given by

$$V(t) = V_0 e^{i\omega t} \quad (3.7)$$

The total current through the capacitor due to the applied alternating voltage is given by

$$I(t) = I_0 e^{i\omega t + \frac{\pi}{2} - \delta} \quad (3.8)$$

where δ is the phase shift as the current leads the voltage by a phase angle in the case of A.C circuit containing a capacitor. Then the total impedance is given by

$$Z^*(\omega) = \frac{V(t)}{I(t)} = \frac{1}{i\omega \varepsilon^*(\omega) C_0} \quad (3.9)$$

For a given frequency the sample capacitor can be formally described as a parallel circuit of ideal resistor R_p and ideal capacitor C_p . Then the total impedance is given by

$$\frac{1}{Z^*(\omega)} = \frac{1}{R_p} + i\omega C_p \quad (3.10)$$

R_p and C_p can be measured by network analysers.

Comparing equations 3.9 and 3.10, the real and imaginary part of the dielectric function can be written as

$$\varepsilon' = \frac{C_p}{C_0} \quad (3.11)$$

$$\varepsilon'' = \frac{1}{R_p \omega C_0} \quad (3.12)$$

where the dielectric loss tangent $\tan \delta$ is given by

$$\tan \delta = \frac{\varepsilon''}{\varepsilon'} \quad (3.13)$$

3.2.2 Data evaluation

A relaxation process in isothermal dielectric data is characterised by a peak in the ε'' and a step-like decrease of ε' vs log frequency (figure 3.3).

The data close to the relaxation peak are usually well described by the Havriliak-Negami function, which approximates real and imaginary part of ε^*

$$\varepsilon^*(\omega) - \varepsilon_\infty = \frac{\varepsilon_{Sta} - \varepsilon_\infty}{[1 + (i\omega\tau_{HN})^b]^g} \quad (3.14)$$

where ε_{Sta} is the dielectric permittivity at low frequency, ε_∞ is the unrelaxed dielectric permittivity at high frequency, $1/\tau_{HN} = \omega_{HN}$ is the Havriliak-Negami frequency, while b and g are shape parameters of the relaxation peak ($0 \leq b, g \leq 1$).

In addition D.C conductivity is observed at high temperatures and low frequencies, which is given by the following relationship

$$\varepsilon''(\omega) = \frac{G_0}{\omega C_0} \quad (3.15)$$

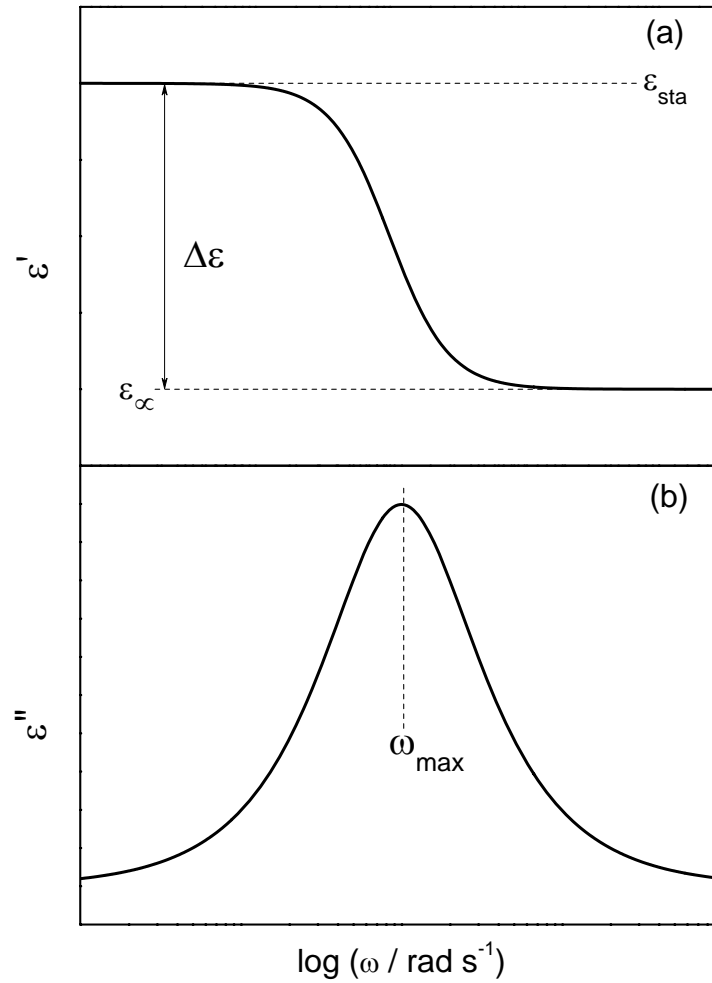


Figure 3.3: Dielectric spectrum showing the typical features of a relaxation process in (a) real and (b) imaginary part of the frequency-dependent permittivity showing the frequency dependence of permittivity $\epsilon^*(\omega) = \epsilon' - i\epsilon''$.

where, G_0 is the D.C, conductivity of the sample in Ω^{-1} .

The α relaxation of glass forming liquids corresponding to the dynamic glass transition is related to cooperative motions of many molecules. A typical feature of such a relaxation process is that, it shows a non - Arrhenius temperature dependence of the characteristic relaxation frequency $\omega_\alpha(T)$, which is usually described by Vogel Fulcher Tamman Hesse (VFT) equation

$$\omega(T)_\alpha = \omega_0 \exp\left(\frac{-B}{T - T_0}\right) \quad (3.16)$$

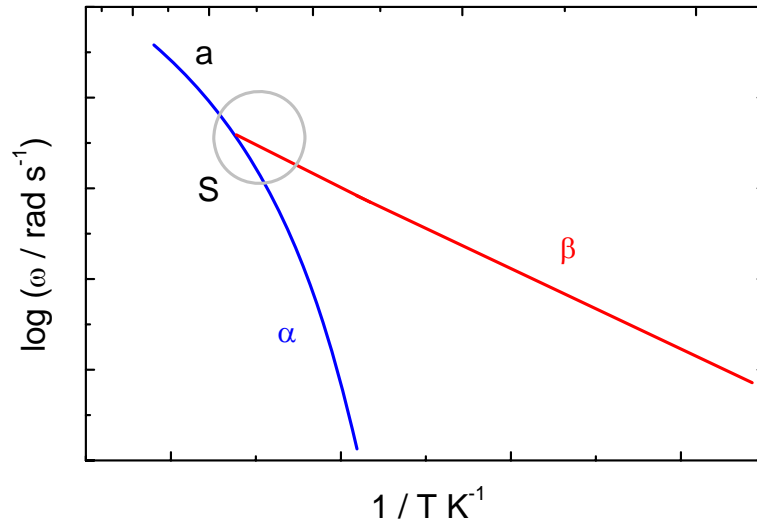


Figure 3.4: Arrhenius plot indicating α , β and, a processes which is separated by the crossover region indicated by an open circle S.

with ω_0 being the limiting frequency for $T \rightarrow \infty$, B the curvature and, T_0 the Vogel temperature.

The secondary relaxation β process also known as Johari- Goldstein modes is related to more local motions in the sample and shows a typical Arrhenius - like temperature dependence

$$\omega_{\beta}(T) = A \exp\left(\frac{-E_a}{RT}\right) \quad (3.17)$$

where E_a is the activation energy, R the gas constant and, A is a pre factor about 10^{14} rad s $^{-1}$.

Due to differences in their temperature dependence α and β relaxations approach each other in the so - called crossover region (figure 3.4).

Chapter 4

Guest - Host system

To study the influence of nanoconfinement on the crystallisation behavior of polymorphic materials, an often investigated pharmaceutical - acetaminophen was selected. Acetaminophen is widely used as an analgesic (pain reliever) and antipyretic (fever reducer) drug. It is known that, acetaminophen can exist in three different crystalline forms. Amorphous acetaminophen with a glass transition around room temperature can be produced by melt quenching. To impose nanoconfinement on the chosen model guest system, suitable porous media were selected. The porous media were chosen in such a way that the inner surface walls are easily wettable by the guest molecule, have good thermal and mechanical stability during the infiltration step and during measurement, and does not change the chemical composition of the infiltrated guest molecule (no decomposition of acetaminophen). In order to serve this purpose two different porous media with comparable surface properties and different pore geometry, controlled porous glass (CPG) and porous alumina, were selected. Both types of host systems have a narrow pore size distribution.

4.1 Guest System

Acetaminophen ($C_8H_9NO_2$), whose chemical structure is shown in figure 4.1, commercially well known as paracetamol, was selected as the guest system. It has a molecular weight of $151.16 \text{ g mol}^{-1}$. The samples were purchased from Sigma-Aldrich (CAT No. 103-90-2) with a purity $\geq 99\%$. Two well known polymorphs [71] of acetaminophen are form I having a monoclinic structure and form II with orthorhombic structure. The thermodynamic parameters of these two forms are listed in table 4.1. X-ray scattering data for both the forms are shown in figure 4.2. It is also known that a metastable form III of acetaminophen exists although many details of this form are unknown, since it was produced only by accident

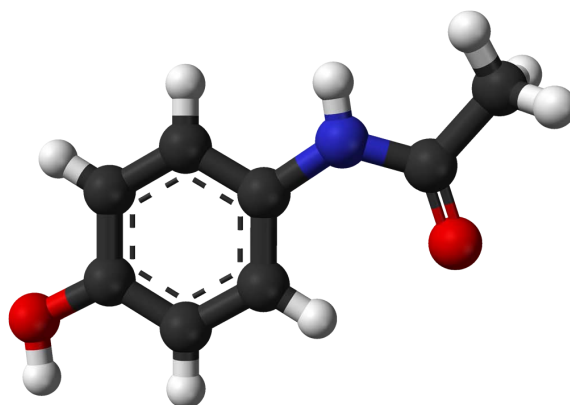


Figure 4.1: Chemical structure of acetaminophen (gray: carbon, white: hydrogen, red: oxygen, blue: nitrogen)

in thin capillaries or in between glass plates. A speculative melting temperature of about 140°C is given in reference [72] and first XRD data is reported in reference [73]. Amorphous acetaminophen has a T_g of about 24 °C and can be obtained by rapid melt quenching. However, the life time of amorphous acetaminophen is usually rather limited to few hours under ambient conditions.

Table 4.1: Thermodynamic parameters such as melting point T_m , enthalpy of melting ΔH_m and, density ρ of different forms of acetaminophen taken from reference [74].

Crystalline form	T_m (°C)	ΔH_m (kJ mol ⁻¹)	ρ (g cm ⁻³)
Form I	168 ± 1	28.1 ± 0.6	1.293
Form II	155 ± 1	26.9 ± 0.4	1.336

4.2 Host Media

Preparation of controlled porous glass (CPG) and porous alumina which are used as nanoconfining media are briefly discussed in the following sub-sections.

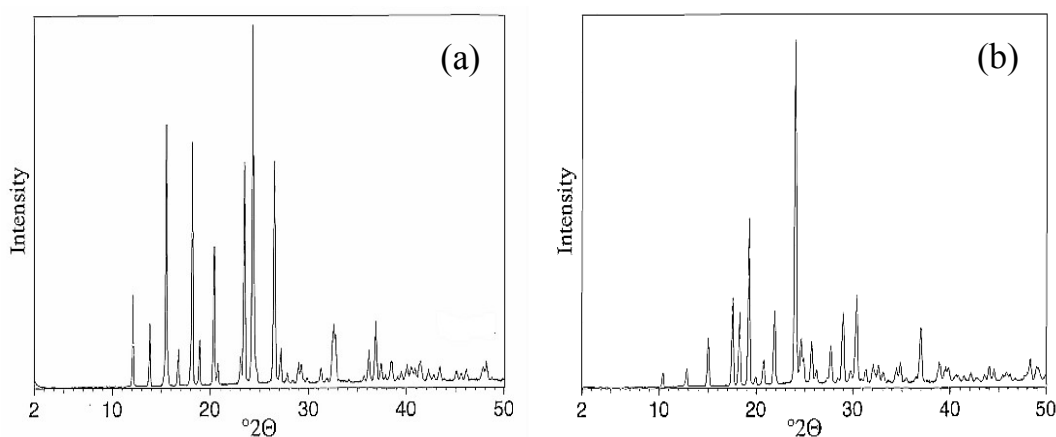


Figure 4.2: Powder X-ray diffraction pattern for (a) monoclinic (form I) and (b) orthorhombic (form II) paracetamol. Taken from [71].

4.2.1 Controlled Porous Glass (CPG)

Sodium borosilicate glasses with a composition of 70 wt % SiO_2 , 23 wt % B_2O_3 and 7 wt % Na_2O was used in the preparation of nanoporous silica glass monoliths using sol-gel process. The procedure to obtain controlled porous glass is described in detail in reference [75]. Textural properties of the porous glass used in this thesis work are listed in table 4.2. The parameters were estimated based on mercury porosimetry for pore diameters 10 -100 nm and nitrogen absorption was used for 4.6 nm pores. Porous glass membranes having thickness of 300 μm and pore diameters in the range 4 - 100 nm were used for the experiments. These substrates are mechanically stable and have narrow pore size distribution (figure 4.3(a)). All the pores are interconnected and there is no anisotropy in the sample. The final CPGs have a sponge like morphology as shown in figure 4.3 (b), which is a typical outcome for spinodal decomposition. The inner pore walls are untreated and have high surface energy. To estimate the surface energy, contact angle measurements of acetaminophen on a ordinary glass plate were performed [76] using a Data Physics OCA 20 instrument with the Sissle drop method. The contact angle was estimated as $\theta = 19.91^\circ$ at 171°C .

4.2.2 Porous alumina

Self-ordered porous alumina layers were prepared by electrochemical two - step anodization according to procedures reported in references [77–79]. Unlike, controlled porous glass the porous alumina have isolated cylindrical pores. The pores are arranged on a hexagonal lattice packing which extends over 10 - 20 lattice constants [80] and have well defined pore

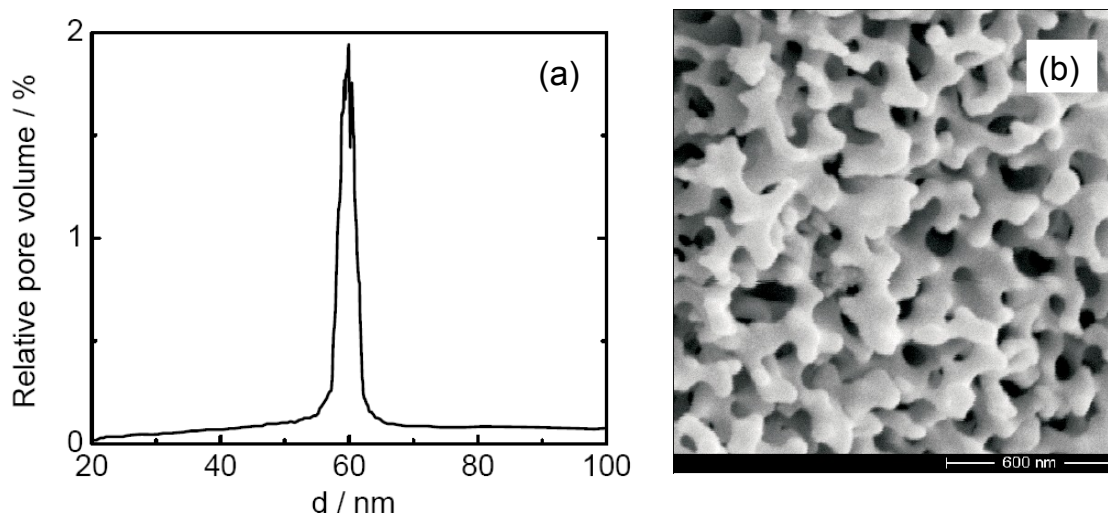


Figure 4.3: (a) Pore size distribution for CPG having pore diameter of 60 nm as obtained from mercury porosimetry measurements, (b) Scanning electron microscopy of controlled porous glass.

Table 4.2: Textural properties of CPG membranes used as host systems. Average pore diameter d , internal surface area μ , specific pore volume ν , and porosity P .

d in nm	μ in $m^2 g^{-1}$	ν in $cm^3 g^{-1}$	P in %
4.6	110	0.108	20
10	76	0.20	32
22	81	0.40	42
43	36	0.36	44
60	30	0.43	43
103	30	0.53	55

diameters. The pore size and the depth can be controlled by type of electrolyte used and the magnitude of the electrical potential applied. Pore diameters of 25, 35, 60, 180 and 400 nm with pore depth of 100 μm were used for infiltration of acetaminophen. The calculated porosity for templates with 25, 35, and 180 nm pores is 10% and 40 - 50% in the case

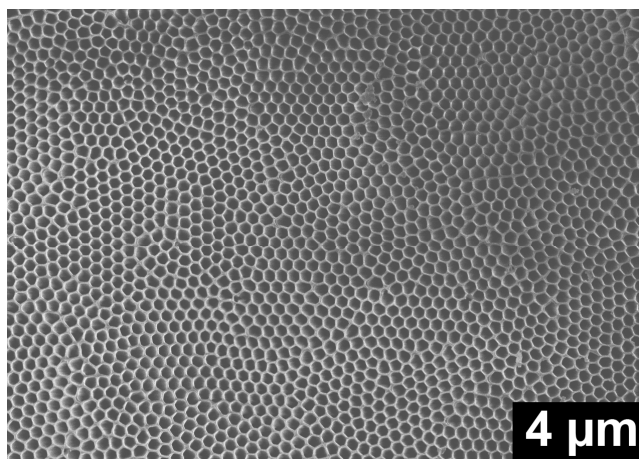


Figure 4.4: (a) Scanning electron microscopy of self ordered porous alumina.

of 60 and 400 nm pores. The contact angle of acetaminophen on a flat alumina surface measured at 171°C [76] was found to be $\theta = 26.78^\circ$. The porous alumina layer is supported by aluminium substrates to have good mechanical stability. These aluminum substrates can be removed when required upon suitable chemical etching.

4.3 Infiltration of guest molecule in host system

Infiltration of the acetaminophen guest system into the nanoporous media was performed using molten acetaminophen. This procedure is advantageous compared to the other methods such as infiltrating acetaminophen solutions, since high degrees of filling can be achieved (nearly 100 %) what would have been impossible with solvent filling.

Porous Glass

Controlled porous glasses are filled after carefully drying the host system under vacuum at 180°C for 2 hours to remove entrapped moisture. The dried porous glass is then immersed in molten acetaminophen maintained at 180°C. The filled substrates are then removed from the molten acetaminophen and cooled to room temperature at ambient conditions. The bulk acetaminophen surface layer is then removed carefully with a scalpel. Small pieces of filled CPG substrates with a size of 2 mm × 2 mm having a mass 4-6 mg were then encapsulated in 10 μ l hermitically sealed pans for DSC measurements or used for WAXS measurements.

Porous alumina

Porous alumina substrates having a circular geometry with a diameter of 20 mm were used for the experiments. The alumina membranes were dried at 180 °C for 2 hours in nitrogen atmosphere to remove the residual moisture. Then a few milligrams of acetaminophen are placed on the surface of the alumina substrate. Acetaminophen melts on the top surface of the alumina maintained at 180°C and fills the pores. The hot substrates are then removed from the oven, cooled to room temperature, and cleaned with a scalpel to remove the acetaminophen on the top surface. The supporting aluminum layer at the bottom of the substrate was partially removed by chemical etching. For the DSC measurements removal of the bottom aluminum layer is important step to have better signal from the tiny amount of sample in the pores. After chemical etching the small pieces of the sample with a size of about 2 mm × 2 mm are encapsulated in the 10 μ l hermitically sealed pans for DSC measurements.

Chapter 5

Amorphous acetaminophen

In the recent years, amorphous pharmaceutical drugs [81–83] including acetaminophen have been of prime interest. Amorphous formulation of acetaminophen like any other pharmaceutical, has the advantages of enhanced solubility and bio-availability when compared to a well ordered crystalline state. These advantages of amorphous state are due to higher mobility of the individual molecules. Amorphous solids in the glassy state can be described as a frozen liquid having a structure which corresponds basically to that of the liquid at the glass transition temperature (T_g). All the glasses are in a state of non-equilibrium and try to reach the equilibrium liquid state at $T < T_g$, a phenomenon well known as physical aging [84, 85]. This process in the disordered material leads to densification [86] of the system affecting the dynamics [84]. In particular it leads to an increase in the α relaxation time. This shows that there is remaining mobility in the solid state. In addition localised motions known as secondary relaxation β or Johari - Goldstein modes occur below the glass transition (T_g). What is discussed so far are equilibration effects in glassy solids which are not crystallisable. For crystallisable substances however, the crystalline state is preferred due to lower free energy when compared to equilibrium liquid at any temperature below the melting point. Even below the glass transition temperature the remaining mobility can be sufficient enough to crystallise the system over a long period of time [87–89]. This is a major problem for pharmaceutical applications, since the life time of the amorphous state must be longer than the typical shelf life of the product in order to serve its purpose. This is usually not the case.

To understand the details, the crystallisation of quenched bulk acetaminophen is investigated close to T_g . The experimental results will be presented in section 5.1. It will be shown that dielectric spectroscopy is a powerful tool to study not only the relaxation behaviour but, also crystallisation kinetics and that the results are consistent with results from conventional DSC

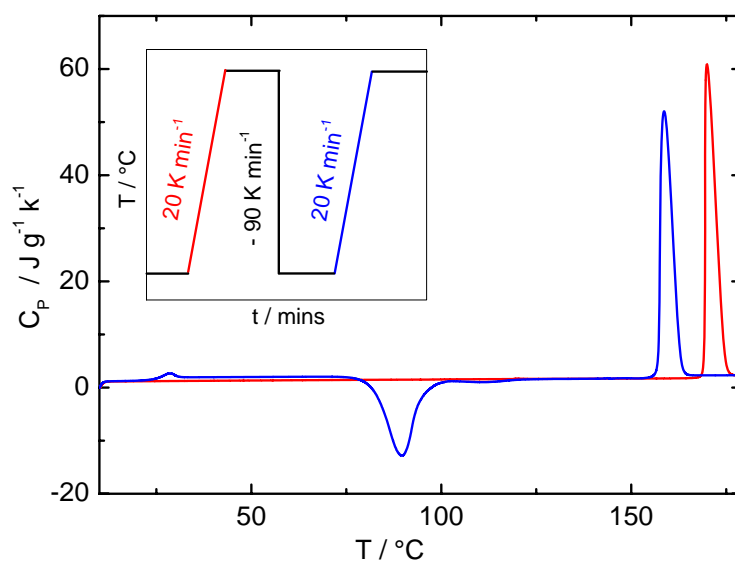


Figure 5.1: DSC heating scan performed on as received and quenched bulk acetaminophen showing endothermic peaks corresponding the melting of form I (red curve) and II (blue curve) respectively. The second heating scan (blue curve) shows in addition a glass transition at 24 $^{\circ}\text{C}$ and a exothermic crystallisation near 80 $^{\circ}\text{C}$. Inset: Thermal program used for the heating scans.

measurements on similarly prepared bulk samples. In section 5.2 it will be demonstrated that nanoconfinement is an interesting method to prevent the crystallisation of acetaminophen and to stabilise its amorphous state.

5.1 Bulk acetaminophen

As a first step standard DSC experiments have been performed in order to characterise calorimetric properties and crystallisation behaviour of bulk acetaminophen. The first heating run on as received sample is shown in figure 5.1, where melting of crystals of form I of acetaminophen around 169 $^{\circ}\text{C}$ is seen. There is no exothermic crystallisation peak observed in the heating run indicating that the sample is completely crystalline before the heating scan. A second heating scan after quenching the sample (figure (5.2)) shows typical features of initially amorphous but crystallisable sample. Obviously cooling rates of about -90 K min^{-1} are sufficient enough to prevent crystallisation of molten acetaminophen completely. During the heating scan one first observes the thermal glass transition at $T_g \approx 24^{\circ}\text{C}$. The calorimetric relaxation strength for completely amorphous acetaminophen was found to be $\Delta C_p \approx 0.7 \text{ J g}^{-1} \text{ K}^{-1}$ (see also figure(5.3)). Upon further heating the liquid acetaminophen cold crystallises around 60-90 $^{\circ}\text{C}$ seen as a exothermic dip in the DSC scan. Parallel polari-

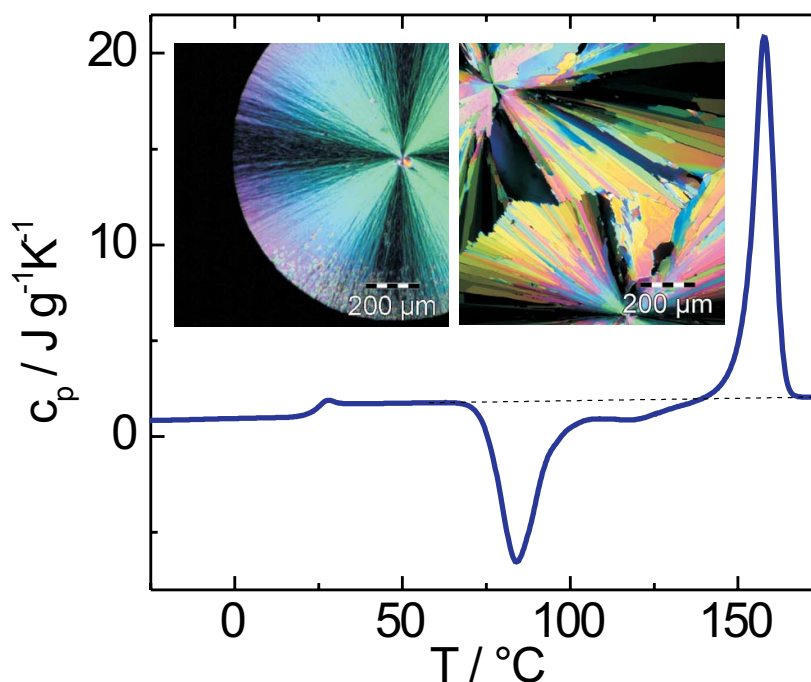


Figure 5.2: DSC scan performed at 10 K min^{-1} on a completely amorphous acetaminophen after melt quenching. The dashed line indicates the interpolated C_P of liquid. The insets show the spherulite grown from a ultra viscous liquid at $T_c = 40^\circ\text{C}$ on the left and after transformation at $T \approx 120^\circ\text{C}$ on the right.

sation microscopy experiments on acetaminophen revealed that few large spherulites grow in a highly viscous environment as shown in the insert of figure 5.2. This finding is consistent with others for acetaminophen [72] and other small molecular organic liquids [90]. Further heating in the DSC scan leads to a small dip around 120°C which may indicate a solid-solid transition. At similar temperatures a transition is seen in the polarization microscopy experiments where, the spherulites change to large flat crystals around 120°C (right insert of figure 5.2). Further heating leads to melting of the crystals seen as endothermic peak with the maximum around 157°C . This value is in well agreement with the melting temperature of form II crystals reported in the literature. Note, that the acetaminophen samples (15 mg) are for DSC measurements are filled in a Hyper DSC aluminium foil before encapsulated in a $30 \mu\text{l}$ closed pan in order to avoid droplet formation.

Isothermal crystallisation kinetics of initially amorphous acetaminophen produced by rapid melt quenching was investigated for different temperatures in the range $48^\circ\text{C} < T_c < 60^\circ\text{C}$. In the temperature range chosen, acetaminophen shows a strong tendency to cold crystallise even during the heating scan (figure 5.2). The isothermally achieved degree of crystallinity

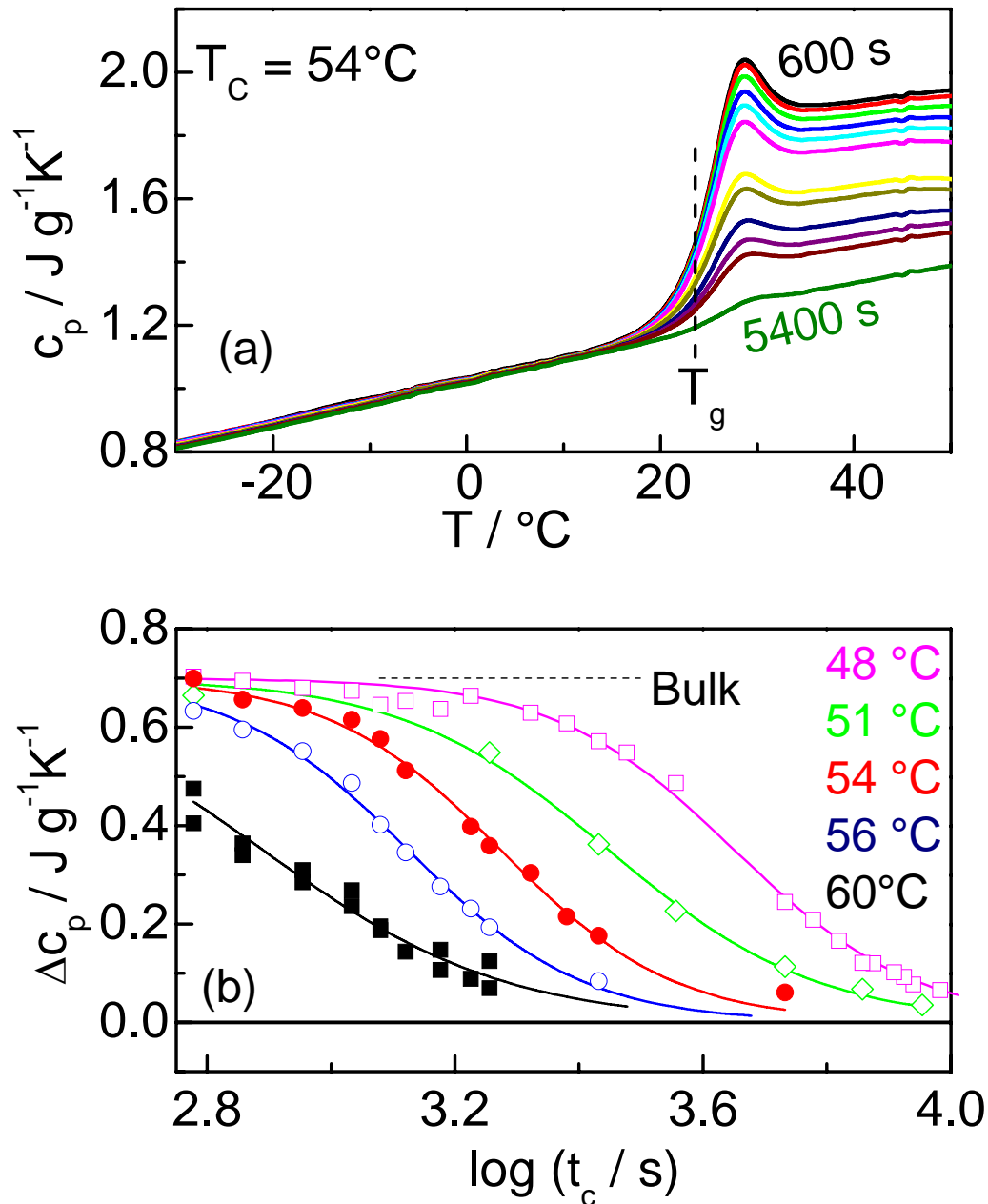


Figure 5.3: (a) Thermal glass transition step in a heating scan measured after isothermal crystallisation for and subsequent cooling to -40°C . $t_c = 600, 780, 900, 1080, 1200, 1320, 1680, 1800, 2100, 2400, 2700, 5400$ secs, (from top to bottom). (b) The time dependence of the calorimetric step height ΔC_P measured after isothermal crystallisation at different crystallisation temperatures T_c

cannot be estimated from the enthalpy of melting (ΔH_m) in a subsequent heating scan since further crystallisation would occur during heating. On the other hand the degree of crys-

tallinity can be determined assuming a simple two phase model from the strength of glass step (ΔC_P) if the samples are cooled to -40°C and reheated after the isothermal crystallisation at different temperatures. Since the glass step height is proportional to the amorphous fraction of acetaminophen, the degree of crystallinity can be then estimated using the relationship

$$D_c = 1 - \frac{\Delta C_P(t_c)}{\Delta C_{P,0}} \quad (5.1)$$

where $\Delta C_P(t_c)$ is the height of the glass transition measured after isothermally crystallising the sample for t_c seconds and $\Delta C_{P,0}$ ($= 0.7 \text{ Jg}^{-1}\text{K}^{-1}$) is the step height of the glass transition of 100 % amorphous acetaminophen.

Thermal glass transition step measured after isothermal crystallisation at 54°C for different times (t_c) are shown in figure 5.3 (a). Since the sample crystallises with time, the amorphous content decreases systematically seen as a reduction in the step height of the glass transition. The dependence of ΔC_P on the isothermal crystallisation time (t_c) is shown in figure 5.3 (b). From these curves one can estimate the half times τ_c corresponding to the time where the strength of the glass step reaches 50 % of the initial value $\Delta C_{P,0}$, i.e., 50 % of the sample is crystalline. As seen in figure 5.3 (b) the half time decreases with the increase in isothermal crystallisation temperature indicating that, the temperature dependence of crystallisation is dominated by that of the mobility. Similar conclusions can be drawn from isothermal crystallisation experiments using dielectric spectroscopy as discussed below.

Dielectric spectra for nearly 100 % amorphous acetaminophen quenched from 180°C to liquid nitrogen temperature with a rate of -100 Kmin^{-1} are shown in figure 5.4. Dielectric isotherms are measured starting from -120°C much below the T_g . At such low temperatures the existence of a secondary relaxation also known as Johari-Goldstein process (β) is indicated by a broad peak in $\Delta\varepsilon''$ having a weak dielectric relaxation strength ($\Delta\varepsilon_\beta < 0.2$) (figure 5.4 (b)). Such secondary relaxations are a common finding for many organic glass forming liquids [91, 92]. The temperature dependence of the secondary relaxation β is well described by the Arrhenius equation (3.17). The estimated values are $A = 10^{12} \text{ rad s}^{-1}$ for the pre factor and, $E_A = 20 \text{ kJ mol}^{-1}$ for the activation energy.

The isothermal measurements above $T_g = 24^\circ\text{C}$ in steps of 4 K shows a prominent α peak in the imaginary part of the dielectric function $\varepsilon''(\omega)$ and a corresponding step-like feature in the real part $\varepsilon'(\omega)$. In addition contributions due to the DC conductivity are observed in the

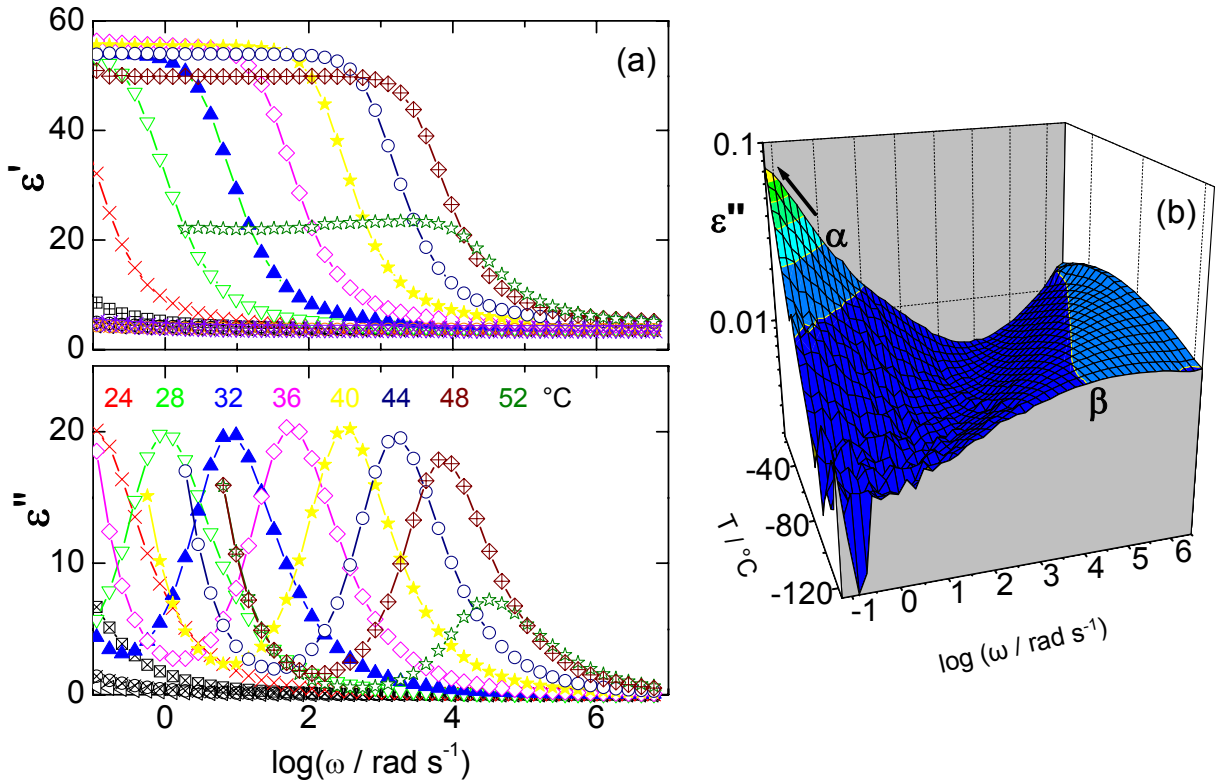


Figure 5.4: (a) Dielectric isothermal spectra for amorphous acetaminophen measured in the temperature range 12-60 °C in steps of 4 °C. (b) Two-dimensional plot of dielectric loss (ϵ'') versus temperature and logarithm frequency for the β processes in the glassy state.

imaginary part of the dielectric function at low frequencies. The strength of the α relaxation remains constant until 48 °C ($\Delta\epsilon_\alpha \approx 53 \pm 3$). For temperatures above 48 °C, the intensity of the relaxation goes down continuously, due to the beginning of the crystallisation during stepwise heating. The α relaxation is due to re-orientation of dipoles. When the system crystallises the number of dipoles contributing to the α process decreases leading to the reduction in the relaxation strength ($\Delta\epsilon_\alpha$). For temperatures above 56 °C, acetaminophen is completely crystalline and no significant α relaxation is observed. When the peak maxima are plotted against inverse temperature also known as Arrhenius plot, one obtains the temperature dependence of the α relaxation well described by Vogel-Fulcher-Tammann (VFT) equation 3.16 [93]. The VFT parameters obtained from a free fit are $\Omega = 10^{20.3} \text{ rad s}^{-1}$ for the limiting frequency for $T \rightarrow \infty$, $B = 1670 \text{ K}$ for the curvature of the α relaxation trace, and $T_\infty = 220 \text{ K}$ for the Vogel temperature.

Based on the above parameters it is possible to estimate the $\alpha\beta$ crossover where α and the β

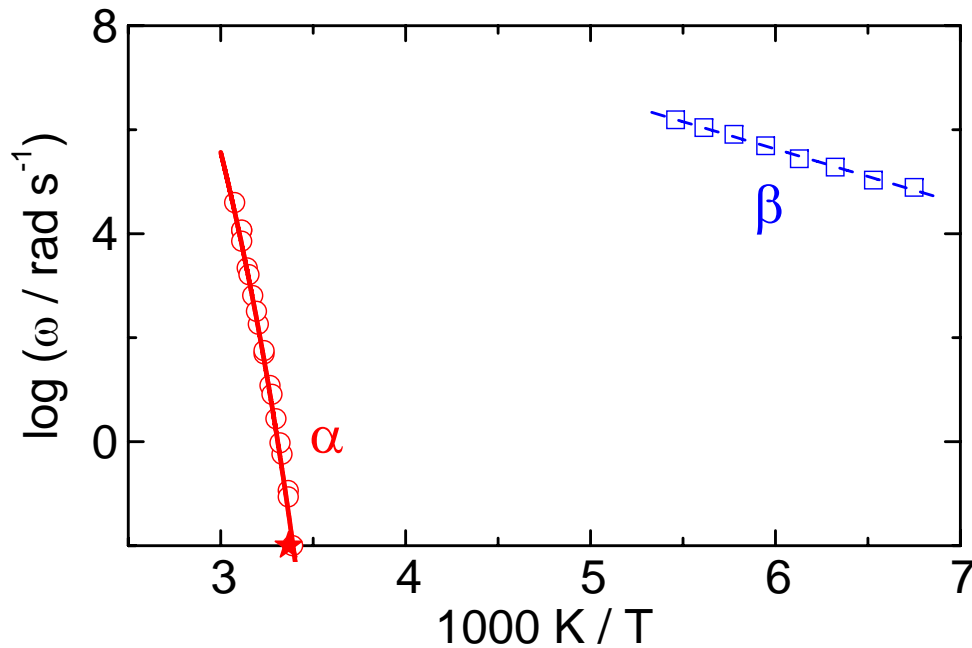


Figure 5.5: Arrhenius plot for α and β processes for acetaminophen. The solid red line is the free VFT fit for the α relaxation and the dashed line is the Arrhenius fit for the β process. The star indicates the DSC glass transition T_g identified with relaxation time of $\tau_\alpha = \omega_\alpha^{-1} = 100s$.

traces should merge. It was found in the GHz range corresponding to a Donth temperature of $T_{\alpha\beta} = 150 \pm 20$ °C. It has been reported for many glass forming liquids that in this region many properties of the dynamic glass transition α and the VFT parameters change. Apart from such effects [94–96] changes in the crystallisation kinetics has been reported.

In order to follow the crystallisation kinetics of acetaminophen, isothermal measurements on melt quenched samples were performed at temperatures T_c between 60 °C and 22 °C. As a representative example isothermal measurements at 46 °C are shown in the figure 5.6. As seen in the figure 5.6, the α relaxation strength corresponding to the step height in the real part of the dielectric function $\varepsilon'(\omega)$ decreases systematically with the increase in the crystallisation time (t_c). The same trend is observed in the imaginary part $\varepsilon''(\omega)$ of the dielectric function. Since the number of dipoles contributing to the α relaxation is proportional to the fraction of amorphous material, the dielectric strength can be used to estimate the degree of crystallinity using the relationship

$$D_c = 1 - \frac{\Delta\varepsilon_\alpha(t_c)}{\Delta\varepsilon_{\alpha,0}} \quad (5.2)$$

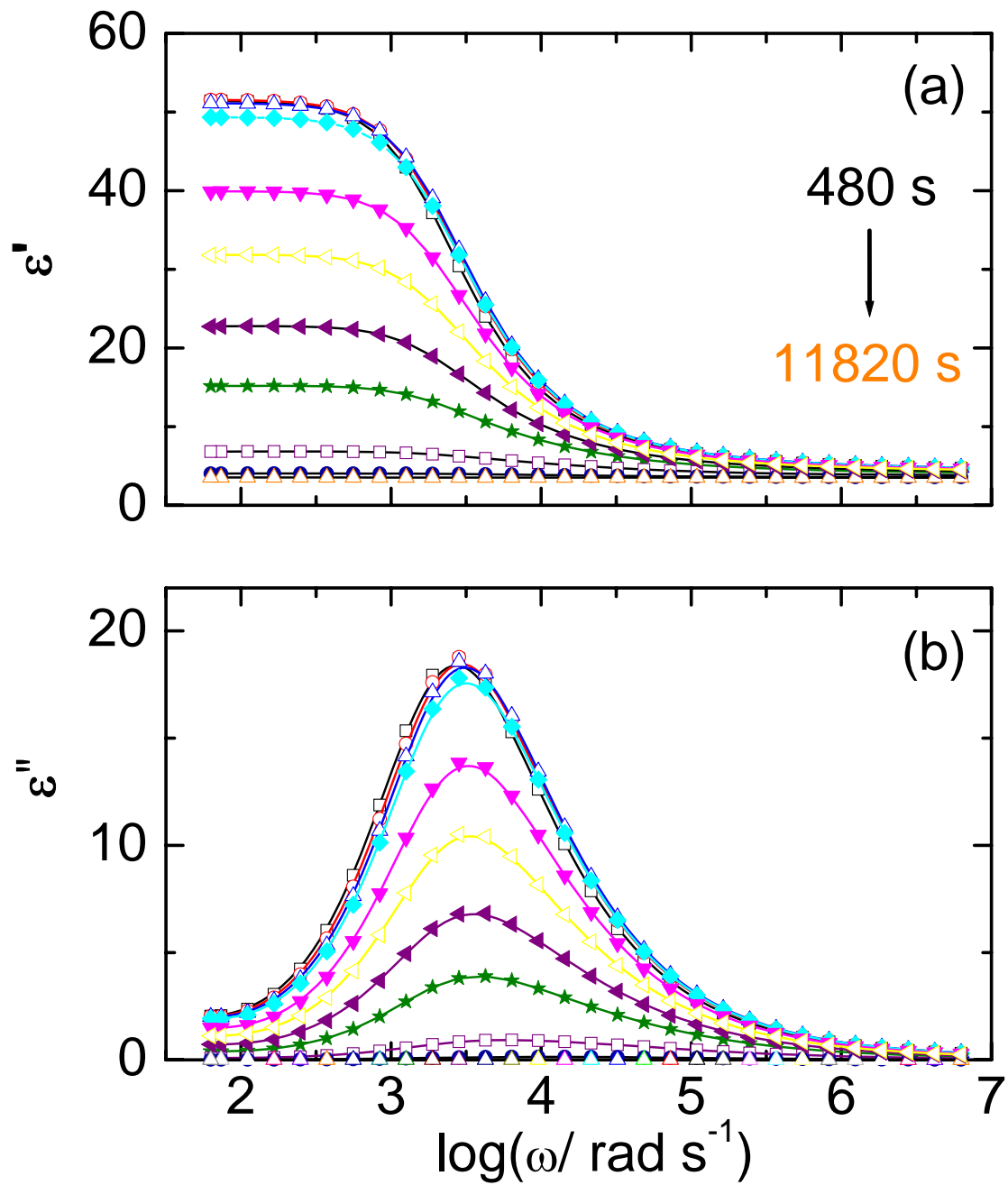


Figure 5.6: (a) Real (ϵ') and (b) imaginary (ϵ'') dielectric function measured during isothermal crystallisation at $T_c=46$ °C.

where $\Delta\epsilon_{\alpha,0}$ is the dielectric α relaxation strength of completely amorphous acetaminophen. It can be clearly seen in figure (5.6(b)) that, there is no significant change neither in the shape nor in the position of the peak, although the peak intensity in the imaginary part of dielectric function $\epsilon''(\omega)$ decreases with the increasing crystallisation time (t_c). Only when the system

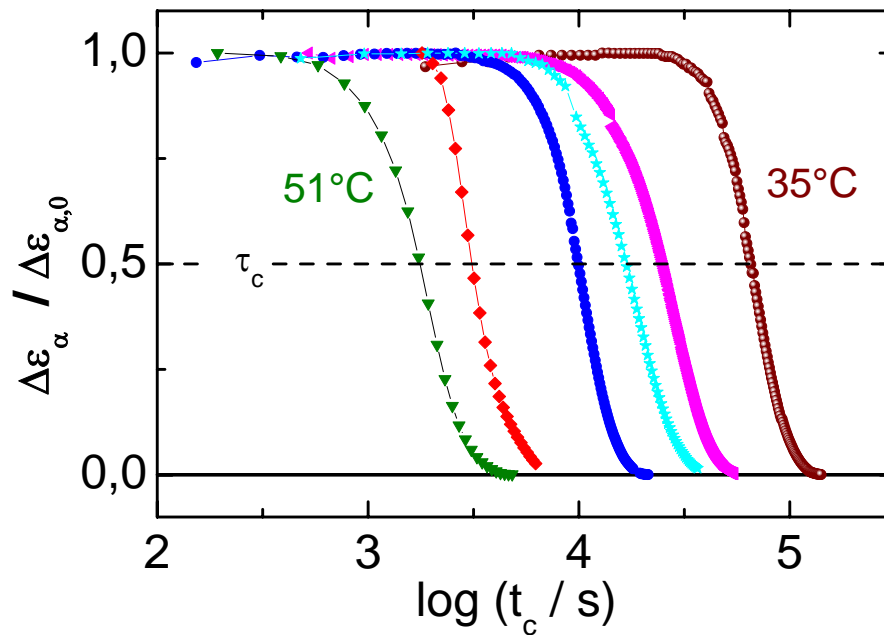


Figure 5.7: Time dependence of the normalised α relaxation strength ($\Delta\varepsilon_\alpha/\Delta\varepsilon_{\alpha,0}$) measured during isothermal crystallisation ($T_c = 51, 48, 46, 40, 38, 35$ °C).

reaches high degrees of crystallinity ($D_c > 90\%$), small changes in peak position and shape are observed. The situation can be well described by a two phase model considering only amorphous and crystalline phase without additional phases such as rigid amorphous phase as discussed for semi-crystalline polymers [97, 98]. The small changes in the α relaxation at higher crystallinity values D_c , can be due to small fraction of amorphous acetaminophen entrapped between the large crystalline spherulites as seen in figure 5.2.

The normalised α relaxation strength ($\Delta\varepsilon_\alpha/\Delta\varepsilon_{\alpha,0}$) from isothermal crystallisation measurements at different temperatures is plotted versus log crystallisation time in figure 5.7. From such a plot the half times (τ_c) can be estimated corresponding to the time where the dielectric strength ($\Delta\varepsilon_\alpha(t_c)$) of the α relaxation reaches 50 % of the initial value $\Delta\varepsilon_{\alpha,0}$ for the amorphous sample. It can be clearly seen from the figure 5.7 that, the half times (τ_c) increases with the decreasing temperature. This shows that the mobility dominates the nucleation rate in the temperature range where isothermal measurements were performed. To parameterise the crystallisation kinetics the Avrami equation

$$X = 1 - \exp(-k t_c^n) \quad (5.3)$$

can be used. Where X is the normalised degree of crystallinity, k the rate constant and n the Avrami exponent. Using the data from dielectric experiments on acetaminophen the Avrami exponent n was estimated to be 3.5 indicating that the crystalline growth is three dimensional [99].

A comparison of half times (τ_c) from dielectric and differential scanning calorimetry is shown in the figure 5.8. The half times from both dielectric and DSC experiments are obviously identical for a given crystallisation temperature T_c . As expected the τ_c value increases non linearly with the decreasing crystallisation temperature due to reduced mobility at low temperatures. It can also be seen from figure 5.8, that the temperature dependence of the half times is less steep than that of the α relaxation time. The stronger temperature dependence of the α relaxation time indicates that the nucleation rate is enhanced at low temperatures like sketched in figure 2.3. Both the dielectric and Differential Scanning Calorimetry experimental techniques give identical information about the crystallisation kinetics, but dielectric measurements allow to monitor changes during the overall crystallisation process.

5.2 Acetaminophen in nanopores

Amorphous state is favoured for pharmaceutical application due to its better solubility and bio-availability. However the tendency of the amorphous pharmaceutical drugs to crystallise during the storage is an issue in the pharmaceutical industry. As a consequence control release of the drug becomes impossible. To prevent the transformation to crystalline state, in the following section it will be shown that the amorphous state of the drug can be preserved for longer periods of times by confining it in a nanoporous host system.

Figure 5.9 provides information about the crystallisation kinetics of acetaminophen filled in controlled porous glass with a diameter of 103 nm. The samples were crystallised isothermally at temperature T_c for a specific time t_c . Isothermal crystallisation temperature was approached from the glassy state obtained by quenching the molten acetaminophen initially held at 180 °C to -40 °C with a cooling rate of -100 K min⁻¹ in the DSC instrument. The degree of crystallinity D_C used in figure 5.9 is estimated by measuring ΔC_p of the glass transition after the isothermal crystallisation step.

Like in the case of bulk acetaminophen the crystallisation is faster at higher crystallisation temperature T_c showing indications for the mobility dominating crystallisation kinetics of acetaminophen in the nanoporous media. To compare the changes in the crystallisation ki-

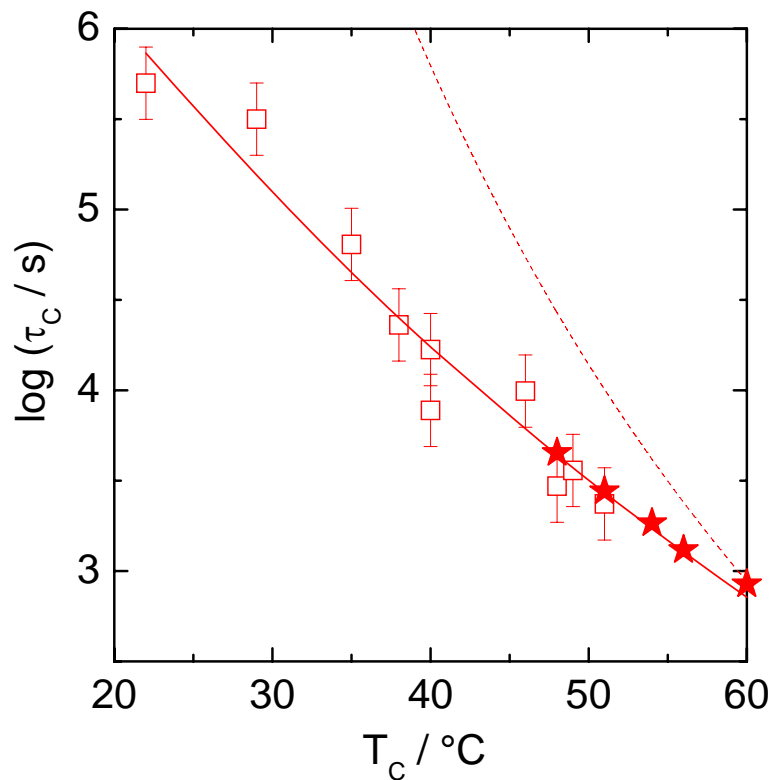


Figure 5.8: Half times τ_c as obtained from dielectric (\square) and calorimetric (\star) crystallization experiments at different temperatures T_c . The solid line is a guide to the eye. The temperature dependence of the α relaxation time (taken from figure 5.5) is indicated by the thin dashed line corresponding to $\log(\omega_\alpha(60^\circ\text{C})\tau_c(60^\circ\text{C})/\omega_\alpha(T))$.

netics of acetaminophen confined to porous glass (having a diameter of 103 nm) with the bulk, the half time (τ_c) of both the cases are plotted for different temperatures in figure 5.9 (b). Although the temperature dependence of τ_c in pores is comparable to the bulk situation, one can clearly see that the crystallisation in the interconnected 103 nm pores is slowed down by almost 5 times. The transformation interval in the isotherms shown in figure 5.9 (a) is only slightly broader than that for bulk. This can be parameterised in terms of an Avrami exponent n having a value of 1.5 for $T_c = 70^\circ\text{C}$ and 2.5 for $T_c = 50^\circ\text{C}$ compared to $n = 3.5$ for bulk acetaminophen as estimated in the previous section. The smaller Avrami exponent n for acetaminophen in porous media may be due to the changes in the growth mechanism. Since the crystals must occupy pores having a sponge like morphology (there is no ordinary three - dimensional growth like in the bulk).

Strong confinement effects are observed for acetaminophen confined to CPGs with 10 nm

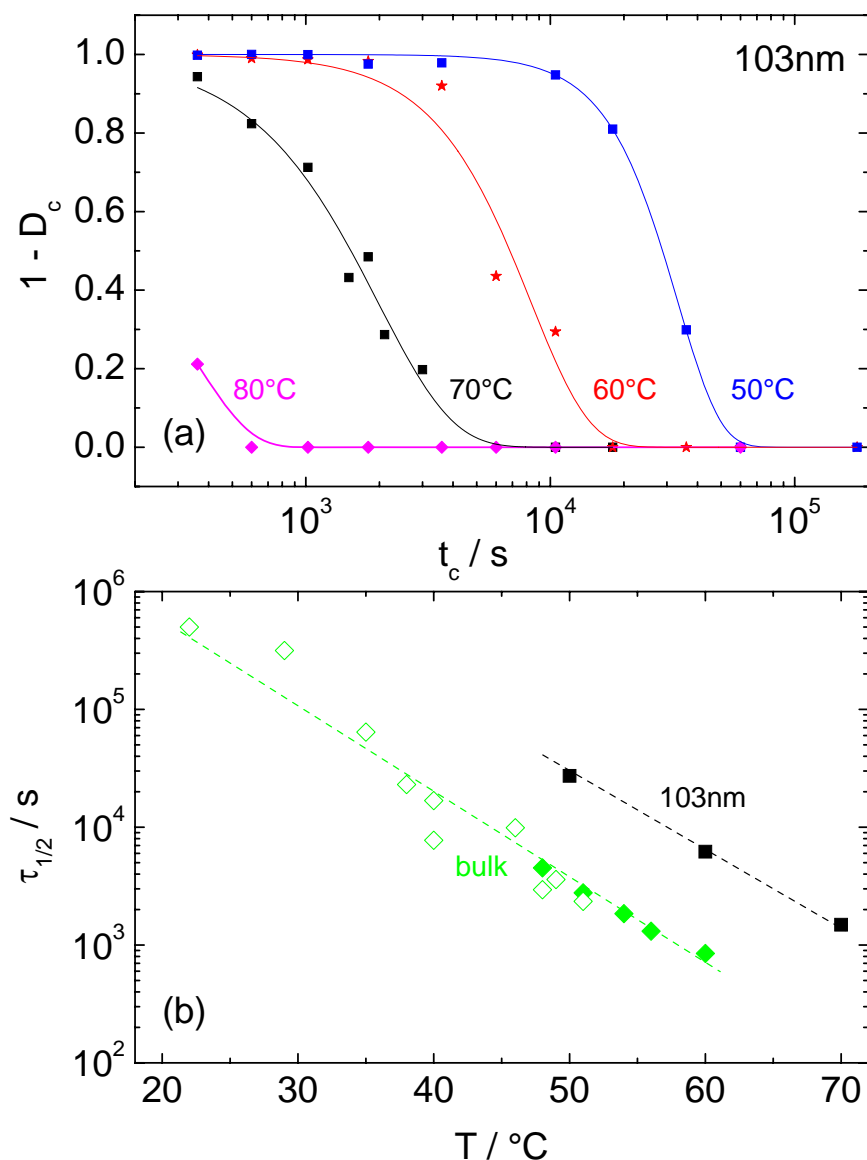


Figure 5.9: (a) Crystallisation kinetics of acetaminophen in CPG having an average pre diameter of 103 nm. The solid lines are fits using Avrami equation. (b) Temperature- dependent half times τ_c for acetaminophen in bulk and confined to 103 nm CPG. Data for acetaminophen in 103 nm pores (■) taken from part (a), for bulk acetaminophen from dielectric spectroscopy(◇) and DSC(◆).

pore diameter. The corresponding DSC curves are shown in figure 5.10. The first heating scan performed after the preparation step shows a significant melting peak. Crystallisation of acetaminophen occurs during the preparation in the presence of thick surface layer. It will be shown in section 6.1 that the melting peak around 130 °C corresponds to form I of acetaminophen in 10 nm pores. The small peak around 160 °C might be a small fraction of

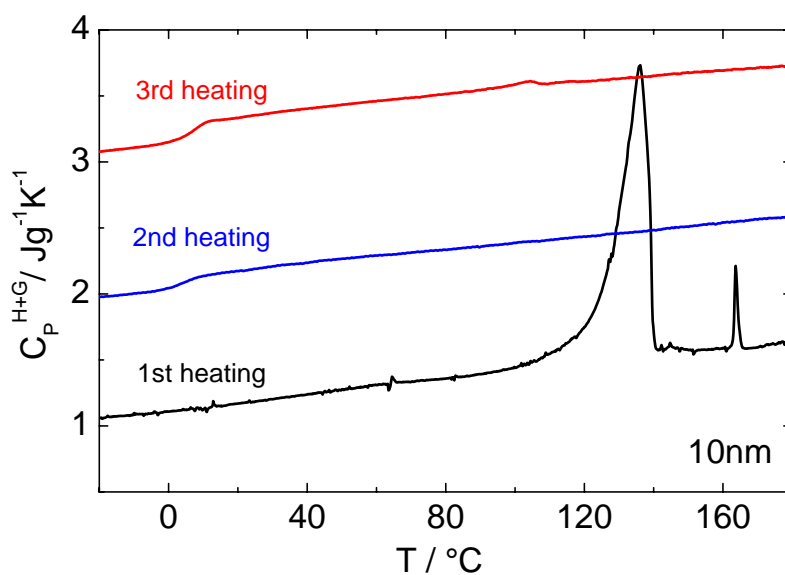


Figure 5.10: DSC heating scans (10 K min^{-1}) for acetaminophen infiltrated in 10 nm CPG. The curves are shifted by $1 \text{ J g}^{-1} \text{ K}^{-1}$. The heating scans were performed after using the thermal program described in the text.

acetaminophen on the surface of the CPG. The second heating scan measured after quenching the sample from $180 \text{ }^\circ\text{C}$ to $-40 \text{ }^\circ\text{C}$ with a rate of -100 K min^{-1} does not show any crystal melting, but only a glass step around $10 \text{ }^\circ\text{C}$. The third heating scan performed after isothermal crystallisation at $T_c = 80 \text{ }^\circ\text{C}$ for 2 hours indicates a similar behaviour and a clear glass transition is seen around $10 \text{ }^\circ\text{C}$. The absence of melting peaks upon further heating shows that the sample is still completely amorphous. Melting of form I acetaminophen is only seen in the first heating scan, i.e. in a sample where crystallisation occurs in the acetaminophen surface layer during the sample preparation step. Only in the presence of crystalline acetaminophen on the CPG surface crystallisation occurred in the pores.

When acetaminophen is filled in controlled porous glass having pore diameters smaller than 10 nm further changes in the crystallisation behaviour are observed. The heating scans of acetaminophen infiltrated in 4.6 nm CPG are shown in figure 5.11. The first heating scan shows a broad glass transition in the temperature range 10 to $40 \text{ }^\circ\text{C}$ but no indication for a melting peak. The second heating scan after quenching with -90 K min^{-1} looks similar and shows a glass transition step but no melting peak. The third heating scan measured after isothermal crystallisation at $35 \text{ }^\circ\text{C}$ for 2 hours (refer 5.11) and fourth after 10 days (figure 5.12 (a)) also does not show any indication for a melting peak. Similar behaviour was observed after storing the sample at $35 \text{ }^\circ\text{C}$ after 18 months (data not shown). The crystallisation

temperature was chosen as 35 °C since, it should be the most efficient crystallisation temperature for acetaminophen in 4.6 nm CPG. The crystals should melt around 50-60°C in 4.6 nm according to the Gibbs-Thompson plot which as presented later in the later section 6.1. Crystallisation of acetaminophen below the glass transition too seems to be unlikely due to depressed mobility. Calorimetric experimental results for acetaminophen filled in 4.6 nm porous glass clearly show that the crystallisation is completely suppressed for significant periods of time.

Note that the glass transition for acetaminophen filled in 4.6 nm CPG is broader compared to that in the bulk samples. This might be due to changes in the density and spatial inhomogeneous mobility of the acetaminophen molecules. It is known that acetaminophen can form

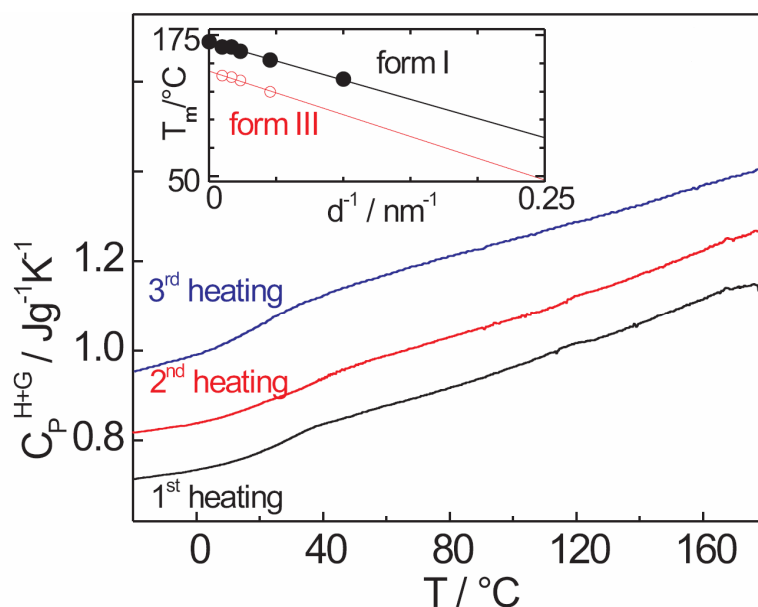


Figure 5.11: DSC heating scan for acetaminophen infiltrated in 4 nm CPG. Inset: Melting temperature T_m vs. inverse pore diameter $1/d$ for I and III crystalline forms of acetaminophen. The lines are fits to Gibbs-Thompson equation for cylindrical pores. The curves are shifted by $0.1 \text{ J g}^{-1} \text{ K}^{-1}$. The heating scans were performed after using the thermal program described in the text.

hydrogen bonds. This may lead to the formation of an immobilised surface layer close to the hydrophilic pore walls having a thickness of few molecules of acetaminophen. Similar behaviour was also observed for several other organic molecules like water [100], glycerol and salol [58] capable of forming hydrogen bonds, when confined to similar nanoporous host systems. These attributed to the formation of immobilised surface layer having a thickness of about 0.4 - 1 nm thickness. Calorimetric measurements on commercial Vycor porous glasses with a pore diameter of 4 nm showed more pronounced indications for such a two phase be-

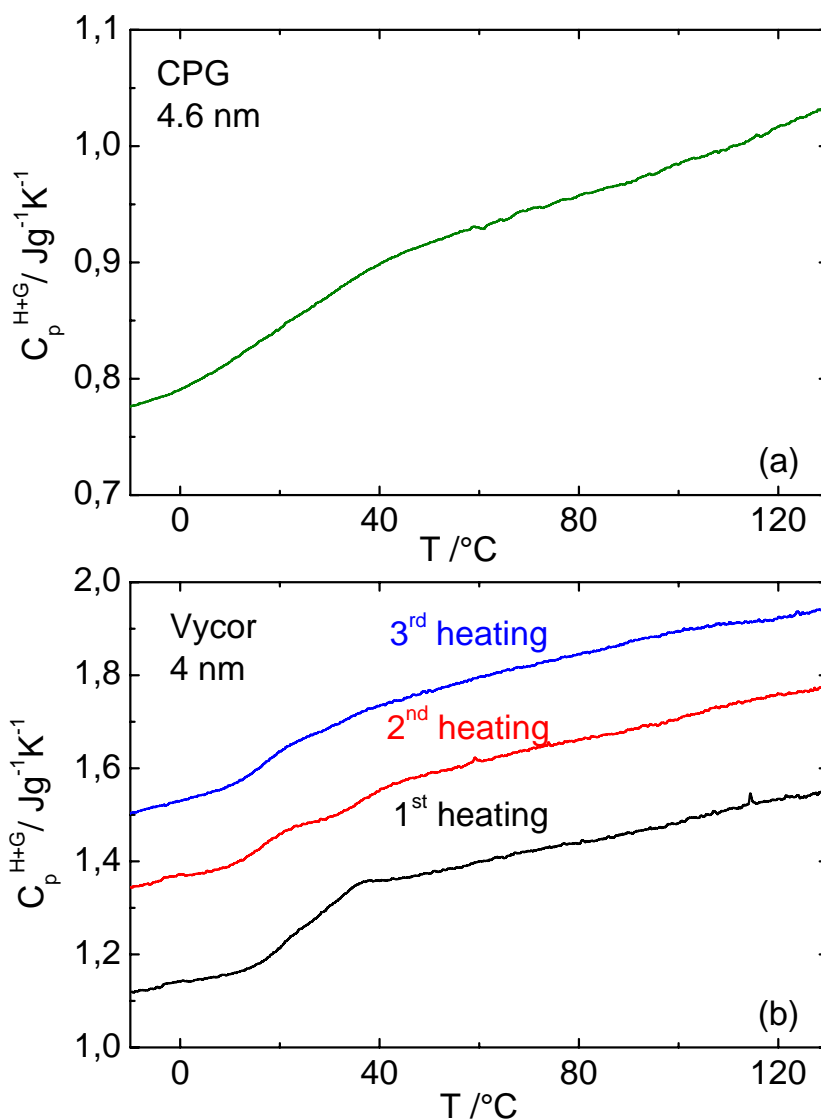


Figure 5.12: (a) DSC heating scan for acetaminophen infiltrated in 4.6 nm CPG measured after melt quenching and isothermal crystallisation at 35°C for 10 days and (b) DSC heating scans for acetaminophen infiltrated in commercial Vycor porous glass 7930 with 4 nm pores indicating the absence of crystalline fraction and two distinct glass transitions. The curves are vertically shifted by 0.2 $\text{Jg}^{-1}\text{K}^{-1}$ for the sake of clarity (1st - after the preparation; 2nd - heating after cooling with -100 Kmin^{-1} ; 3rd heating - after isothermal annealing at 35 °C for 2hrs).

haviour. A two step feature is seen instead of a broad glass transition as shown in figure 5.12 (b). It can also be said that the packing of amorphous acetaminophen in the smaller pores is very sensitive to the nature of the walls of the host system under investigation. However, in accordance with the results for CPGs with 4.6 nm pores crystallisation of acetaminophen infiltrated in commercial Vycor glass was never observed.

From the experimental results presented above it can be inferred that nano confinement effects can be exploited to stabilise amorphous drugs. Thermodynamic effects as well as changes in the nucleation mechanism and molecular mobility can result in improved life time of amorphous drugs in nanopores. This will be presented in detail in section 7.1.

Chapter 6

Polymorphic acetaminophen under Nano-confinement

More than 80 % of the pharmaceuticals exhibit polymorphism [18]. Acetaminophen is no exception to this and two different crystalline forms (monoclinic form I melting around 169 °C and orthorhombic form II melting around 157 °C) are well investigated. Different approaches were reported to produce these two forms either from melt or from solution [71, 82, 101, 102]. A third polymorph form III of acetaminophen, which is unstable in bulk was also reported under special conditions, i.e. confined between thin glass plates or in glass capillaries [72, 73, 101]. Previous studies indicated that from III is a transient form in bulk. A solid - solid conversion from the transient form III to II was discussed, based on the transformation of spherulites to small stacked platelets observed in the light microscope around 120 °C [72] and might be indicated by a small dip in the DSC heating scans (figure 5.2) around the same temperature.

Limited information regarding the physical properties of metastable form III exists from the X-ray scattering [73] and RAMAN spectroscopy [72] measurements. The bulk melting temperature and other thermodynamic parameters of the metastable form III was not known since a direct method was not reported to produce significant amount of form III so far. Since metastable crystalline forms have better solubility and bio-availability there is huge interest to stabilise them [2].

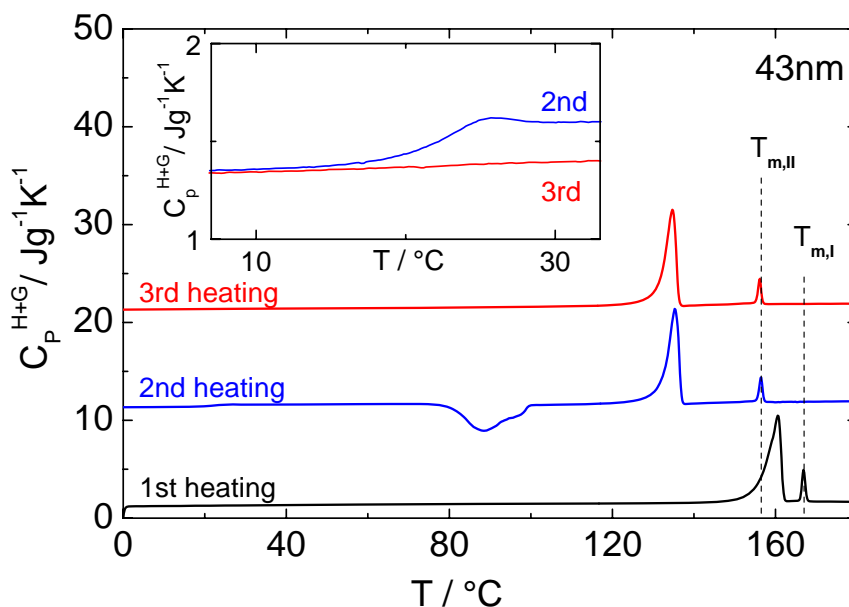


Figure 6.1: DSC heating scans for acetaminophen infiltrated in CPG having an average pore diameter of 43nm. First heating scan is performed after removing the surface layer from the sample preparation step. Second heating after quenching and third heating after quenching and isothermal crystallisation at 80°C for 2 hrs. The curves are shifted vertically by 10 J g⁻¹K⁻¹ for the sake of clarity. The insert shows a zoom around glass transition region. Heat capacities of host-guest (C_p^{H+G}) system are plotted. The bulk melting temperatures of form I ($T_{m,I}^\infty = 167^\circ\text{C}$) and form II ($T_{m,II}^\infty = 156^\circ\text{C}$) are indicated by dotted vertical lines

6.1 Melting of form III acetaminophen in CPGs

In this chapter it will be shown that controlled porous glasses having pore diameters in the range 20 - 100 nm can be used to produce and stabilise form III of acetaminophen. This allows to determine thermodynamic parameters of form III which were unknown so far. Differential scanning calorimetry and wide angle X-ray scattering (WAXS) measurements were used to characterise metastable form III of acetaminophen.

DSC heating scans for acetaminophen filled in 43 nm CPG after different thermal treatment is shown in figure 6.1. The first heating scan of acetaminophen in 43 nm pores crystallised during the sample preparation step in presence of a bulk acetaminophen surface layer shows a major melting peak around 160 °C. This melting peak is assigned to melting of monoclinic form I of acetaminophen. As seen in figure 6.1, there is no indication for cold crystallisation showing that the sample crystallised completely during cooling to room temperature in the sample preparation step. The additional melting peak having a very small intensity seen in the first heating scan around 167 °C indicates the melting a small fraction of acetaminophen

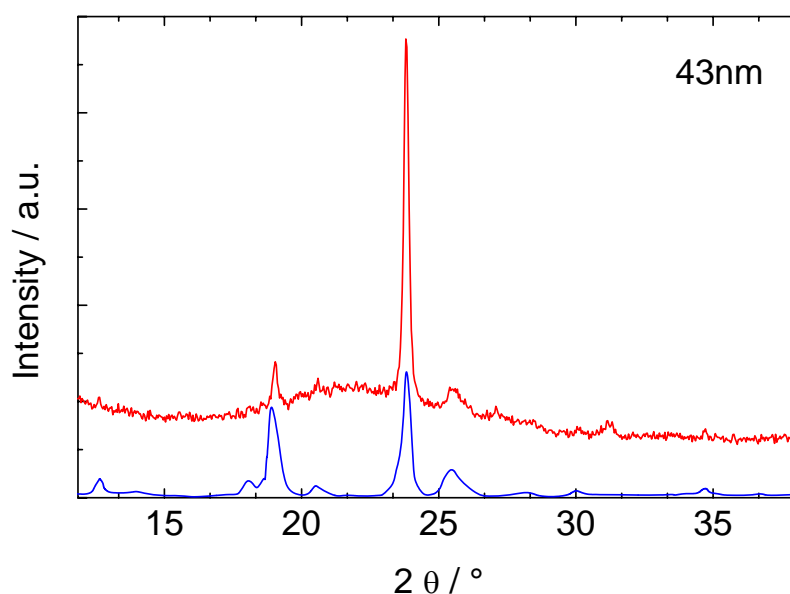


Figure 6.2: Wide angle X-ray scattering curves for acetaminophen infiltrated in 43nm CPG measured at room temperature. The red curve is measured after isothermally crystallising in the DSC instrument at 80 °C for 2 hours equivalent to third heating in the DSC heating scans. The broad halo is attributed to the amorphous porous glass. The blue curve corresponds to data reported by Peterson *et al.* [73] for form III acetaminophen. The curves are vertically shifted for the sake of clarity.

form I remaining on the top surface of the filled CPG after cleaning. The second heating scan in figure 6.1 shows that the sample is nearly 100 % amorphous after quenching the sample rapidly from 180 °C to -40 °C in the DSC instrument with a nominal rate of -200 K min⁻¹. This is confirmed by the glass transition step around 24 °C (insert figure 6.1) similar to that of bulk acetaminophen and a significant cold crystallisation peak around 80 °C. These cold crystallised acetaminophen melts around 135 °C slightly below the speculative melting of form III (\approx 139 °C) in bulk-like samples as reported by Giordano *et al* [103]. The tiny melting peak at 157 °C corresponds to melting of form II crystals on the surface of the CPG. This behaviour is comparable to melting of form II in the case of bulk acetaminophen reheated from a glassy state (figure 5.1). The third heating scan measured after isothermal crystallisation at 80 °C for 2 hours shows melting of form III as observed in the second heating scan. The absence of cold crystallisation of acetaminophen in 43 nm pores during the third heating scan indicates that the sample has reached 100 % crystallinity during the isothermal step. The WAXS pattern obtained for identically prepared samples is comparable to that one reported by Peterson *et al* [73] for form III of acetaminophen obtained by chance, in thin glass capillaries (figure 6.2).

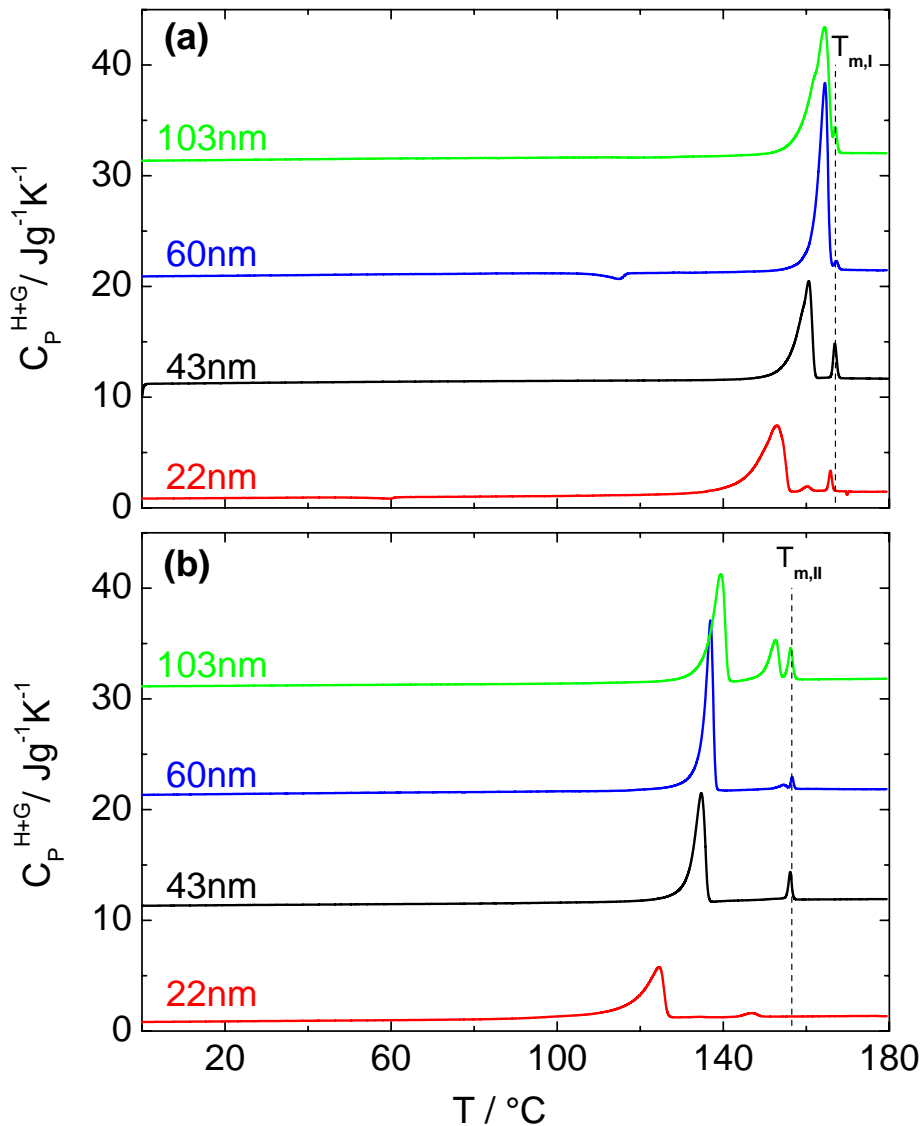


Figure 6.3: DSC heating scans for acetaminophen infiltrated in CPGs having pore diameters in range 22 to 103 nm. (a) first heating scan shows the melting of form I and (d) the third heating scan after isothermal crystallisation for 2 hrs at 80 °C shows melting of form III. The dashed lines in (a) and (b) corresponds to bulk melting temperature of form I ($T_{m,I}^\infty = 167^\circ\text{C}$) and form II ($T_{m,II}^\infty = 156^\circ\text{C}$) respectively.

First and third heating scans on acetaminophen filled to CPGs with different pores diameters are shown in figure 6.3. In the first heating scan, melting of form I is always seen. Depending on the pore diameter the melting point shifts from 165 °C in case of 103 nm to 153 °C for acetaminophen in 22 nm pores (figure 6.3 (a)). It can be seen further in first heating scans that, the additional small melting peaks do not shift with the pore diameter. This observation is consistent with the idea that this peak is only from the small fraction of re-

maining acetaminophen on the surface of the CPGs. The third heating scans (figure 6.3 (b)) measured on samples which are quenched and isothermally crystallised at 80 °C for 2 hours shows melting of form III in all CPGs . The third heating scans show no glass transition and no cold crystallisation peak. The heat of melting is always similar to the values obtained in the second heating scans. The third heating scan too shows shift in the melting point from 140 °C in the case of 103 nm pores to 125 °C for acetaminophen in 22 nm pores. Obviously, form III and form II of acetaminophen do co-exist in 103 nm pores, indicating a transition to bulk like behaviour where melting of form II is observed exclusively when a similar temperature program is used (section 5.1). The additional peak around 152°C corresponds to melting of form II crystals of acetaminophen in 103 nm pores. For all the pore diameters a small melting peak around 156 °C is observed. These small melting peaks correspond to melting of form II crystals of acetaminophen.

Melting peaks of form I in the first heating and form III in the third heating show a reduction in the melting temperature with the decreasing pore diameter in accordance with the Gibbs - Thompson equation, which predicts for cylindrical pores with diameter d

$$T_m^\infty(d) = T_m^\infty - \frac{4 T_m^\infty \sigma_c}{d \Delta H_m^\infty \rho_c} \quad (6.1)$$

where σ_c is the surface tension (most likely between crystal and immobilised liquid like acetaminophen layer at the pore walls, i.e. $\sigma_c = \sigma_{cl}$), ΔH_m^∞ the heat of melting and ρ_c is the density of the crystal in bulk. It is commonly assumed [51, 57] that equation 6.1 describes the melting point depression in CPG having a sponge like morphology reasonably well.

A Gibbs - Thompson plot containing the melting points obtained from the DSC scans as discussed before is shown in figure 6.4. The $T_{m,I}$ values for form I from the first heating scans (black, solid squares) and the $T_{m,III}$ values for form III from the third heating (red solid circles) are plotted. The melting temperatures of form II in pores (blue solid rhombus) are determined from further annealing experiments which will be discussed in detail in section 6.2. The extrapolation of melting temperatures of form I and form II from small diameters to infinitely large crystals ($d \rightarrow \infty$) yields the bulk melting temperatures form I and II as indicated by half filled symbols in figure 6.4. By extrapolating the melting temperature of form III in pores to infinitely large d values the melting temperatures of bulk form III can be estimated. The extrapolated melting temperature of form III is $T_{m,III}^\infty = 143$ °C. The open symbols (circles, diamonds and squares) in figure 6.4 were obtained from DSC measurements performed on acetaminophen filled in porous alumina. The melting point depression

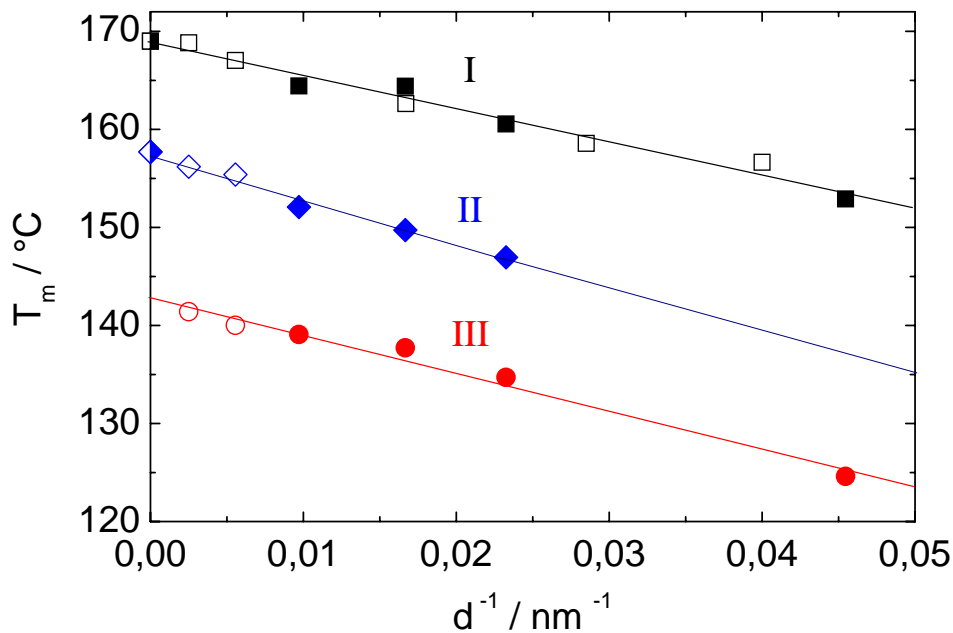


Figure 6.4: Gibbs - Thompson plot for three different forms of acetaminophen showing melting temperature T_m as a function of inverse pore diameter ($1/d$). Solid symbols represent acetaminophen in CPGs and the open symbols correspond to acetaminophen infiltrated in mesoporous alumina and, the half symbols represent the bulk melting temperature T_m^∞ of individual crystalline forms. The solid lines represent linear fits based on equation 6.1.

of acetaminophen in porous alumina and in controlled porous glass is practically identical as shown in figure 6.4. This can be explained based on the fact that the contact angles of acetaminophen melt on alumina ($\theta \approx 27^\circ$) and silica glass ($\theta \approx 20^\circ$) are quite comparable. This indicates that the surface energies for both the host - guest systems are similar. Molten acetaminophen wets both the surfaces quite well. An alternative explanation is that the crystal in both cases is only in contact with an immobilised non - crystallisable acetaminophen layer having a thickness around 1 nm covering the pore walls.

Apart from the bulk melting temperature of form III acetaminophen another thermodynamic parameter which can be estimated is the enthalpy of melting $\Delta H_{m,III}^\infty$ of form III. This can be done in two different ways. The first version involves the use of slopes obtained from figure 6.4, for form I, one gets $s_I \approx 340 \text{ K nm}$ and for form III $s_{III} \approx 386 \text{ K nm}$ using a linear fit. Based on these values and the known enthalpy of melting for form I ($\Delta H_{m,I}^\infty = 186.1 \text{ J g}^{-1}$), the heat of melting of form III can be estimated using the relationship

$$\Delta H_{m,III}^\infty = \frac{\Delta H_{m,I}^\infty T_{m,III}^\infty s_I}{T_{m,I}^\infty s_{III}} \quad (6.2)$$

Table 6.1: Thermodynamic properties of all the three crystalline forms of acetaminophen.

Properties	Form I	Form II	Form III
$s_c (\times 10^{-9} K m)$	340	455	386
$\rho_c (kg m^{-3})$	1297	1336	1302
$\Delta H_m^\infty (\times 10^3 J kg^{-1})$	186	178	165
$T_m^\infty (K)$	442	430	416
$\sigma_c (\times 10^{-2} Jm^{-2})$	4.64	6.29	5.25

Underlying assumption is that the ratio σ_c/ρ_c is identical for both forms I and III. The estimated value of enthalpy of fusion for form III is $\Delta H_{m,III}^\infty = 154 \pm 15 J g^{-1}$ [104]. The second version is based on a comparison of the enthalpy of melting in the first and the third heating scans as shown in figure 6.3. By using the known enthalpy melting of form I in bulk ($\Delta H_{m,I}$) the mass m of acetaminophen in a filled CPG can be estimated using

$$m = \frac{\Delta h_{m,I}}{\Delta H_{m,I}} \quad (6.3)$$

where $\Delta h_{m,I}$ is the enthalpy of melting of form I taken from the first heating scan on host - guest system. Using the mass estimated from equation 6.3 step the enthalpy of melting of form III ($\Delta h_{m,III}$) from the third scan on the same sample, the melting enthalpy of form III ($\Delta H_{m,III}^\infty$) can be estimated. The underlying assumption is that the degree of crystallinity is identical in both scans ($\approx 100\%$ of acetaminophen). The enthalpy of melting for form III was estimated to be $176 \pm 12 J g^{-1}$. The ΔH_m^∞ calculated from both the methods are quite comparable. Note that both the approaches neglect possible changes in ΔH_m in very small pores (pore size dependence of ΔH_m), which would lead to deviations of the estimated values from the bulk enthalpy of melting of form III ($\Delta H_{m,III}^\infty$). However systematic changes depending on pore diameter (d) have not been obtained and one can assume that possible effects are smaller than the experimental uncertainty of the performed DSC measurements.

Based on the slope taken from figure 6.4 and assumptions discussed one can estimate the surface energies σ_I , σ_{II} , σ_{III} for different crystalline forms using the slopes in figure 6.4 according to the following relationship

$$\sigma_c = \frac{\Delta H_m^\infty s_c \rho_c}{4 T_m^\infty} \quad (6.4)$$

The corresponding values for surface energy σ , slopes s_c , crystal density ρ_c , enthalpy of melting ΔH_m^∞ , and the melting temperature T_m^∞ are listed for all the three crystalline forms of acetaminophen in table 6.1. Most likely the confined crystal is only in contact with an immobilised / disordered acetaminophen layer covering the pore walls (i.e. $\sigma_c = \sigma_{cl}$). Obviously the surface energies for form II is larger than that of other crystalline forms. Possible consequences of this finding for thermodynamic equilibrium situation in nanopores are discussed later in section 7.2.

6.2 Phase transition form III \rightleftharpoons II of acetaminophen

So far, melting of form I and III were discussed in detail and it was shown that the melting temperatures of the three different forms were consistent with the Gibbs - Thompson relationship. We know from the previous section that, the major fraction melting after cold crystallisation at 80 °C is form III for all the pore diameters. In this subsection a rigorous and efficient way to produce form II will be described in detail. A special temperature program as shown in figure 6.5 (a) is employed to produce nearly 100 % form II in the CPGs. The initial step to produce form II is to vitrify the sample. This is done by quenching the molten acetaminophen held at 180 °C in the pores to - 40 °C with a cooling rate of - 100 K min⁻¹. Cold crystallisation of form III appears during reheating with a rate of 10 K min⁻¹ to a temperature ($T_{cl}^u = 135$ °C) where form III is partially molten. Then the sample is cooled to lower cycling temperature ($T_{cl}^l = 100$ °C) and reheated to upper cycling temperature (T_{cl}^u). This cooling and heating to a partially molten state is repeated one to six times. In case of the last cycle the final heating is not stopped at T_{cl}^u but the sample is reheated to 180 °C in order to see which crystals are formed.

The results of such experiments including different number of cycling steps are shown in the figure 6.5 (b), where acetaminophen infiltrated in CPG having a pore diameter of 43 nm is chosen as an representative example. Major fraction that melts in the final heating scan after one cycle is form III of acetaminophen as seen in figure 6.5 (b). However minor

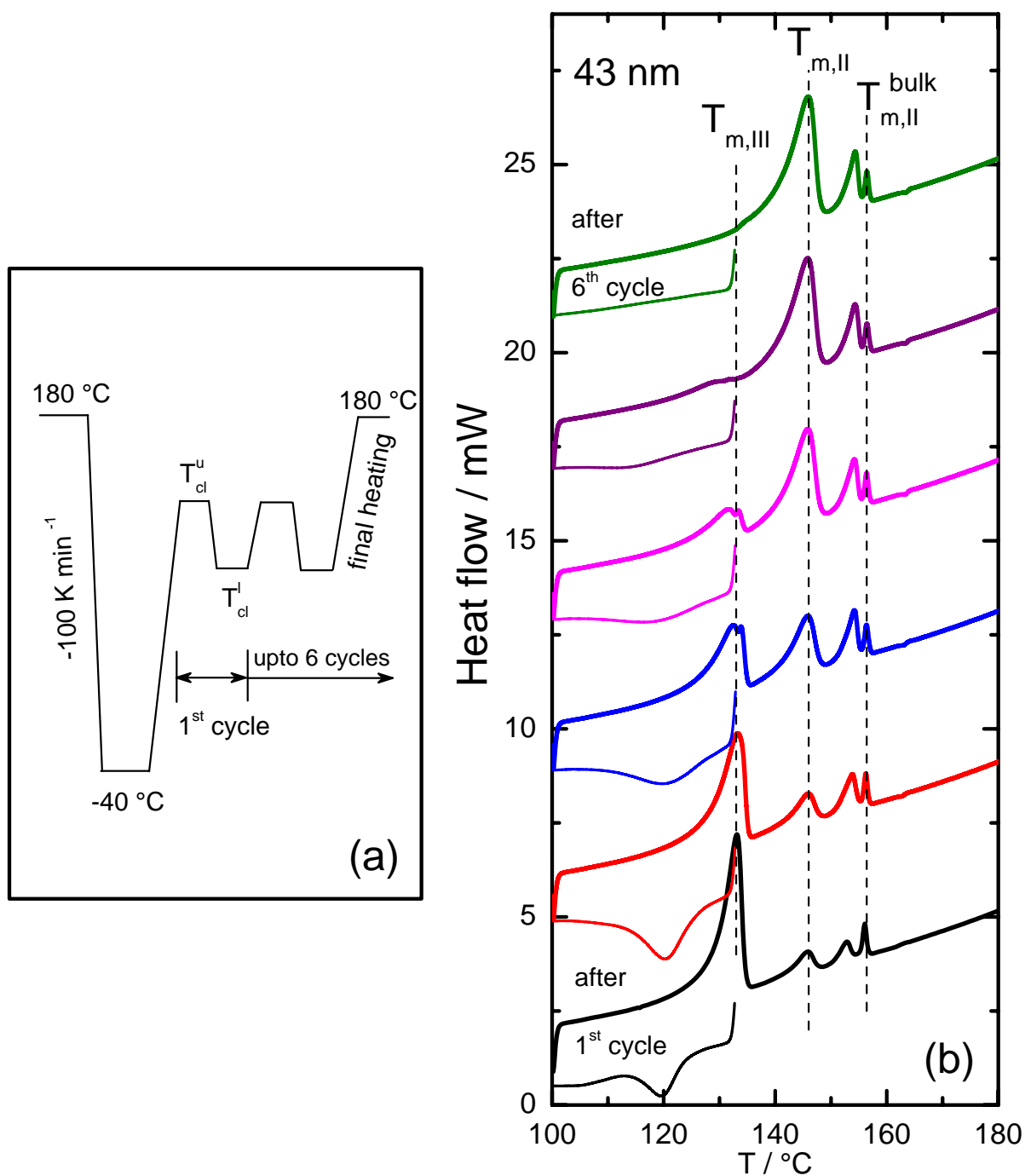


Figure 6.5: (a) Temperature program used to convert form III to form II in the 43 nm CPG pores. (b) DSC heating scans (thick black curves) represent the final heating scan after one cycle and the thick green curve after six cycling steps. The preceding cooling scans to the lower cycling temperatures are shown as thin curves. The curves are shifted by 4 mW for the sake of clarity. T_{cl}^u is the upper cycling temperature limit which in this case is 135 °C and T_{cl}^l is the lower cycling limit which is 100 °C for the given pore diameter. Except the initial quenching which is performed from 180 °C to -40 °C with a rate of -100 K min⁻¹ all other heating and cooling rates are performed at ± 10 K min⁻¹.

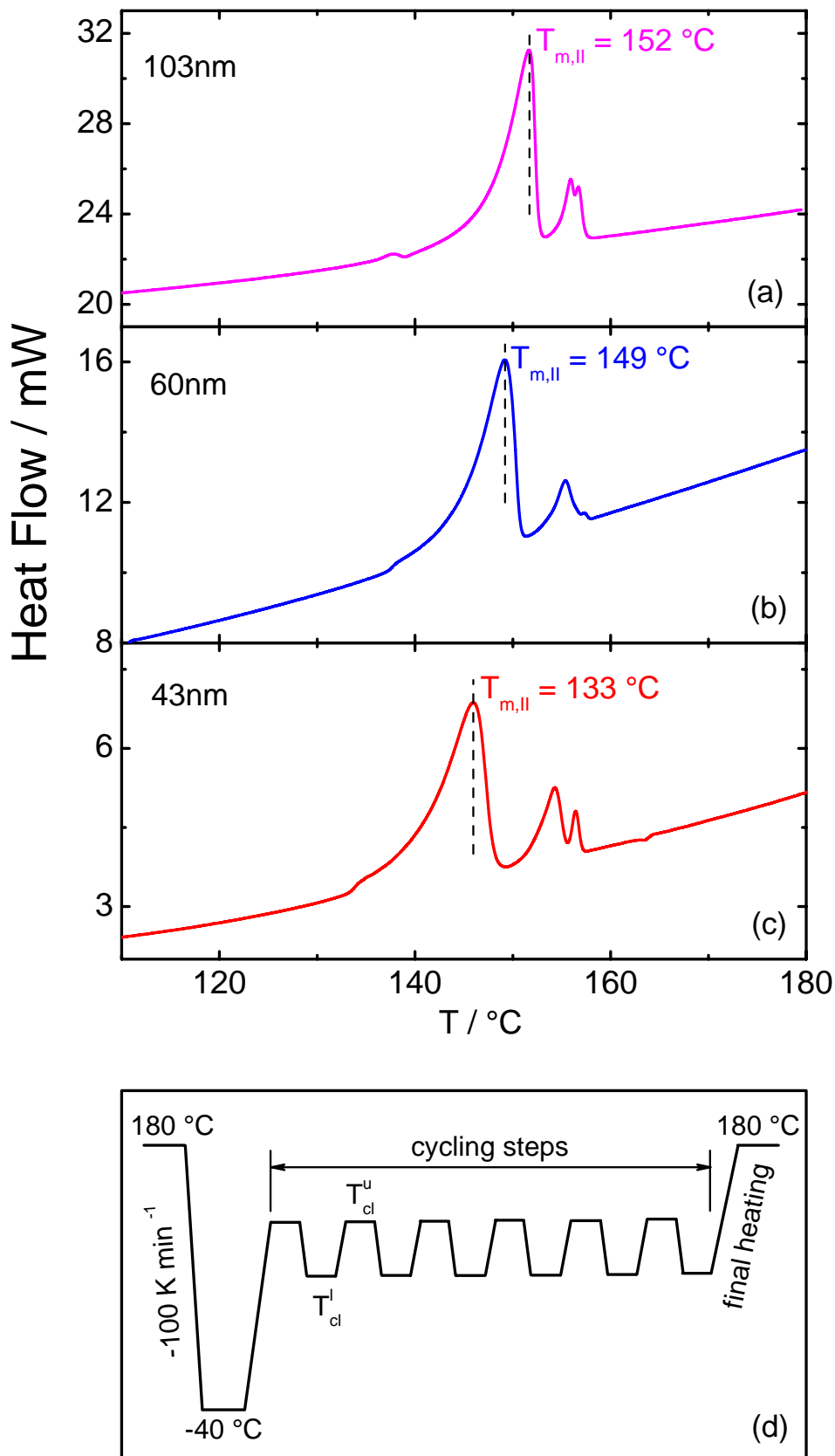


Figure 6.6: Final heating scans after applying the program as shown in part (d) to acetaminophen infiltrated in CPGs having an average pore diameter of (a) 103 nm with upper cycling temperature $T_{cl}^u = 137\text{ °C}$, and lower cycling temperature $T_{cl}^l = 100\text{ °C}$ (b) 60 nm with upper cycling temperature $T_{cl}^u = 135\text{ °C}$, and lower cycling temperature $T_{cl}^l = 110\text{ °C}$, (c) 43 nm with upper cycling temperature $T_{cl}^u = 133\text{ °C}$, and lower cycling temperature $T_{cl}^l = 100\text{ °C}$. (d) temperature program employed for conversion of form III to form II for all the three pore diameters shown here.

fractions of form II (and form I) do already exist. The preceding cooling step also shows a significant crystallisation peak near 120 °C. At that temperature, fraction of the confined acetaminophen melting as form III recrystallises. Upon increasing the number of cycling steps, both the melting peak of form III and the preceding crystallisation peak decreases systematically. On the other hand the fraction of form II increases systematically from a small fraction after the first cycle to almost 100 % after six cycles. After the sixth cycle there is no indication for melting of form III. In all the final heating scans shown in figure 6.5 (b), there is tiny peak melting around 156 °C which is assigned to melting of form II on the top surface of the CPG or large cracks as discussed in the previous section. In addition to melting of form II in the pores and the bulk form II on the surface there is an indication for a tiny additional melting peak. This is most likely melting of a very small fraction of form I with a very small size entrapped in between the major form II crystals. This can be also seen in the experiments presented in the last section of this chapter. If the cycling experiments are carried out in between 135 °C and 100 °C it is clearly seen that form II can be effectively produced. This finding indicates that, there is a phase transition temperature ($T_{\text{III}=\text{II}}$) between form III and II in 43 nm pores should be around 120 °C. This finding seems to be consistent with results for bulk acetaminophen in the literature [72] and in our studies on bulk acetaminophen where a small dip in DSC heating scan and changes in the optical microscope are seen at around 120 °C which may indicate a form III to form II transition (figure 5.2).

The observed conversion from form III to form II during cycling between 100 °C and 135 °C as shown in figure 6.5 occurs similarly for acetaminophen infiltrated in CPGs with other pore diameters. In figure 6.6 the final heating scan for acetaminophen in pores with three different diameters (43 nm, 60nm and 103 nm) are shown after six cycling steps according to figure 6.6 (d). Depending on pore diameter, slightly different upper cycling T_{cl}^{u} and the lower cycling temperature T_{cl}^{l} where chosen (refer figure 6.6 caption for details). Systematic reduction in melting point of form II is observed from larger to smaller pores in accordance with the Gibbs - Thompson relationship. On low the temperature side of the major melting peak of form II, a tiny peak is observed indicating a remaining fraction of form III after the cycling steps. At higher temperatures for the largest pores (103 nm) there is an indication for a double peak, for smaller pore diameters it is observed as two distinct peaks for acetaminophen. Most likely these two peaks correspond to form II on the surface or in larger cracks melting around 157 °C and a small fraction of entrapped form I crystals.

In order to estimate the temperature range where the transition between form III and II occurs, three different upper cycling temperatures (T_{cl}^{u}) were chosen. In figure 6.7 results

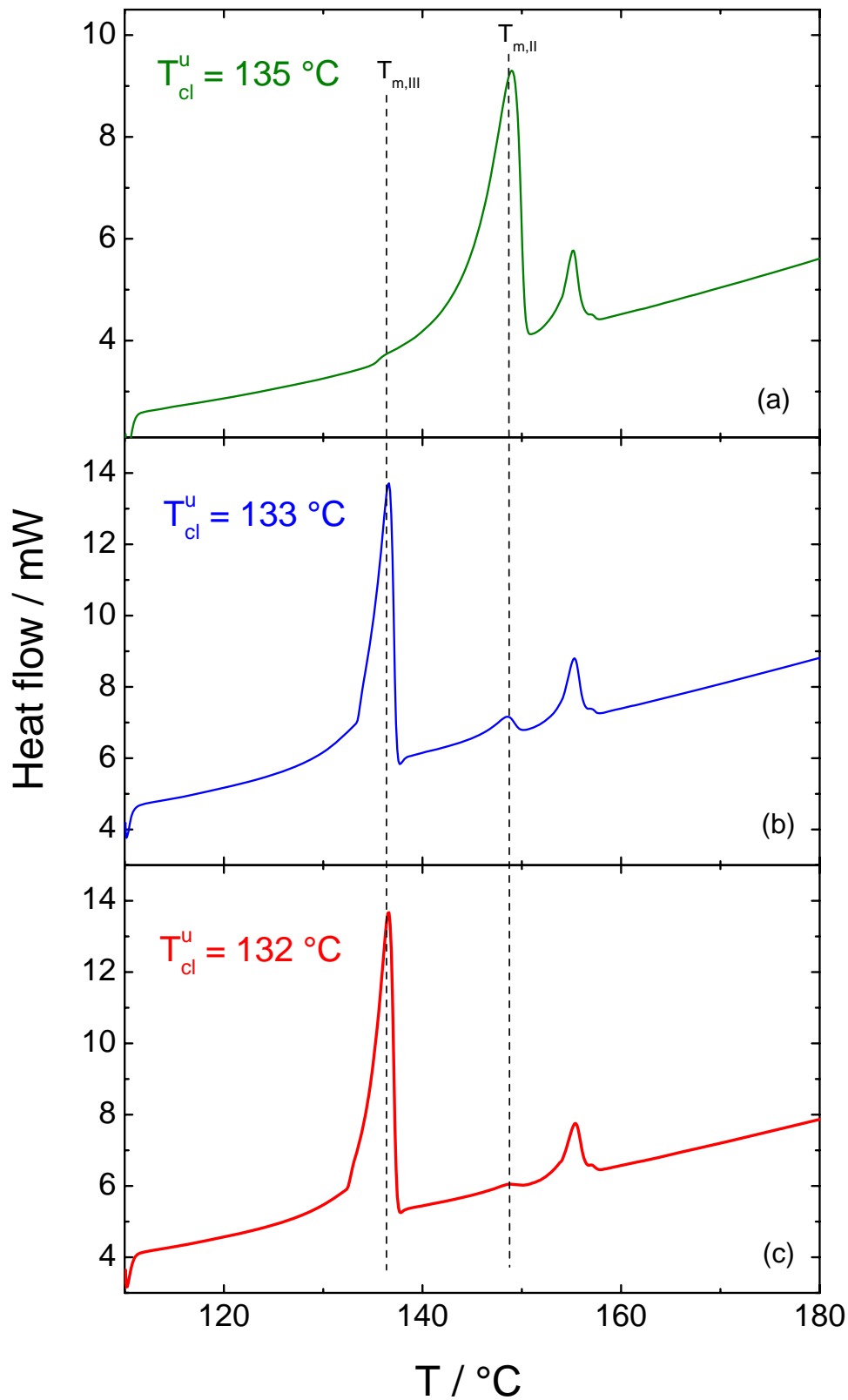


Figure 6.7: Final heating scan for acetaminophen infiltrated in 60 nm CPG after cycling steps as shown in figure 6.6 (d) for different upper cycling temperature (a) $T_{cl}^u = 132\text{ °C}$, (b) $T_{cl}^u = 133\text{ °C}$ and, (c) $T_{cl}^u = 135\text{ °C}$

for acetaminophen infiltrated in 60 nm CPG are presented. Final heating scans are shown using the temperature program with six cycles as shown in figure 6.6 (d). For the highest upper cycling temperature ($T_{cl}^u = 135$ °C, figure 6.7 (a)) melting of form II is observed in the final heating scan. Significant changes are observed in the final heating scans when the upper cycling temperature is reduced by only 2 °C as shown in figure 6.7 (b) and (c) where only melting of form III is seen. This may indicate that there is a transition temperature slightly below 135 °C. However the effect of kinetics should not be underestimated, since the transitions might be only slower or hindered for temperatures below 135 °C. It is possible that form II is thermodynamically stable in a certain temperature interval below 135 °C. Although, dramatic changes in the kinetics by a temperature change of only 2 °C are not so likely. It has to be noted that for upper cycling temperature below 135 °C the melting peaks of form III seem to be sharper when compared to conventional melting of form III. This might be due to the further perfection of form III crystals in the pores during cycling where the sample is heated and cooled repeatedly. The measurements clearly show that nearly 100 % form II can be produced in 60 nm pores by employing the cycling program described above only if the upper temperature limit is suitable and not too low. Similar trend is observed for acetaminophen infiltrated in CPGs having pore diameters in the range 40 - 103 nm. In 43 nm pores form II is not found below $T_{cl}^u \approx 133$ °C and for 103 nm pores it disappears below $T_{cl}^u = 135$ °C.

In order to get a better understanding of the transitions between form III and form II of acetaminophen in the pores, another suitable temperature program as shown in figure 6.8 (d) was applied. The initial steps of the program are quite similar to that one used to produce form II in the pores (figure 6.6 (d)). The only difference is an additional step after producing form II in the pores. Once nearly 100 % form II is produced, then the sample is heated to a temperature ($T_{cl}^{u,II}$) where form II is partially molten. It is then cooled to lower cycling temperature T_{cl}^l in the range 100 - 110 °C depending on the pore diameter. Individual cycling steps are shown in different colours in figure 6.8 (d) and the corresponding heating and cooling scans in figure 6.8 (a) to (c) for acetaminophen infiltrated in different pore diameters. For more details of the temperature program ($T_{cl}^u, T_{cl}^l, T_{cl}^{u,II}$) refer to the caption of figure 6.8.

The first cooling step after partial melting of cold crystallised form III crystals show crystallisation peaks around 130 °C for acetaminophen infiltrated in 103 and 60 nm pores (violet curves in figure 6.8 (a) and (b) respectively), while for the acetaminophen in 43 nm pores (figure 6.8 (c)) the crystallisation temperature is shifted to 120 °C. For all pore diameters the heating scan to $T_{cl}^{u,II}$ after the sixth cycling step shows only melting of form II (red curve),

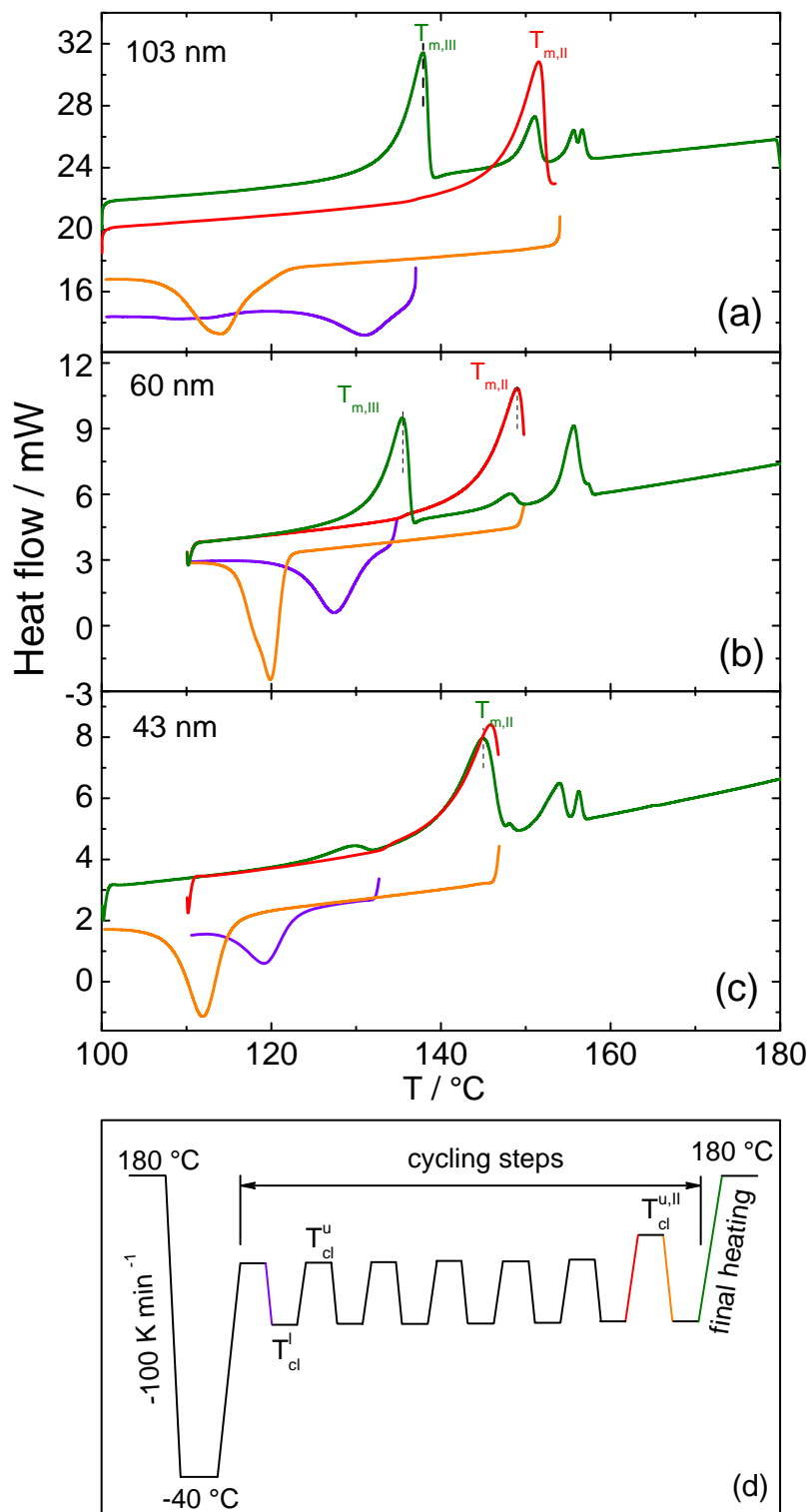


Figure 6.8: First cooling scans (violet curves), the intermediate heating scans (red cures) to $T_{cl}^{u,II}$ the final cooling scans (orange curves), and the final heating scans (green curves) to 180 °C for acetaminophen infiltrated in CPGs having an average pore diameter (a) 103 nm with upper cycling temperature $T_{cl}^u = 137$ °C, lower cycling temperature $T_{cl}^l = 100$ °C and, the second upper cycling temperature $T_{cl}^{u,II} = 154$ °C; (b) 60 nm with upper cycling temperature $T_{cl}^u = 135$ °C, lower cycling temperature $T_{cl}^l = 110$ °C and, the second upper cycling temperature $T_{cl}^{u,II} = 150$ °C (c) 43 nm with upper cycling temperature $T_{cl}^u = 133$ °C, lower cycling temperature $T_{cl}^l = 100$ °C and, the second upper cycling temperature $T_{cl}^{u,II} = 147$ °C. (d) Temperature program employed to vary the crystallisation temperature systematically.

an indication for practically complete conversion to form II. The cooling step (orange curve) after heating to the second upper cycling temperature ($T_{cl}^{u,II}$) shows crystallisation peaks at significantly at lower temperatures in the range 110 - 120 °C depending on the pore diameter. The final heating scan (green curves) for acetaminophen infiltrated in porous glass with an average pore diameter of 103 nm (figure 6.8 (a)) and 60 nm (figure 6.8 (b)) shows preferentially melting of form III in the pores. However, acetaminophen in 43 nm CPG shows a completely reversed trend, where only melting of form II is seen in the final heating scan. These measurements indicate that low temperature crystallisation during the cooling step (yellow curves) after heating to $T_{cl}^{u,II}$ leads to formation of form III which melts in the final heating scan for acetaminophen in 103 nm and 60 nm. High temperature crystallisation (blue curves) in the presence of remaining form III crystals acting as nuclei leads to formation of a significant fraction of form II for acetaminophen in 103 nm and 60 nm. A possible interpretation is that crystallisation temperature decides which form is growing. There might be a transition at $T_{III=II}$ between the crystallisation temperatures occurring under different conditions. Interestingly, acetaminophen in 43 nm CPG shows always melting of form II in the final heating scan, indicating that the transition $T_{III=II}$ might have shifted to lower temperature (< 110 °C). However, the shift cannot be too large since, we also know from the previous section that isothermal crystallisation at 80 °C for 2 hours (refer figure 6.3 (b)) leads to production of form III in the CPGs having pore diameters in the range 22 - 103 nm.

The above described measurement for acetaminophen infiltrated in 103 nm and 60 nm pores clearly indicate that crystallisation at different temperatures lead to different crystalline forms. In order to conform these findings the program was slightly modified. The final cooling step after melting form II was performed at different cooling rates in order to change the crystallisation temperature. The temperature program is identical to that shown in figure 6.8 (d) until the heating step to the second upper cycling temperature ($T_{cl}^{u,II}$). Only the final cooling scans (orange curves) are performed at three different rates to $(-10, -4, -1 \text{ K min}^{-1})$.

Results for acetaminophen infiltrated in CPG with 103 nm pores using this modified program are presented in figure 6.9 show that, neither the melting of form II nor crystallisation of form III during the first cooling is affected. This is expected since, the program is identical until that step. However significant changes are observed in the cooling (orange curves) scans from $T_{cl}^{u,II}$ to 100 °C. For the highest cooling rate (-10 K min^{-1}) as shown in figure 6.9 (a), crystallisation occurs around 110 °C. The major fraction which melts after this treatment in the final heating scan (red curve) is form III. When intermediate cooling rates (-4 K min^{-1}) are used the crystallisation peaks seems to shift to higher temperature and the

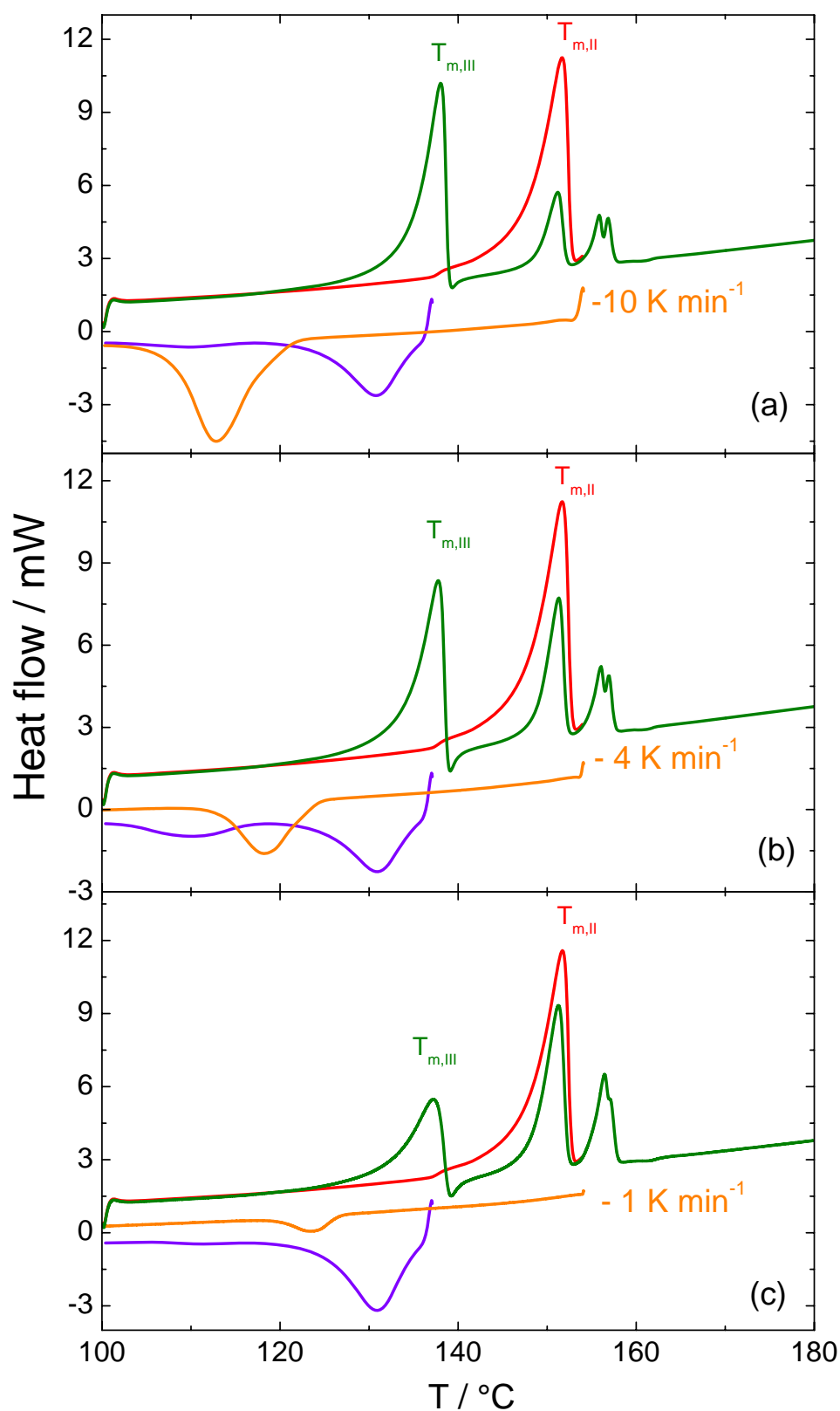


Figure 6.9: DSC scans for acetaminophen infiltrated in 103 nm CPG by employing temperature as shown in figure 6.8 (d). The final cooling scan (orange curves) is performed with a cooling rate of (a) -10 K min^{-1} , (b) -4 K min^{-1} and (c) -1 K min^{-1} . The red curves corresponds to intermediate heating scan to $T_{cl}^{u,II} = 154 \text{ }^\circ\text{C}$. The final heating scan (green curves) shows melting of different fractions of forms III and II, and violet curves corresponds to first cooling scan.

final heating step show melting of form III and II of acetaminophen to an equal extent as in figure 6.9 (b). However, when the melt is cooled with very small cooling rate (-1 K min^{-1}) significant changes are observed (figure 6.9 (c)). The crystallisation peak during the final cooling step (orange curves) shifts significantly to higher temperature (around $120 \text{ }^\circ\text{C}$) and the final heating scan shows melting of form II as a major fraction. These findings seem to be consistent with the idea that it depends on the crystallisation temperature which form of acetaminophen grows in the pores.

Summarising, the results discussed in this section, one can conclude that the crystallisation temperature is a major factor determining the crystalline structure. Form III seems to grow below a certain transition temperature $T_{\text{III}=\text{II}}$ while form II is observed above. The exact transition temperature ($T_{\text{III}=\text{II}}$) between form III and II is difficult to estimate. However it can be concluded that the transition between form III and form II of acetaminophen occurs in the temperature range $100 - 135^\circ\text{C}$ for all pore diameters in the range $43 - 103 \text{ nm}$.

6.3 Crystallisation of form I in CPGs

In this section it will be shown that high temperature crystallisation leads to formation of form I of acetaminophen. In order to find out where form I acetaminophen would crystallise a different temperature program was used shown as inserts in (figure 6.10 (a) and (b)). The infiltrated samples containing form I are heated to a temperature ($164 \text{ }^\circ\text{C}$ for 60 nm and $158 \text{ }^\circ\text{C}$ for 43 nm CPG) and held at for 3 minutes. Most of the form I crystals should be molten afterwards considering the melting points of form I of acetaminophen in pores determined in the previous section (refer figure 6.3 (a)). Then the sample is cooled (blue curves in figure 6.10) and reheated to $180 \text{ }^\circ\text{C}$ (red curves in figure 6.10) to estimate the melting temperature of form I crystals of acetaminophen in the pores.

The results clearly show that, form I crystallises around $150 \text{ }^\circ\text{C}$ in the case of 60 nm pores and around $140 \text{ }^\circ\text{C}$ in the case of acetaminophen infiltrated in 43 nm CPG. We also know that homogenous nucleation close to melting point is very difficult due to thermodynamic reasons. Observed crystallisation close to the melting of form I in the pores is initiated by the remaining stable crystals acting as a nucleating agent during the cooling step. Both the scans shown in figure 6.10 (a) and (b) were performed after storing the acetaminophen infiltrated in the CPGs at room temperature for two years after removing the bulk surface layer. The first heating scans (not included in figure 6.10) show that form I is stable for long periods

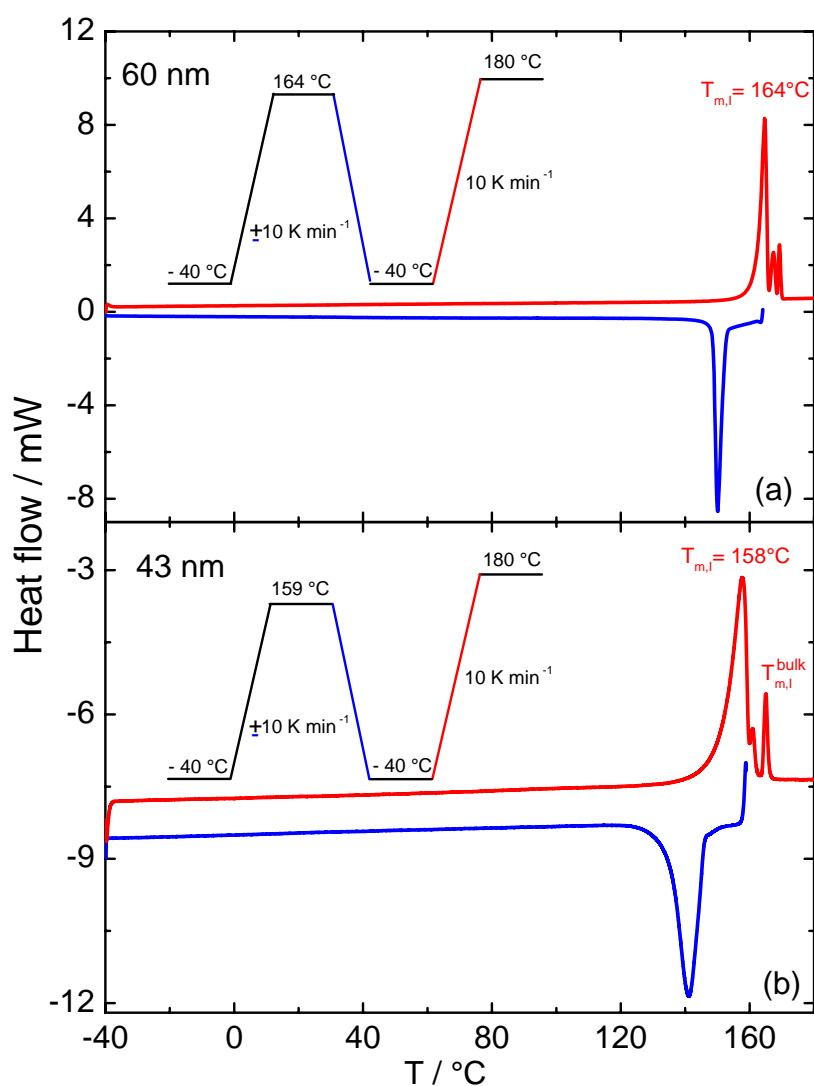


Figure 6.10: Shows the melting (second heating - red curves) and crystallisation (cooling step - blue curves) of form I acetaminophen infiltrated in (a) 60 nm and (b) 43 nm. The first heating from -40 °C to 164 °C for acetaminophen in 60 nm and to 159 °C in 43 nm (which not shown here) is performed with a rate of 10 K min⁻¹. For both the diameters the cooling (blue curves) step to -40 °C is performed at a rate of -10 K min⁻¹. The final heating to 180 °C is performed at a rate of 10 K min⁻¹.

of time at room temperature. We also know from the previous chapter that form III in the CPGs too is stable for long time scale. This shows that once a crystalline form is formed, it remains stable at room temperature for significant amount of time. Solid - solid transitions close to room temperature are obviously very unlikely. This indicates that it is hard to access the thermodynamic equilibrium state since only one form can be energetically favoured. This is the reason why in this work crystals grown from the melt at different temperatures are often considered.

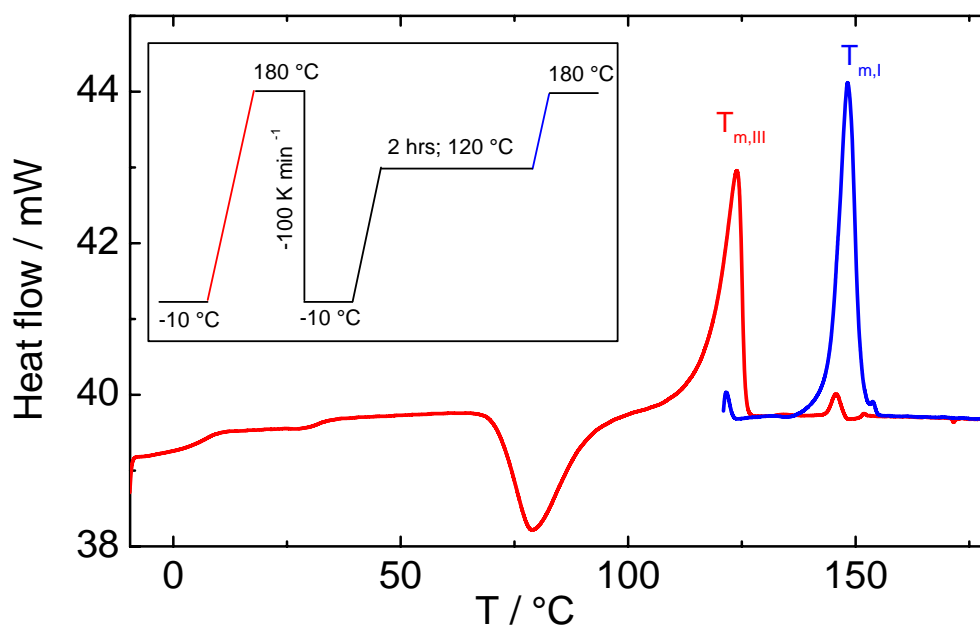


Figure 6.11: Melting of form III and a crystal which might be similar to form I, for acetaminophen infiltrated in CPG having an average pore diameter of 22 nm. First heating scan (red curves) performed at 10 K min^{-1} shows melting of form III acetaminophen. The final heating scan (blue curve), after isothermally annealing the infiltrated sample at $120 \text{ }^\circ\text{C}$ shows melting of form I acetaminophen in the pores. The heating rate used for both the scans is 10 K min^{-1}

An interesting finding is observed for acetaminophen infiltrated in 22 nm CPG. Figure 6.11 shows the melting of form III and, a crystalline form similar to form I acetaminophen in 22 nm CPG. The first heating (red curves) of initially glassy sample from $-10 \text{ }^\circ\text{C}$ to $180 \text{ }^\circ\text{C}$ shows melting of form III in the pores as observed for acetaminophen infiltrated in other pore diameters. However the final heating scan (blue curves) which was performed after annealing the melt quenched sample at $120 \text{ }^\circ\text{C}$ for 2 hours shows a new feature, melting of form I (or an intermediate having a melting point 4 K below the melting of form I and a slightly reduced enthalpy of melting (Δh_m) compared to melting peak seen in very first heating scans on freshly prepared samples)^a. We know from the previous experiments (figure 6.10) that form I crystallises close to its melting point in presence of form I seeds. However, for acetaminophen infiltrated in porous glass having an average pore diameter of 22 nm, a direct transition from a semi-crystalline state containing form III crystals at $120 \text{ }^\circ\text{C}$ to form I is observed when annealed close to the melting of form III in the pores. In larger pores form

^aFurther indications for the existence of an intermediate growing in this temperature range seem to exist but need further investigation.

II grows under similar conditions. In all the experiments performed on acetaminophen infiltrated in 22 nm CPG melting of form II was never observed. Another interesting aspect is the observance of two glass steps, one below room temperature and the other one around 30 °C. These findings indicate that a immobilised surface layer having a higher T_g a thickness around 2 nm. The performed isothermal experiments strongly indicate that crystallisation of form I occurs already above 120 °C for acetaminophen infiltrated in 22 nm pores.

To conclude, it was shown in this section that high temperature crystallisation leads to form I crystals. This form grows for temperatures $T_c \geq 140$ °C for diameters $103 \text{ nm} \geq d \geq 43$ nm and at temperatures $T_c \geq 120$ °C for $d = 22$ nm. Interestingly there seems to be a direct transition between the temperature intervals where form III and form I do grow in 22 nm pores. Occurrence of form I at high temperatures might explain the existence of form I in freshly prepared samples. For such a case T_c should be high since crystallisation starts from a bulk surface layer containing a larger number of heterogenous nuclei.

Chapter 7

Discussion

7.1 Amorphous acetaminophen in bulk and in CPGs

The properties of amorphous acetaminophen have been studied in the framework of this thesis work by DSC and dielectric spectroscopy. It was shown in chapter 5 that completely glassy acetaminophen can be achieved by using cooling rates higher than -100 K min^{-1} . Subsequent DSC heating scans show a pronounced glass step ($\Delta C_P \approx 0.7 \text{ J g}^{-1} \text{ K}^{-1}$) of amorphous acetaminophen at $T_g \approx 24^\circ \text{C}$. During further heating a cold crystallisation is observed around 80°C . Isothermal crystallisation experiments by DSC and dielectric spectroscopy show consistently that the half time τ_c reduces systematically with the increase in the isothermal crystallisation temperature T_c . It was observed that the height of the glass step ΔC_P after isothermal crystallisation decreases with the increase in crystallisation time t_c . The half time is about 10^6 s at T_g and approaches 10^3 s at 60°C . This indicates that the crystallisation kinetics of bulk acetaminophen is dominated by mobility. The situation can be well described by a two phase model i.e, assuming crystalline and amorphous fractions. There are no indications for a rigid amorphous fraction like sometimes discussed for semicrystalline polymers.

Dielectric measurements on bulk acetaminophen starting from the glassy state at -20°C up to 50°C where crystallisation starts to appear, show the typical relaxation behaviour known for glass forming liquids with a strong cooperative α relaxation and a weak Johari - Goldstein (JG) β process. The temperature dependence of α relaxation can be parameterized using the Vogel - Fulcher - Tamman (VFT) equation, with $\Omega = 10^{20.3} \text{ rad s}^{-1}$ which is the limiting frequency for $T \rightarrow \infty$, $B = 1670 \text{ K}$ for curvature of α relaxation trace and, $T_\infty = 220 \text{ K}$ for the Vogel temperature. The Johari - Goldstein β relaxation at low temperatures shows an

Arrhenius like temperature dependence with an activation energy $E_A = 20 \text{ kJ mol}^{-1}$.

When acetaminophen is infiltrated in CPGs changes in the crystallisation behaviour are observed. Although CPGs have a sponge like morphology with inter connected pores, crystallisation in porous glass with $d = 103 \text{ nm}$ takes five times longer than that of bulk acetaminophen. Similar effects are indicated for other pore diameters between 100 nm and 20 nm . In case of 10 nm pores crystallisation occurs only in the presence of a thick acetaminophen layer on the CPG piece, while acetaminophen in 4 nm pores never crystallise. To understand the prominent changes in the crystallization mechanism of acetaminophen in pores, the following three effects should be considered:

1. Equilibrium thermodynamics predicts that crystallisation is completely suppressed below a critical size d^* , since the surface energy contributions overcompensate the energetic advantage associated with the release of the internal energy upon crystallisation. For cylindrical pores the critical diameter d^* can be estimated from

$$d^* = \frac{4 \sigma_c T_m^\infty}{\Delta H_m^\infty \rho_c (T_m^\infty - T)} \quad (7.1)$$

where σ_c is the surface energy, ΔH_m^∞ the enthalpy of melting, T_m^∞ the bulk melting temperature and, ρ_c is the density of the individual crystalline form.

2. The changes in the nucleation mechanism can delay the crystallisation if the liquid is confined to isolated pores, since each compartment has to be nucleated individually. Homogenous nucleation would dominate under such conditions when the pore walls are non-nucleating. This would lead to longer crystallisation times (τ_c) under isothermal conditions or would require large under-cooling in non - isothermal crystallisation experiments. The number of heterogenous nuclei will be reduced in nanopores with non - nucleating walls since particles with dimensions larger than pore diameter cannot enter. Moreover, nuclei might be less efficient since growth perpendicular to the axis of the cylindrical pores might be blocked.
3. The crystallisation kinetics can be significantly slowed down in nanopores when immobilised surface layers having a thickness around 1 nm corresponding to a few molecules of guest system are formed. This effect becomes prominent in very small pores where the interfacial fraction is huge due to very high surface area and, in cases where the guest molecules can form hydrogen bonds to the pore wall with high surface energy.

The first effect (1) is a thermodynamic equilibrium phenomenon, while the other two (2, 3) would affect the crystallisation kinetics. All the above three mentioned effects should be considered for explaining the observed stabilisation of amorphous acetaminophen in nanopores.

Changes in the crystallisation kinetics in pores with diameters in the range 103 nm to 22 nm might be due to changes in the mobility and, the number of heterogenous nuclei. Both these effects can contribute to the slower kinetics. The number of heterogenous nuclei per volume will be reduced since the bigger ones are sieved out and the cooperative dynamics will be slowed down close to the pore walls. This is because, acetaminophen contains polar groups such as carboxyl (C = O), hydroxyl (O - H) and amino (N - H) groups in its chemical structure and can form inter molecular hydrogen bonds [105]. Controlled porous glass made of SiO₂ is hydroxyl terminated. Hence acetaminophen is capable of forming hydrogen bonds with the inner pore walls of the porous glass under investigation. Such a hydrogen bonded acetaminophen to the surface of inner walls of the porous media having a thickness around 1 - 2 nanometers as discussed in chapter 2 should have a slow α dynamics corresponding to a higher T_g and should be non - or hardly crystallisable.

The behaviour of acetaminophen in 10 nm pores may indicate that changes in the nucleation mechanism dominate in this case. Crystallisation appears either in the presence of an acetaminophen layer on the surface of the CPG platelets in which heterogenous nuclei that do not fit to the pores are enriched or to a very small extent after extremely long isothermal crystallisation times. This can be understood assuming a transition from heterogenous to homogenous nucleation leading to extremely long crystallisation times in the absence of an acetaminophen layer on the surface of CPG platelets.

Equilibrium thermodynamics may explain the existence of amorphous acetaminophen in 4 nm pores. If the critical diameter d^* is larger than the average pore diameter d of the host system, then acetaminophen can not crystallise at all [57,106]. The critical diameter for form III of acetaminophen at 35 °C was estimated based on equation 7.1 to be $d^* = 3.6$ nm [107] i.e., acetaminophen confined to pores having a diameter around 4 nm is very close to this limit. The effective pore diameter might be even smaller since it can be assumed that the immobilised acetaminophen layers at the walls cannot really crystallise. As a consequence it is very unlikely that acetaminophen can crystallise in the pores with diameters around 4 nm due to thermodynamic reasons. At lower temperatures d^* decreases but at T_g and below crystallisation kinetics is surely too slow to achieve the crystalline state on accessible time scales.

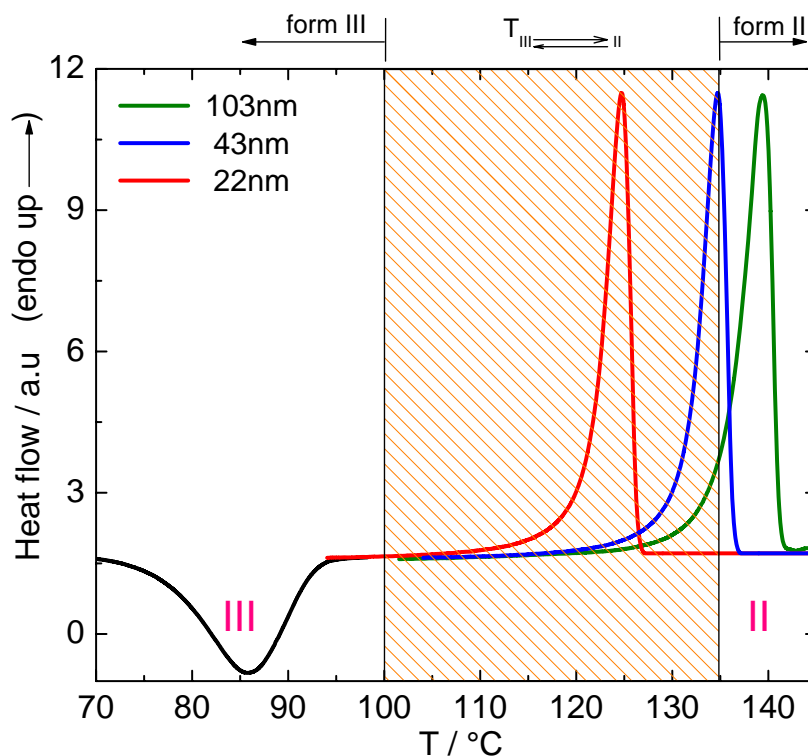


Figure 7.1: A scheme showing the temperature ranges where form III and II are stable. Crystallisation is shown as an exothermic peak and the large endotherms indicate melting of form III acetaminophen infiltrated in CPGs having 22 nm, 43nm and 103 nm pore.

7.2 Melting of form III acetaminophen in CPGs

It was shown in chapter 6 that form III of acetaminophen can be rationally produced in nanopores with diameters in the range 103 nm to 22 nm starting from glassy acetaminophen. In the recent years there were many speculations about the properties of form III of acetaminophen which seems to be metastable in bulk and was obtained only under special conditions [72, 73, 101]. However, melting of form III was never reported for bulk acetaminophen. Thus, thermodynamic parameters such as bulk melting point ($T_{m,III}^{\infty} \approx 143^{\circ}\text{C}$) and enthalpy of melting ($\Delta H_{m,III}^{\infty} \approx 177 \times 10^3 \text{ J kg}^{-1}$) of form III could be determined for the first time based on data for acetaminophen infiltrated in CPGs in the framework of this thesis [104].

In order to understand why form III melts in the pores, consider the situation sketched as a scheme in figure 7.1. Cold crystallisation during the heating scans is observed at low temperatures ($\approx 80^{\circ}\text{C}$) for all three pore diameters shown. The shaded region in figure 7.1 is considered as interval where transition between form III and II occurs. This transition inter-

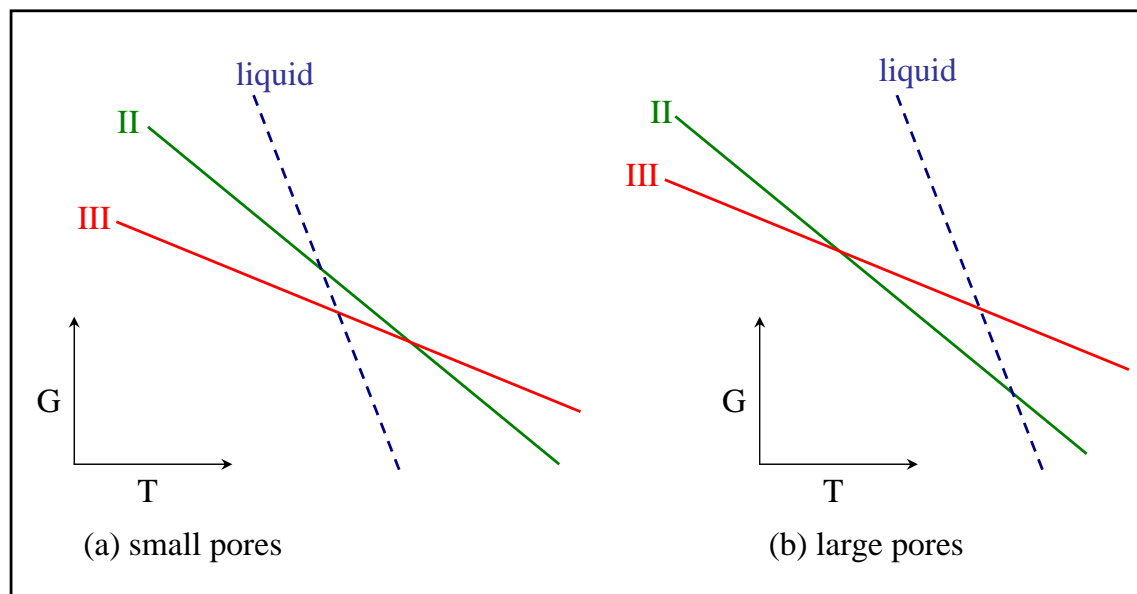


Figure 7.2: A scheme showing melting and transition between form III and II for acetaminophen in CPGs having (a) small pore diameters and (b) large pore diameters. This scenario does not fit to the experimental findings.

val is estimated based on experimental results for different pore diameters shown in chapter 6 (refer figure 6.8). At temperatures below and above form III and form II of acetaminophen are assumed to be thermodynamically stable, respectively. This can be concluded from the finding that form III is growing exclusively at temperatures below 100 °C while cycling experiments in the temperature range 110 °C to 135 °C lead to the formation of form II for pore diameters between 103 nm and 43 nm.

As seen in figure 7.1 melting of form III occurs depending on the pore diameter above or in the transformation interval. In principle, this could be the reason why cold crystallised samples show melting of form III unlike form II in the case of bulk. Thermodynamically this could be a consequence of a changing relation between melting temperature of form III ($T_{m,III}$) and transition temperature $T_{III=II}$. Neglecting the existence of form I one may expect an enantiotropic to a monotropic transition if the melting temperature of form III is reduces more rapidly than $T_{III=II}$ with decreasing pore diameter. This scenario is sketched in figure 7.2. However, such a purely thermodynamic phenomenon would be accompanied by a changing relation between $T_{m,III}$ and $T_{m,II}$ (refer figure 7.2), which is not experimentally observed in the relevant pore diameter range ($10 \text{ nm} < d < 103 \text{ nm}$). Moreover, form II can be produced below the melting temperature of form III. This would not happen if form III would be thermodynamically stable until it melts.

Obviously, thermodynamics alone cannot explain why melting of form III is observed in nanopores and kinetics is playing an important role in our host - guest systems. In the conventional DSC heating scans melting of form II is not observed for pores in the diameter range 22 - 103 nm, although thermodynamically it seems to be stable above $T_{\text{III} \rightleftharpoons \text{II}}$. Note that a certain fraction of acetaminophen melts as form II in pores having diameters larger than 100 nm, and that the DSC heating scans for bulk acetaminophen (figure 5.2) shows a small peak around 120 °C, also seen as a transition from spherulites to a staked platelets in the optical microscopy (figure 5.2 insert). This may indicate that there is a solid - solid transition form III \rightarrow form II [72], which is fast in case of bulk samples but kinetically hindered in nanopores. Accordingly the slow solid - solid transition cannot appear during the DSC heating scan in the small temperature interval between $T_{\text{III} \rightleftharpoons \text{II}}$ and $T_{\text{m,III}}$ where form III melts, i.e., the observation that form III melts in nanopores can be explained based on kinetic arguments. It was shown that for acetaminophen infiltrated in CPGs having pore diameter of 103 nm the crystallisation kinetics is slowed down due to changes in the nucleation mechanism and or surface interaction (section 7.1). In a similar way the solid - solid transition form III \rightleftharpoons form II might be slowed down. In any case it seems to be clear based on the performed experiments that for acetaminophen in CPGs having pore diameters larger than 40 nm, melting of form III in the DSC heating scans occurs in a non - equilibrium state, i.e, in a temperature range where form II should be stable due to thermodynamic reasons.

7.3 Transitions among three forms of acetaminophen in CPGs

In chapter 6 it was shown that all three forms of acetaminophen can be produced in pores by employing special temperature programs. Summarising the results it depends basically on two parameters, temperature and pore size, which form is growing in the pores. This indicates that thermodynamics is important since both parameters enter the Gibbs free energy. The temperature determines the volume contribution (ΔG_v) and, the pore size on the surface energy term (σA) (equation 2.9). Thus, the appearance of different crystalline forms in the pores will be discussed on the basis of a thermodynamic picture in this section.

Figure 7.3 (a) shows the temperature ranges where different forms of acetaminophen are considered to be stable in CPGs having a pore diameter around 60 nm. Like discussed earlier, form III grows below 100 °C. Cycling experiments (figure 6.5) in the temperature range 110 to 135 °C show that the fraction of form II increases with number of cycles. Crystallisation of form II from the melt or a transition of form III to form II is observed (figure 6.8). At temperatures above 145 °C form I of acetaminophen grows from the melt (figure 6.10).

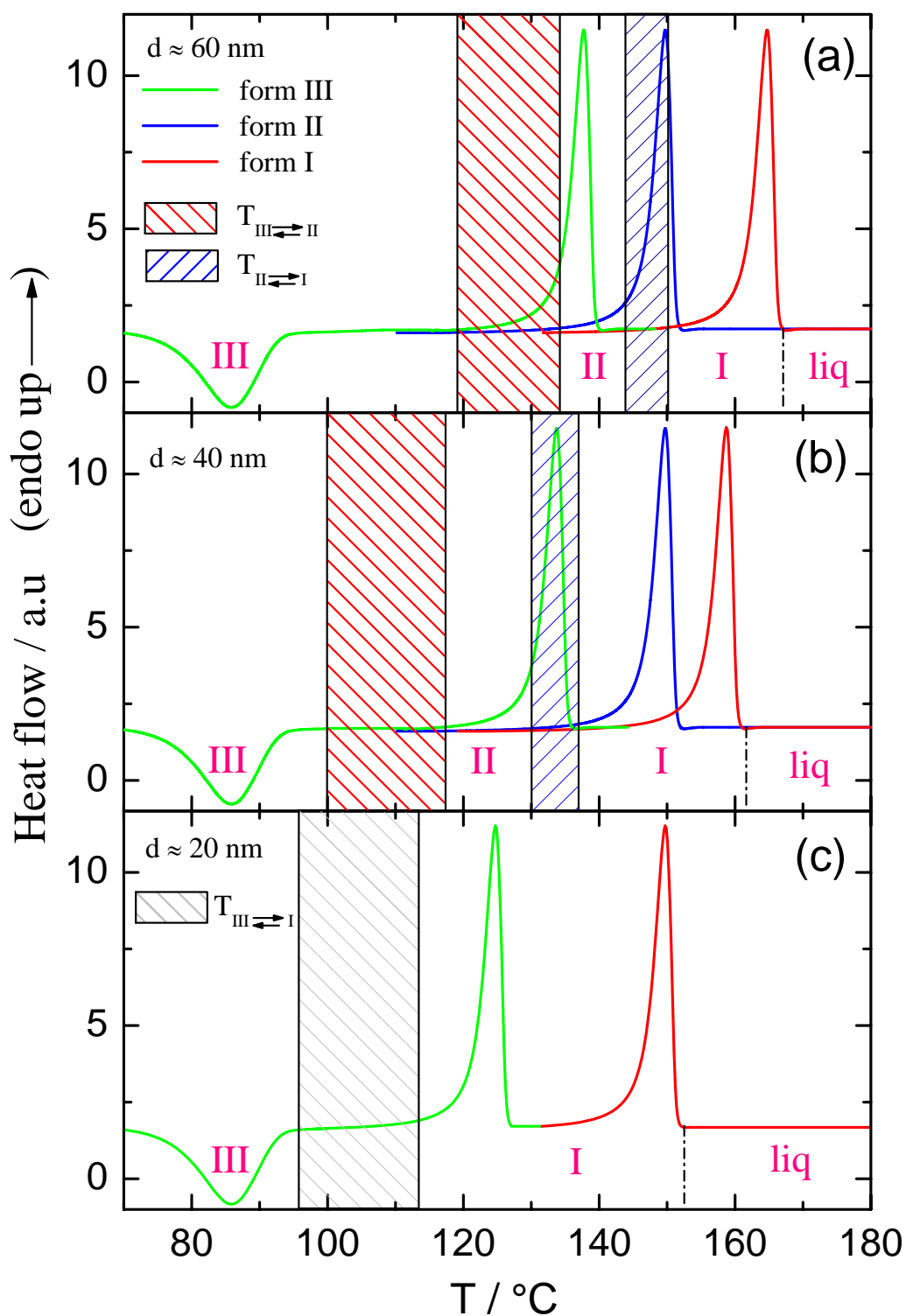


Figure 7.3: A scheme showing the phase behaviour, crystallisation and melting curves for acetaminophen in CPGs having an average pore diameter of about (a) 60 nm, (b) 40 nm and (c) 20 nm. Exothermic peaks are observed around 80 °C for all the three pore diameters. The red shaded area corresponds to the transition temperature interval where form III \rightleftharpoons form II transition occurs, the blue shaded area corresponds to form II \rightleftharpoons form I transition temperature interval, and the gray shaded area corresponds to form III \rightleftharpoons form I transition interval. The endothermic peak corresponding to melting of form I (red curves), form II (blue curves) and form III (green curves).

Like indicated in figure 7.3 (b) the phase transition temperature $T_{\text{III}=\text{II}}$, does depend on the diameter of the pores. $T_{\text{III}=\text{II}}$ shifts to lower temperatures with the reduction in the average pore diameter. This can be concluded from the findings for systems with $40 \leq d \leq 100$ nm crystallised at different temperatures using various programs (figures 6.5 - 6.9). Note that, the crystalline form II melts seemingly in all cases in a non - equilibrium state i.e, in a temperature range where for energetic reasons form I is the most stable crystalline form like discussed in the previous section.

Form I is observed in the pores with $40 \leq d \leq 100$ nm by high temperature crystallisation at 140 °C to 150 °C after providing enough seeds (figure 6.10), and after isothermal crystallisation around 120 °C in 22 nm pores from the melt (figure 6.11). One can conclude that, form I is thermodynamically stable for larger pores above 140 °C but, already above 120 °C for small pores. Obviously, the low temperature limit of its stability range is also pore diameter dependent.

For acetaminophen infiltrated in CPGs having pore diameters in the range 40 -100 nm melting and crystallisation of all the three crystalline forms are seen. Completely different behaviour is observed for acetaminophen infiltrated in CPGs having an average pore diameter of 22 nm. For such diameters the infiltrated acetaminophen undergoes obviously a direct transition from form III to form I (figure 6.11). Only melting of these two forms was been observed. Thus, only form I and form III are incorporated as stable form in sketch in figure 7.3 (c). This experimental finding indicates that the phase transition temperature between form II and I ($T_{\text{II}=\text{I}}$) shifts more rapidly to lower temperatures than the transition temperature $T_{\text{III}=\text{II}}$ with decreasing pore diameter. In other words, it can be concluded that the small temperature range where form II is considered as the most stable form in large pores ($d \geq 40$ nm) becomes narrower if the diameter decreases. The stability range of form II disappears for acetaminophen infiltrated in CPGs having pore diameters around 20 nm. In order to understand how the phase behaviour changes with pore diameter, free energy plots for the individual crystalline forms and, the phase diagrams would be required. An approach giving such information will be presented in the last section of this chapter.

7.4 Thermodynamic modeling and free energy simulations

In this section a thermodynamic model is discussed, which can describe qualitatively quite well the phase behaviour, and the transitions among individual crystalline forms of acetaminophen depending on the pore diameter of the host system. The proposed model is

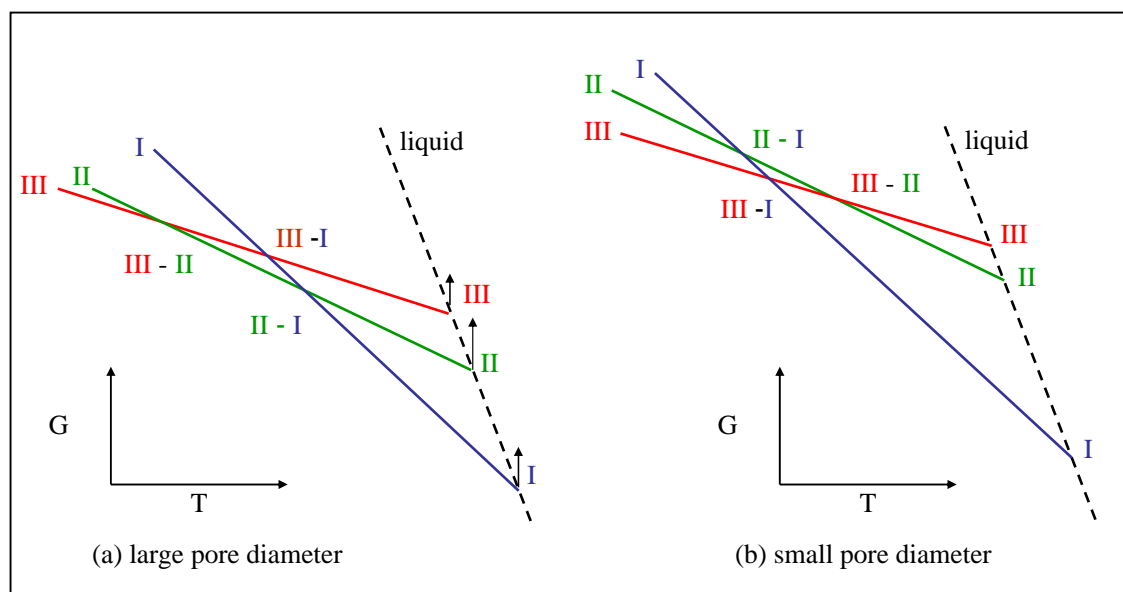


Figure 7.4: A thermodynamic model showing the Gibbs free energies and the phase transitions for given pairs of crystalline forms of acetaminophen infiltrated in CPGs having (a) large pore diameters and (b) small pore diameters. The vertical arrows in (a) represents the shift in the free energy for a given crystalline form of acetaminophen when the average pore diameter of the CPG is reduced due to surface energy contributions.

developed based on the experimental observations discussed earlier in this chapter. In particular the knowledge about the diameter dependence of the melting and the transition temperatures. Information about the enthalpy of melting (ΔH_m) and the surface energy (σ) from calorimetric measurements will be incorporated at later stage. Basically, the equilibrium situation of nanosized crystals filling the pores is described considering the influence of volume and surface energy contributions.

Figure 7.4 shows a simplified sketch of the Gibbs free energy versus temperature for two different pore diameters. This plot predicts the relative position of phase transitions among pairs of crystalline forms of acetaminophen infiltrated (a) in large pores ($d \geq 60$ nm) and, in (b) CPG's having small pore diameters ($d \leq 20$ nm). Based on the discussion in the previous section, we assume that form III is the most stable form of acetaminophen at low temperatures for all pore diameters ($d \geq 20$ nm). Consequently, form III should have the least free energy compared to other crystalline forms in this temperature range. For larger pores ($d \geq 40$ nm) a phase transition form III \rightleftharpoons form II occurs at temperatures between 100 °C and 135 °C depending on the diameter of the pores. Once the phase transition temperature $T_{\text{III}=\text{II}}$ is reached, then the free energy of form II should become the least and it is the most stable crystalline form. As already shown in figure 7.3 (a) an additional phase transition form II

\rightleftharpoons form I occurs for large pore diameters at higher temperatures. Above the phase transition temperature $T_{II\rightleftharpoons I}$, form I becomes the most stable form. In this temperature range form I has the least free energy among the three crystalline forms of acetaminophen until its melting point. Above the melting point the liquid is the most stable state. Note that both form III and form II of acetaminophen can melt according to this picture only in a non - equilibrium state (like discussed in the previous section) since form II or form I are thermodynamically more stable at the melting temperature respectively.

Figure 7.4 (b) shows the situation for acetaminophen in CPGs with small diameters ($d \leq 20$ nm). As discussed in the previous sections the surface energy contributions become more prominent when the pore size is reduced. This effect (indicated by vertical arrows in figure 7.4 (a)) leads to a shift of the melting point in accordance with the Gibbs - Thompson relationship (equation 2.32). From the Gibbs - Thompson plot in figure 6.4, where no crossing of the melting lines for different forms is observed, one can conclude that the system is and remains enantiotropic for all investigated pore diameters. The main difference in case of small pores compared to the situation in CPGs with larger pores is that the transition form III \rightleftharpoons form I occurs directly without intermediate temperature range where form II is stable. All other solid -solid transitions (III \rightleftharpoons II, II \rightleftharpoons I) are completely hidden and do not occur in equilibrium. This is because, the free energy of form II is at all temperatures higher than that of either form III or form I. Hence the occurrence of form II is not expected for acetaminophen in CPGs having diameters $d \leq 20$ nm like experimentally observed.

The fundamental reason for this qualitative change in the phase behaviour depending on pore diameter d , can be due to the huge surface energy contributions in small pores which not only affect the melting points, but also the phase transitions between crystalline forms of acetaminophen infiltrated in pores. Since the surface energy of each crystalline form in contact with the same environment is different, the transitions between different crystalline forms do shift. If we consider the form III \rightleftharpoons form II transition, we know that it will shift to lower temperatures for acetaminophen in small pores when compared to acetaminophen in larger pores. The same trend seems to exist for the phase transition form II \rightleftharpoons form I, it also occurs at lower temperatures for acetaminophen in pores with smaller diameters. In small pores ($d \leq 20$ nm) however, both transitions are completely hidden since at all temperatures either the free energy of form I or that of form III is smaller than that of form II. Thus, only the transition III \rightleftharpoons I can appear in equilibrium. In order to get this change from three phase to two phase behaviour with decreasing pore diameter, the shift of $T_{I\rightleftharpoons II}$ in pores should be more pronounced compared to that of $T_{II\rightleftharpoons III}$, which does not contradict the experimental

finding. This corresponds to surface energies of form III and form II which are smaller than that of form I (table 6.1). According to this picture form II is not observed in small pores ($d \leq 20$ nm), since form I has a much lower surface energy. Thus, the stability range of this form increases for small d values. Generally spoken the free energy balance for small crystals is not determined by the volume contributions but dominated by their surface energies. This can change the phase behaviour tremendously.

The free energy difference between liquid and crystalline state of a system incorporates volume and surface energy contributions, which can be expressed mathematically as in equation 2.8. When the size of the crystal is reduced by enforcing an external nano confinement, the volume term becomes negligible and the surface term dominates ($V \sim r^3 \ll A \sim r^2$). This effect can be clearly seen considering the pore size dependence of the surface area to volume ratio for different CPG's used in the experiments (table 4.2).

The free energy difference between liquid and a nanosized crystal of an individual crystalline form under confinement can be written as

$$G_l^{Pores} - G_{II}^{Pores} = G_l^{bulk} - G_{II}^{bulk} - \left(\frac{A}{V}\right) \left(\frac{\sigma_{II}}{\rho_{II}}\right) \quad (7.2)$$

$$G_l^{Pores} - G_I^{Pores} = G_l^{bulk} - G_I^{bulk} - \left(\frac{A}{V}\right) \left(\frac{\sigma_I}{\rho_I}\right) \quad (7.3)$$

where σ_I, σ_{II} are the surface energies between both the forms and liquid (in our case more precisely a liquid like layer at the pore walls), $\left(\frac{A}{V}\right)$ is the surface area to volume ratio, and ρ the density of the crystal.

Using equations 7.2 and 7.3 the free energy difference between form II and I in the pores can be estimated as follows

$$G_{II}^{Pores} - G_I^{Pores} = [(G_{II}^{bulk} - G_I^{bulk})] + \frac{A}{V} \left[\left(\frac{\sigma_{II}}{\rho_{II}}\right) - \left(\frac{\sigma_I}{\rho_I}\right) \right] \quad (7.4)$$

In order to get information about the phase transition temperature $T_{II=I}$, the main task is to describe the free energy difference ($\Delta G = G_{II}^{bulk} - G_I^{bulk}$) as a function of temperature. Assuming that the temperature dependence of the ratio $\left(\frac{\sigma}{\rho}\right)$ is negligible or at least comparable for both forms in equation 7.4. The most simple approximation is based on a linearisation of Gibbs free energies close to the melting points. Which requires only the information about the melting temperatures and, the melting enthalpies of both forms. More

detailed approaches incorporate the difference between the C_p values of liquid and form I in the temperature interval between both melting temperatures. Sacchetti estimated based on these parameters the free energy difference between two known crystalline forms of acetaminophen, neglecting higher order correction terms using the equation [45]

$$\begin{aligned}
G(T)_{II}^{bulk} - G(T)_I^{bulk} &= (\Delta H_{l,I} - \Delta H_{l,II}) - (T_{m,II} - T_{m,I})C_{p,l} \\
&+ (T - T_{m,I})C_{p,I} - (T - T_{m,II})C_{p,II} \\
&- T \left[\left(\frac{\Delta H_{l,I}}{T_{m,I}} \right) - \left(\frac{\Delta H_{l,II}}{T_{m,II}} \right) \right] \\
&- TC_{p,l} \ln \left(\frac{T_{m,II}}{T_{m,I}} \right) + TC_{p,I} \ln \left(\frac{T}{T_{m,I}} \right) \\
&+ TC_{p,II} \ln \left(\frac{T}{T_{m,II}} \right)
\end{aligned} \tag{7.5}$$

Considering higher order corrections one gets a non - linear description of the free energy difference $\Delta G(T)$ between the two polymorphs having the form ^a

$$\begin{aligned}
G(T)_{II}^{bulk} - G(T)_I^{bulk} &= (\Delta H_{l,I} - \Delta H_{l,II}) - (T_{m,I} - T_{m,II})(C_{p,l} - C_{p,I}) \\
&+ (T_{m,II} - T)(C_{p,I} - C_{p,II}) \\
&- T \left[\left(\frac{\Delta H_{l,I}}{T_{m,I}} \right) - \left(\frac{\Delta H_{l,II}}{T_{m,II}} \right) \right] \\
&- T(C_{p,l} - C_{p,I}) \ln \left(\frac{T_{m,I}}{T_{m,II}} \right) \\
&+ T(C_{p,II} - C_{p,I}) \ln \left(\frac{T_{m,II}}{T} \right)
\end{aligned} \tag{7.6}$$

which requires further knowledge about the C_p values of liquid and both the polymorphs. Similarly, one can estimate the free energy differences between forms III and II, and between form III and I based on the expressions

$$G_{III}^{Pores} - G_{II}^{Pores} = [(G_{III}^{bulk} - G_{II}^{bulk})] + \frac{A}{V} \left[\left(\frac{\sigma_{III}}{\rho_{III}} \right) - \left(\frac{\sigma_{II}}{\rho_{II}} \right) \right] \tag{7.7}$$

$$G_{III}^{Pores} - G_I^{Pores} = [(G_{III}^{bulk} - G_I^{bulk})] + \frac{A}{V} \left[\left(\frac{\sigma_{III}}{\rho_{III}} \right) - \left(\frac{\sigma_I}{\rho_I} \right) \right] \tag{7.8}$$

In order to come to a more quantitative description of the phase behaviour and to check the

^aThe mathematical treatments for the estimation of free energy changes between two different crystalline forms of acetaminophen in bulk state, including the correction terms in specific heat C_p are discussed in appendix A.

Table 7.1: Thermodynamic parameters used to estimate free energy differences as shown in figure 7.6 and 7.7.

$T_{m,I}$	$T_{m,II}$	$T_{m,III}$
443.15 K	430.15 K	416. 15 K
$\Delta C_{P,l-I}$	$\Delta C_{P,I-II}$	$\Delta C_{P,II-III}$
559 J kg ⁻¹ K ⁻¹	50 J kg ⁻¹ K ⁻¹	10 J kg ⁻¹ K ⁻¹
σ_I	σ_{II}	σ_{III}
4.485×10^{-2} J m ⁻²	5.533×10^{-2} J m ⁻²	5.344×10^{-2} J m ⁻²
ΔH_I	ΔH_{II}	ΔH_{III}
180×10^3 J kg ⁻¹	178×10^3 J kg ⁻¹	177×10^3 J kg ⁻¹
ρ_I	ρ_{II}	ρ_{III}
1297 kg m ⁻³	1336 kg m ⁻³	1302 kg m ⁻³

consistency with the thermodynamic parameters estimated in this work, we have performed some simulations aimed to get a consistent picture based on equations (7.4 - 7.6).

We started with the experimentally observed parameters given in table 6.1, but varied them slightly in their uncertainty range. This was done in order to get the right sequence of the transitions according to the free energy picture in figure 7.4, derived based on experimental facts. A certain optimum are the thermodynamic parameters listed in table 7.1. It has to be

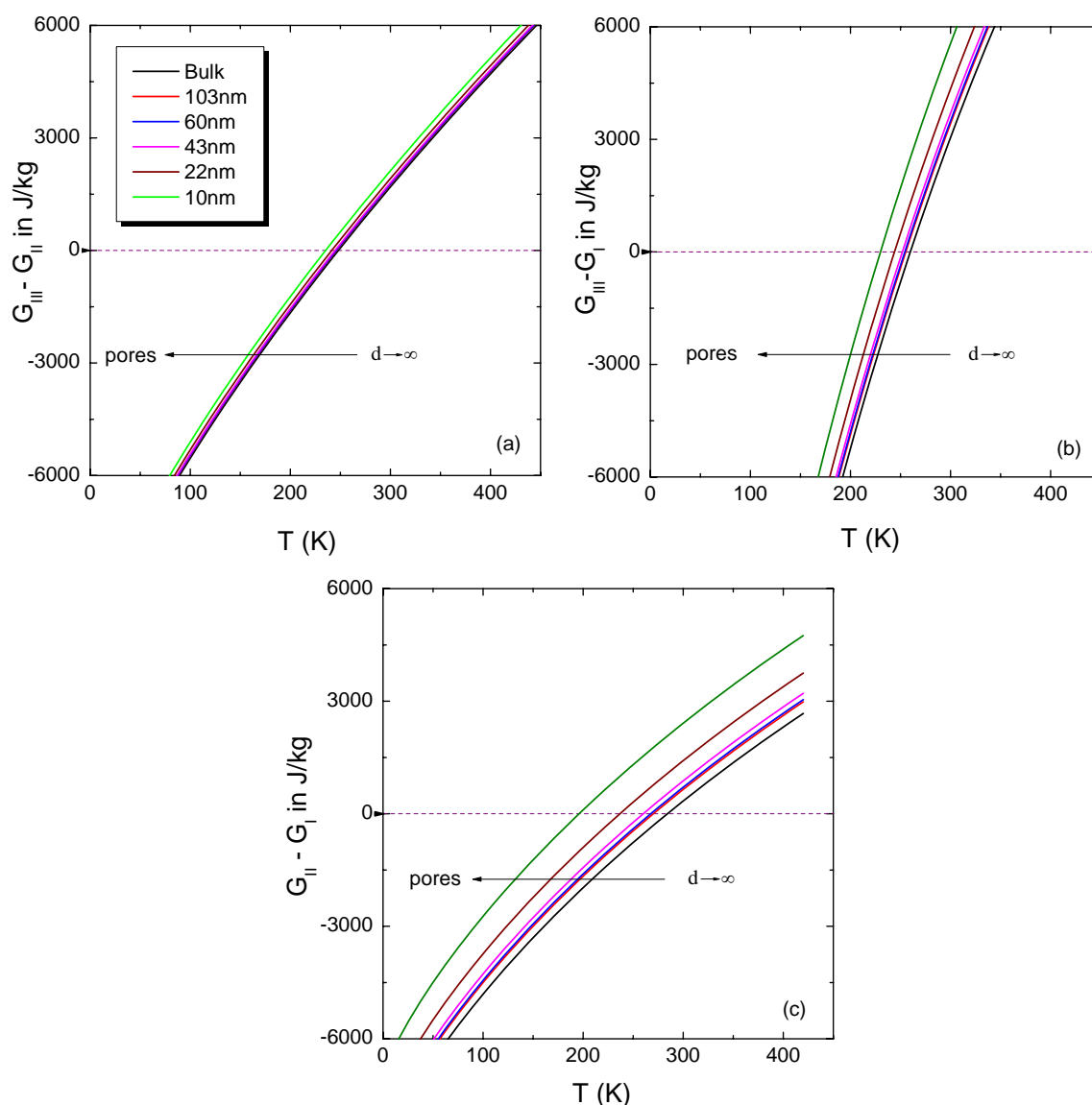


Figure 7.5: Temperature dependence of free energy difference of acetaminophen between (a) form III and II, (b) form III and I, (c) form II and I. The estimation of the free energy difference is based on equation 7.6 and the parameters listed in table 7.1.

noted here that the ΔC_p differences are not known precisely since it is hard to estimate them based on our DSC experiments. Thus, realistic values which result in a reasonable overall scenario are chosen for the simulation.

Free energy differences between pairs of crystalline forms of acetaminophen infiltrated in CPGs calculated based on the parameters in table 7.1 are shown in figure 7.5. Transitions between one crystalline form to another occur at a temperature, where the free energy dif-

ference between the individual crystalline forms is zero. In order to understand the stability of a crystalline form in a temperature range consider figure 7.5 (a), where the free energy difference between form III and II acetaminophen is shown. Form III is stable at low temperatures i.e., in the temperature range where the free energy change ($\Delta G = G_{\text{III}} - G_{\text{II}}$) is negative.

The plots shown in figure 7.5 are based on the assumptions that (i) the surface energy (σ) and density (ρ_c) of a given crystalline form of acetaminophen does not change with the temperature, that (ii) the ΔC_p values are constants and, (iii) the enthalpy of melting (ΔH_m) of a crystalline form does not change with the average pore diameter of the CPGs used. These approximations are made since the expansion coefficients $\Delta\rho/\Delta T$ of the different crystalline forms are small (and unknown). The $\Delta H(d)$ is constant as indicated by linear dependencies in the Gibbs - Thompson plot (figure 6.4) in accordance with the equation 6.1, where ΔH is treated as a constant. The ΔC_p assumption is a zeroth approximation due to the lack of information.

Figure 7.5 shows that, the phase transition temperature between different crystalline forms indeed depend on the pore diameter of the CPGs. For the chosen parameter set, the main trends are in accordance with the experimentally observed trends as shown in figure 7.3. All the transition temperatures ($T_{\text{III}=\text{II}}$, $T_{\text{II}=\text{I}}$, $T_{\text{III}=\text{I}}$) shift systematically to lower temperature, if the pore diameter decreases (corresponding to smaller crystal sizes). This effect is most pronounced for the transition between form II and form I (figure 7.5 (c)) and, weakest for the transition between form III and form II (figure 7.5 (a)). This results in a pore diameter (crystal size) dependent sequence of the phase transition temperatures as shown in figure 7.6. For large pore diameters the transition form III \rightleftharpoons form II occurs at low temperatures, form III \rightleftharpoons form I transition at intermediate temperatures and, that between form II \rightleftharpoons form I at the highest temperature 7.6 (a). In case of acetaminophen in CPG having an average pore diameter around 20 nm (figure 7.6 (b)), the phase transitions among the three crystalline forms seem to occur in a very small temperature interval. This shows that we are close to a triple point where all three forms would co-exist. For acetaminophen infiltrated in even smaller pores, a completely reversed trend is observed (figure 7.6 (c)). The form III \rightleftharpoons form II transition occurs at the highest temperature although, it is not much shifted compared to large pores since $T_{\text{I}=\text{II}}$ and $T_{\text{III}=\text{I}}$ decrease significantly more with decreasing pore diameter. Looking more carefully on the Gibbs free energy plots sketched in figure 7.4, one can see that these trends fit to the predictions of this model. It becomes clear that the form III \rightleftharpoons form II and form II \rightleftharpoons form I transitions in small pores are fictive transitions, which do not appear in equilibrium.

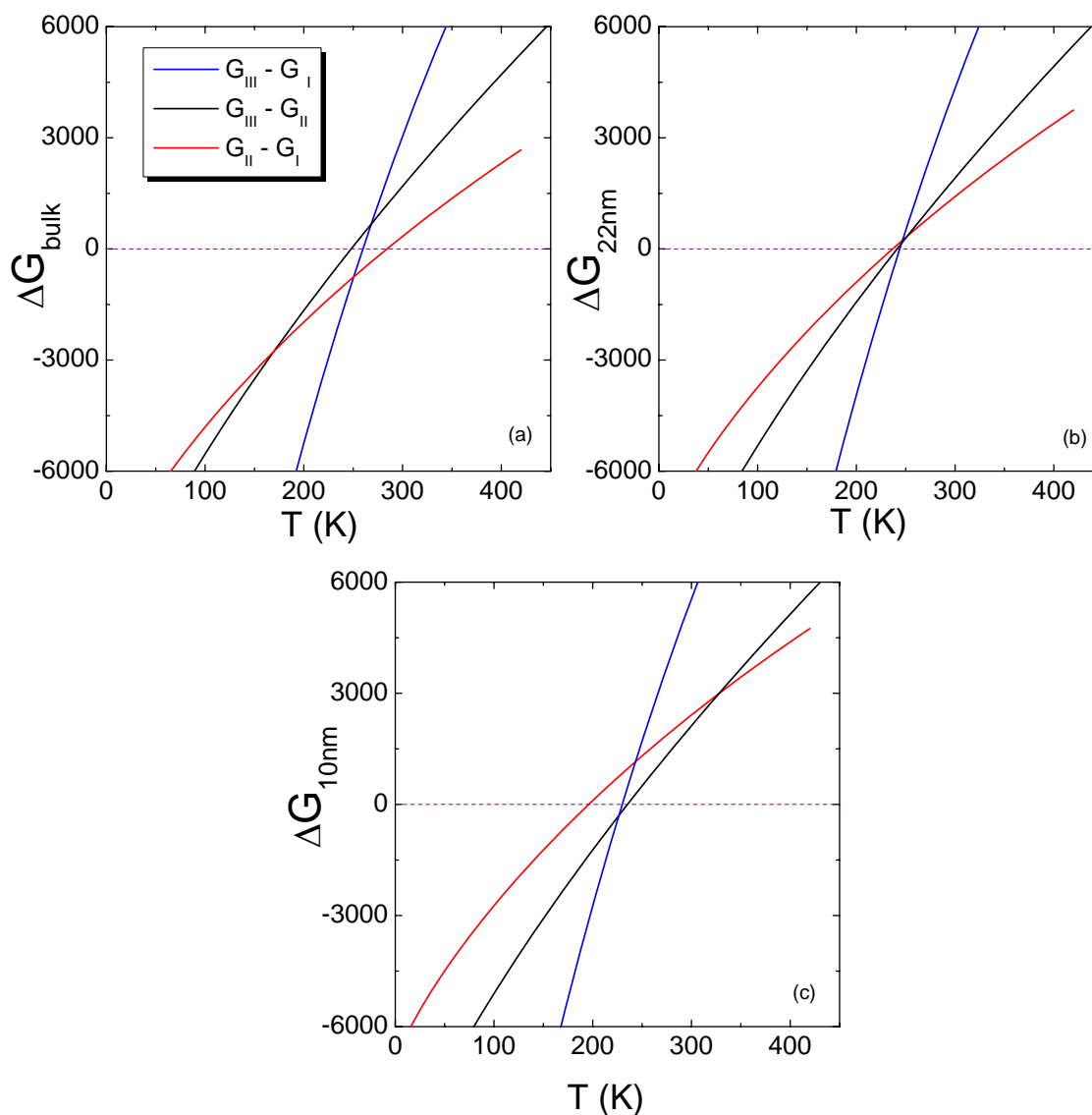


Figure 7.6: Temperature dependence of the free energy difference between different crystalline forms of acetaminophen in (a) bulk, (b) 22 nm pores and (c) 10 nm pores.

Summarising the information about the transition temperature dependence on pore diameter we can construct some kind of phase diagram. Such a phase diagram would describe the stability of different crystalline forms as a function of temperature and inverse pore diameter (figure 7.7). According to this picture form III is always stable at low temperatures. Transitions to other crystalline forms occur below the melting temperature of all the crystalline forms. At even higher temperatures liquid state is the most stable one. Depending on the pore size, different crystalline forms would appear at intermediate temperatures. Form I is

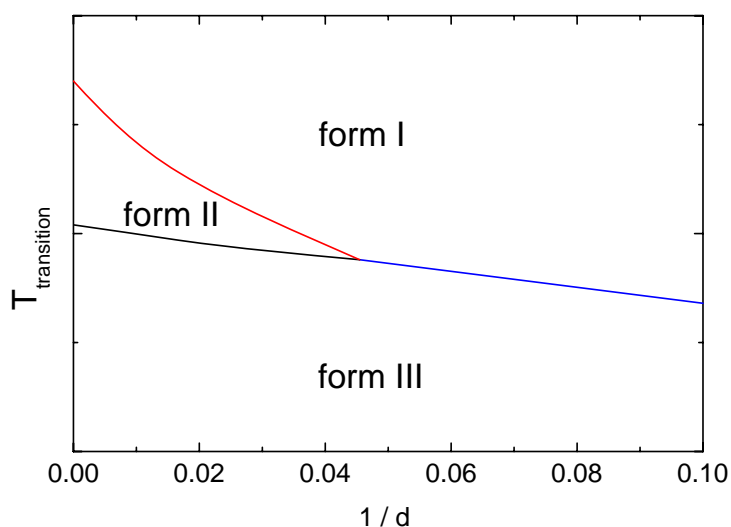


Figure 7.7: A hypothetical phase diagram indicating the stability limits of all the three crystalline forms of acetaminophen.

found in CPGs having diameters below 20 nm, while form II as well as form I are seen for pore diameters significantly larger than 20 nm. At $d \approx 20$ nm a triple point occurs, i.e., all three crystalline forms are energetically equal. Note, that experiments and simulations indicate commonly that a triple point at $d_3 \approx 20$ nm. The corresponding temperature T_3 from the simulations is however, much lower than that taken from experiments. In general, the transition temperatures between different crystalline forms predicted by the simulations are approximately 100 K below the experimentally observed values. This might be a consequence of large uncertainties in the parameters used for the simulations and the delicate dependence of the free energy differences on small changes of these parameters. This is in particular true for temperatures far below melting. Note, that free energy differences between different crystalline forms are in the entire temperature range shown in figure 7.5 below 3 % of the melting enthalpy i.e., small changes can shift the transition temperature tremendously. In particular the C_p values used in the simulation which are responsible for the non-linearity of $\Delta G(T)$ are quite uncertain. It is definitely a crude and finally unrealistic assumption that the C_p difference between different crystalline forms is temperature independent. The real values of ΔC_p differences are basically unknown and only estimated based on more precise experimental values reported for form I and form II. Already, these uncertainties can change the transition temperatures significantly and may explain even shifts of 100 K in transition temperature. The observed deviations may indicate a more pronounced non-linearity of $G(T)$ as assumed in the simulations. The temperature dependence of the free energies and

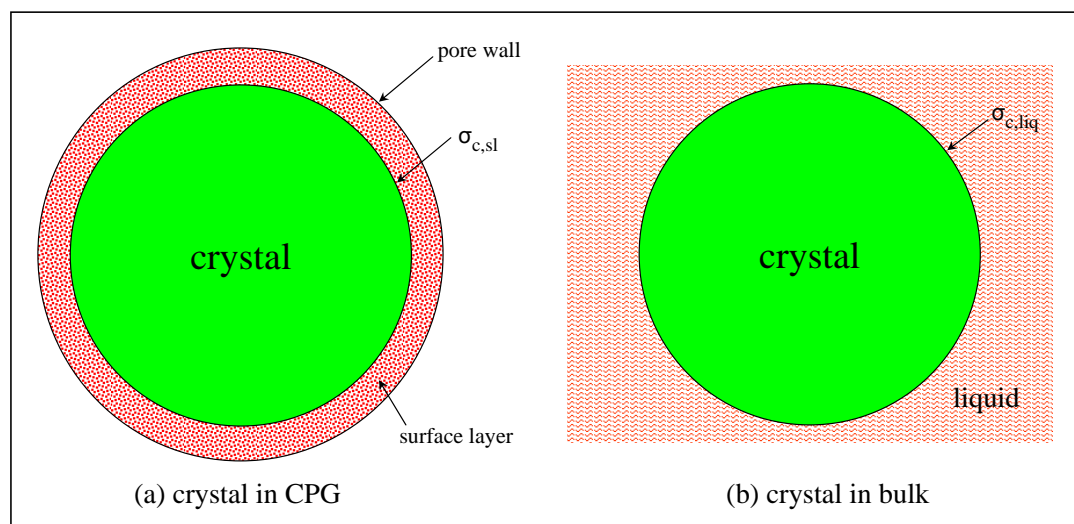


Figure 7.8: A scheme showing a crystal grown in (a) CPGs and (b) bulk situation. The surface layer in the CPGs may lead to a different surface energy ($\sigma_{c,sl}$) compared to a bulk crystal surrounded by liquid ($\sigma_{c,l}$).

the ΔG 's between them far below the melting points might be weak (weaker than shown in figure 7.5), i.e., the surface energy differences between the forms are most important. For small pores, the surface energy contributions decide under these conditions more exclusively which form is stable. The general message might be that acetaminophen in nanopores show "weakly enantiotropic" behaviour with solid - solid transitions slightly below melting.

Finally, one should consider the general implications of the discussed model for early stages of crystallisation in polymorphic bulk systems where the crystals are small. It is shown in this work that the stability of a certain crystalline form is size dependent. This conclusion should also apply to bulk systems containing nanosized crystals. In this sense nanoconfined polymorphic system could help to understand early stages of crystallisation [108]. However, one should be careful with the details, since the properties of the immobilised, disordered surface layer at the pore walls might be different from that of the ordinary liquid leading to other surface energies (figure 7.8). Nevertheless, the consequence for bulk systems is that, during crystal growth different crystalline forms can be thermodynamically stable for a given temperature as discussed by Johari in the case of water [27]. There could be even a thermodynamic explanation for the appearance of metastable crystalline states in polymorphic systems during crystal growth as observed already 100 years ago and summarised by Ostwald in his step rule of stages [4]. Only recently, it was discussed based a thermodynamic background for such a phenomena [109, 110] and, it was shown directly that nano sized crystals undergo changes concerning their crystalline structure during growth [111].

Chapter 8

Conclusions

In this thesis work the influence of nanoconfinement on the crystallisation behaviour of the polymorphic model drug acetaminophen is investigated systematically. Polymorphic state and crystallisation kinetics of acetaminophen infiltrated in nanoporous host systems like controlled porous glass (CPGs) and nanoporous anodized alumina with pore diameters in range $4 \text{ nm} \leq d \leq 400 \text{ nm}$ are investigated by DSC and X-ray scattering. Experiments on bulk acetaminophen are performed, where needed for comparison with the situation in nanopores and to parameterize the dynamics and crystallisation kinetics of amorphous acetaminophen.

As a first step basic studies focused on relaxation behaviour and kinetics of amorphous bulk acetaminophen by dielectric spectroscopy and calorimetry close to and well above the conventional glass transition temperature ($T_g \approx 24 \text{ }^\circ\text{C}$) were performed. Completely amorphous samples can be produced by melt quenching with a cooling rate of -100 K min^{-1} . In the dielectric spectra for amorphous samples a pronounced α - relaxation and a weak secondary Johari - Goldstein relaxation β far below the glass transition were observed. Both the relaxation processes show conventional features of other known organic liquids. Isothermal crystallisation experiments were performed at temperatures above T_g by using dielectric spectroscopy and DSC. Half times (τ_c) estimated from these isothermal crystallisation experiments show consistently that, the crystallisation kinetics in the bulk state is dominated by mobility. Additional polarization microscopy experiments show that only few large spherulites grow in a highly viscous acetaminophen during cold crystallisation at temperatures below $100 \text{ }^\circ\text{C}$, which convert at temperatures near $120 \text{ }^\circ\text{C}$ into stacked platelets.

Nanoconfinement in CPGs with pore diameters $22 \text{ nm} \leq d \leq 103 \text{ nm}$ is shown to be an

efficient approach to produce and stabilise the metastable form III of acetaminophen. Unknown thermodynamic parameters such as melting point ($T_{m,III}$) and the enthalpy of melting ($\Delta H_{m,III}$) for form III of acetaminophen were estimated based on calorimetric measurements for the first time. The appearance of form III in the pores is argued based on thermodynamic reasons. Apart from form III, the two well known crystalline forms of acetaminophen the monoclinic form I and the orthorhombic form II, are prepared in CPGs by employing special thermal treatments. All three forms of acetaminophen infiltrated in nanopores show melting point depression in accordance with the Gibbs - Thompson relationship. Based on calorimetric experiments it is shown that there are temperature intervals where form III, form II and form I do grow. The calorimetric data indicates that, the stability interval of different crystalline forms and the transition temperatures between them depend on pore diameter. A clear indication for such a behaviour and a major consequence of the transition temperature dependence on pore diameter was that, form II is inaccessible for acetaminophen infiltrated in small pores ($d \leq 20$ nm). Based on these experimental observations an equilibrium thermodynamic model is proposed. This model explains the pore size - dependent stability ranges for different crystalline forms, incorporating the huge surface energy contributions to the Gibbs free energy of nano sized crystals. In the case of nano sized crystals, the crystalline form with the lowest surface energy is favoured which is not a priori that form which is energetically preferred in the bulk. Plotting the transition temperatures between crystalline forms in a phase diagram versus pore size, a triple point seems to occur near $d_3 \sim 20$ nm for acetaminophen in CPGs where all three crystalline forms are energetically equal.

The crystallisation of acetaminophen infiltrated in CPGs having large pore diameters (≈ 100 nm) showed that, crystallisation is slowed down five times when compared to the bulk state. It is argued that slowing of the crystallisation process in the larger pores is due to the reduced number of heterogenous nucleus per volume and, the presence thin immobilised layers of acetaminophen close to pore walls of CPGs. Further reducing the average pore diameters of CPGs to $d \approx 10$ nm lead to amorphous acetaminophen in pores. Crystallisation in these host - guest systems is only observed if a thick layer of acetaminophen is present on the top surface of the CPG during the preparation. Crystallisation is completely suppressed for acetaminophen infiltrated in CPGs having pore diameters comparable to the critical size of the nucleus ($d \approx d^* = 4$ nm) since, amorphous state is thermodynamically stable under such a condition.

Above all, it was shown that nanoconfinement can be used to manipulate the crystalline state of polymorphic pharmaceuticals. Conventionally, metastable states can be produced since surface energy contributions dominate the free energy of nanocrystals. Such a thermodynamic strategy should be applicable in many cases to stabilise amorphous drugs as well as metastable crystalline forms which have limited life time in bulk. From the view point of fundamental research, the presented results give new insights into the properties of nano-sized crystals of acetaminophen. This might help in the future to understand early stages of crystallisation where nanosized crystals appear in bulk samples.

Appendix A

Free energy changes between two different crystalline forms (I and II)

This appendix contains mathematical treatment employed to estimate the free energy change of transformation between form I and form II crystalline forms of acetaminophen. The changes in free energy calculated are necessary for the construction of change in free energy plots between all the three known forms of acetaminophen. The thermodynamic parameters such as specific heat C_p , enthalpy of melting ΔH_m can be obtained from the DSC measurements which are essential for the following mathematical treatment.

Gibbs free energy change associated with the phase transition between two different crystalline forms can be written as follows

$$G(T)_{II} - G(T)_I = [H(T)_{II} - H(T)_I] - T [S(T)_{II} - S(T)_I] \quad (\text{A.1})$$

To estimate the above free energy change between form I and II, the temperature dependence of enthalpy $H(T)$ and temperature dependence of entropy $S(T)$ of individual forms should be known. The steps involved to estimate the same are shown below.

Enthalpy difference between form II and I

The temperature dependence of enthalpy of form I can be written as

$$H(T)_I = \int_0^T C_{P,I} d\hat{T} \quad (\text{A.2})$$

where $C_{p,I}$ is the specific heat of form I Then, equation A.2 can be rewritten as follows

$$H(T)_I = \int_0^T (C_{p,I} - C_{p,l}) d\hat{T} + \int_0^T C_{p,l} d\hat{T} \quad (\text{A.3})$$

$$= \underbrace{\int_0^{T_{m,I}} (C_{p,I} - C_{p,l}) d\hat{T}}_{\text{is defined as } \Delta H_I} + \int_{T_{m,I}}^T (C_{p,I} - C_{p,l}) d\hat{T} + \int_0^T C_{p,l} d\hat{T} \quad (\text{A.4})$$

$$H(T)_I = -\Delta H_{l,I} + \int_{T_{m,I}}^T (C_{p,I} - C_{p,l}) d\hat{T} + \int_0^T C_{p,l} d\hat{T} \quad (\text{A.5})$$

The temperature dependence of enthalpy of form II can be written similar to equation A.4

$$H(T)_{II} = \int_0^{T_{m,II}} (C_{p,II} - C_{p,l}) d\hat{T} + \int_{T_{m,II}}^T (C_{p,II} - C_{p,l}) d\hat{T} + \int_0^T C_{p,l} d\hat{T} \quad (\text{A.6})$$

$$H(T)_{II} = -\Delta H_{l,II} + \int_{T_{m,II}}^T (C_{p,II} - C_{p,l}) d\hat{T} + \int_0^T C_{p,l} d\hat{T} \quad (\text{A.7})$$

Then, the enthalpy difference between form II and I is given by

$$\begin{aligned} H(T)_{II} - H(T)_I &= (\Delta H_{l,I} - \Delta H_{l,II}) - \int_{T_{m,II}}^T C_{p,l} d\hat{T} + \int_{T_{m,I}}^T C_{p,l} d\hat{T} \\ &\quad - \int_{T_{m,I}}^T C_{p,I} d\hat{T} + \int_{T_{m,II}}^T C_{p,II} d\hat{T} \end{aligned} \quad (\text{A.8})$$

after rearranging the individual terms the above equation becomes

$$\begin{aligned} H(T)_{II} - H(T)_I &= (\Delta H_{l,I} - \Delta H_{l,II}) - \int_{T_{m,II}}^{T_{m,I}} C_{p,l} d\hat{T} + \int_T^{T_{m,II}} C_{p,I} d\hat{T} \\ &\quad + \int_{T_{m,I}}^{T_{m,I}} C_{p,I} d\hat{T} + \int_{T_{m,II}}^T C_{p,II} d\hat{T} \end{aligned} \quad (\text{A.9})$$

$$\begin{aligned}
&= (\Delta H_{l,I} - \Delta H_{l,II}) - \int_{T_{m,II}}^{T_{m,I}} (C_{p,l} - C_{p,I}) d\hat{T} \\
&+ \int_T^{T_{m,II}} (C_{p,I} - C_{p,II}) d\hat{T}
\end{aligned} \tag{A.10}$$

Assuming the differences $(C_{p,l} - C_{p,I})$ and $(C_{p,I} - C_{p,II})$ as constants in the temperature intervals $(T_{m,II}$ to $T_{m,I})$ and $(T$ to $T_{m,II})$ respectively, the enthalpy difference between form II and I can be written as follows

$$\begin{aligned}
H(T)_{II} - H(T)_I &= (\Delta H_{l,I} - \Delta H_{l,II}) - (T_{m,I} - T_{m,II})(C_{p,l} - C_{p,I}) \\
&+ (T_{m,II} - T)(C_{p,I} - C_{p,II})
\end{aligned} \tag{A.11}$$

Entropy difference between form II and I

Now the temperature dependence of entropy $S(T)$ of individual forms will be shown using similar treatment used for the estimation of enthalpy change for two different forms of acetaminophen.

The temperature dependence of entropy of form I can be written as

$$S(T)_I = \int_0^T \frac{C_{p,I}}{\hat{T}} d\hat{T} \tag{A.12}$$

Then, equation A.12 can be rewritten as follows

$$S(T)_I = \int_0^{T_{m,I}} \frac{(C_{p,I} - C_{p,l})}{\hat{T}} d\hat{T} + \int_0^T \frac{C_{p,l}}{\hat{T}} d\hat{T} \tag{A.13}$$

$$= \int_0^{T_{m,I}} \frac{(C_{p,I} - C_{p,l})}{\hat{T}} d\hat{T} + \int_{T_{m,I}}^T \frac{(C_{p,I} - C_{p,l})}{\hat{T}} d\hat{T} + \int_0^T \frac{C_{p,l}}{\hat{T}} d\hat{T} \tag{A.14}$$

Gibbs Free energy change for form I at the melting temperature $T_{m,I}$ be written as follows

$$\Delta G_{l,I} = \Delta H_{l,I} - T_{m,I} \Delta S_{l,I} \tag{A.15}$$

$$= \int_0^{T_{m,I}} (C_{p,l} - C_{p,I}) d\hat{T} - T_{m,I} \int_0^{T_{m,I}} \frac{(C_{p,l} - C_{p,I})}{\hat{T}} d\hat{T} \tag{A.16}$$

We know that at the phase transition (here at melting), the free energy change $\Delta G_{l,I}$ becomes zero. Then the change in entropy can be estimated as follows.

$$\int_0^{T_{m,I}} \frac{(C_{p,l} - C_{p,I})}{\hat{T}} d\hat{T} = \frac{1}{T_{m,I}} \int_0^{T_{m,I}} (C_{p,l} - C_{p,I}) d\hat{T} \quad (\text{A.17})$$

$$\Delta S_{l,I} = \frac{\Delta H_{l,I}}{T_{m,I}} \quad (\text{A.18})$$

Substituting the above in equation A.14, we get

$$S(T)_I = -\frac{\Delta H_{l,I}}{T_{m,I}} + \int_{T_{m,I}}^T \frac{(C_{p,I} - C_{p,l})}{\hat{T}} d\hat{T} + \int_0^T \frac{C_{p,l}}{\hat{T}} d\hat{T} \quad (\text{A.19})$$

Similarly, the temperature dependence of form II can be written as

$$S(T)_{II} = -\frac{\Delta H_{l,II}}{T_{m,II}} + \int_{T_{m,II}}^T \frac{(C_{p,II} - C_{p,l})}{\hat{T}} d\hat{T} + \int_0^T \frac{C_{p,l}}{\hat{T}} d\hat{T} \quad (\text{A.20})$$

The entropic changes between form II and I can be estimated using similar treatment used for the estimation of changes in enthalpy and it can be mathematically expressed as follows

$$\begin{aligned} S(T)_{II} - S(T)_I &= \left[\left(\frac{\Delta H_{l,I}}{T_{m,I}} \right) - \left(\frac{\Delta H_{l,II}}{T_{m,II}} \right) \right] - \int_{T_{m,II}}^{T_{m,I}} \frac{(C_{p,l} - C_{p,I})}{\hat{T}} d\hat{T} \\ &+ \int_T^{T_{m,II}} \frac{C_{p,I} - C_{p,II}}{\hat{T}} d\hat{T} \end{aligned} \quad (\text{A.21})$$

If differences $(C_{p,l} - C_{p,I})$ and $(C_{p,I} - C_{p,II})$ in the temperature intervals $(T_{m,II}$ to $T_{m,I})$ and $(T$ to $T_{m,II})$ respectively are assumed to be constant, then the entropic difference between form II and I can be written as follows

$$\begin{aligned} S(T)_{II} - S(T)_I &= \left[\left(\frac{\Delta H_{l,I}}{T_{m,I}} \right) - \left(\frac{\Delta H_{l,II}}{T_{m,II}} \right) \right] \\ &- (C_{p,l} - C_{p,I}) \ln \left(\frac{T_{m,I}}{T_{m,II}} \right) + (C_{p,II} - C_{p,I}) \ln \left(\frac{T_{m,II}}{T} \right) \end{aligned} \quad (\text{A.22})$$

Free energy between form II and I

Using equation A.11 and A.22 the free energy change between form II and I at a given temperature T can be expressed using the following equation.

$$\begin{aligned}
 G(T)_{II} - G(T)_I &= (\Delta H_{l,I} - \Delta H_{l,II}) - (T_{m,I} - T_{m,II})(C_{p,l} - C_{p,I}) \\
 &+ (T_{m,II} - T)(C_{p,I} - C_{p,II}) \\
 &- T \left[\left(\frac{\Delta H_{l,I}}{T_{m,I}} \right) - \left(\frac{\Delta H_{l,II}}{T_{m,II}} \right) \right] \\
 &- T(C_{p,l} - C_{p,I}) \ln \left(\frac{T_{m,I}}{T_{m,II}} \right) \\
 &+ T(C_{p,II} - C_{p,I}) \ln \left(\frac{T_{m,II}}{T} \right)
 \end{aligned} \tag{A.23}$$

Bibliography

- [1] W. C. McCrone. *Physics and Chemistry of Organic Solid State*. Interscience, New York, 1965.
- [2] J. Bernstein. *Polymorphism in Molecular Crystals*. Oxford Science Publications, 2007.
- [3] E. Mitscherlich. *Annales des Chimie et des Physique*, 19:350–419, 1822.
- [4] W. Ostwald. *Zeitschrift für Physikalische Chemie*, 22:289, 1897.
- [5] P. H. R. Groth. *Chemische Krystallographie*. W. Engelmann, Leipzig, Erster Teil. 1906b; Zweiter Teil 1908; Dritter Teil. 1910; Vierter Teil. 1917.
- [6] U. Griesser and A. Burger. *Journal of Pharmaceutical Sciences*, 61:133–143, 1993.
- [7] S. Bryn, R. Pfeiffer, M. Ganey, C. Hoiberg, and G. Poochikan. *Pharmaceutical Research*, 12:945–954, 1995.
- [8] C. P. Buckley and A. J. Kovacs. *Colloid and Polymer Science*, 254:695–715, 1976.
- [9] S. Z. D. Cheng. A. Keller. *Polymer*, 19:4461–4487, 1998.
- [10] A. J. Lovinger, S. R. Forrest, M. L. Kaplan, P. H. Schmidt, and T. Venkatesan. *Journal of Applied Physics*, 263:476–482, 1984.
- [11] T. Ogawa, K. Kuwamoto, S. Isoda, T. Kobayshi, and N. Karl. *Acta Crystallographica Section B*, 55:123–130, 1999.
- [12] C. Loisel, G. Keller, G. Lecq, and M. Ollivon. *Journal of the American Oil Chemists Society*, 75:425–439, 1998.
- [13] T. M. Haller, A. L. Rheingold, and T. B. Brill. *Acta Crystallographica C*, 39:1559–1563, 1983.

- [14] McCrone. *Analytical Chemistry*, 22:1225–1226, 1950a.
- [15] M. V. King, B. S. Magdoff, M. B. Adelman, and D. Harker. *Acta Crystallographica*, 9:460–465, 1956.
- [16] F. Cramer, R. Sprinzl, N. Furgac, W. Freist, P. Manor, L. Sprinzll, and H. Sternback. *Biophysica Acta*, 349:351–365, 1974.
- [17] S. H. Kim, G. J. Quigley, F. L. Suddath, A. McPherson, D. Sneden, J. J. Kin, J. Weinzirl, and A. Rich. *Journal of Molecular Biology*, 75:421–428, 1973.
- [18] R. Hilfiker, editor. *Polymorphism*. Wiley-VCH Verlag GmbH & CO. KGaA, 2006.
- [19] J. Bauer, R. Spanton, R. Henry, J. Quick, W. Dziki, W. Porter, and J. Morris. *Pharmaceutical Research*, 18:859–866, 2001.
- [20] C. P. Price, A. L. Grzesiak, and A. J. Matzger. *Journal of American Chemical Society*, 127:5512–5517, 2005.
- [21] M. Lahav and L. Leiserowitz. *Journal of Physics D: Applied Physics*, 26:B22–B31, 1993.
- [22] S. J. Bonafede and M. D. Ward. *Journal of American Chemical Society*, 117:7853–7861, 1995.
- [23] C. A. Mitchell, L. Yu, and M. D. Ward. *Journal of American Chemical Society*, 123:10830–10839, 2001.
- [24] J. Zaccaro, J. Matic, A. S. Myerson, and B. A. Garetz. *Crystal Growth and Design*, 1:5–8, 2001.
- [25] J-M. Ha, M. A. Hillmyer, and M. D. Ward. *Journal of Physical Chemistry B*, 109:1392–1399, 2005.
- [26] M. Alcoutlabi and G. B. McKenna. *Journal of Physics: Condensed Matter*, 17:461–524, 2005.
- [27] G. P. Johari. *Journal of Chemical Physics*, 122:19504–1–19504–5, 2005.
- [28] R. Huttenrauch. *Acta Pharmaceutica Technologica*, 6:55–127, 1978.
- [29] L. Yu. *Advanced Drug Delivery Reviews*, 48:27–42, 2001.

- [30] D. L. Zhou, G. G. Z. Zhang, D. Law, D. J. W. Grant, and E. A. Schmitt. *Journal of Pharmaceutical Sciences*, 91:1863–1872, 2002.
- [31] C. J. Roberts and P. G. Debenedetti. *AIChE Journal*, 48:1140–1144, 2002.
- [32] J. Alie, J. Menegotto, P. Cardon, H. Duplaa, A. Caron, C. Lacabanne, and M. Bauer. *Journal of Pharmaceutical Sciences*, 93:218–233, 2004.
- [33] M. Yoshioka, B. C. Hancock, and G. J. Zografi. *Journal of Pharmaceutical Sciences*, 83:1700–1705, 1994.
- [34] J. L. Green and C. A. Angell. *Journal of Physical Chemistry*, 93:2880–2882, 1989.
- [35] V. Andronis and G. Zografi. *Journal of Non-Crystalline Solids*, 271:236–248, 2000.
- [36] W. C. Stagner and J. K. Guillory. *Journal of Pharmaceutical Sciences*, 68:1005–1009, 1979.
- [37] M. Inagaki. *Chemical and Pharmaceutical Bulletin*, 25:1001–1009, 1977.
- [38] T. J. Anchordoquy and J. F. Carpenter. *Archives of Biochemistry and BioPhysics*, 332:231–238, 1996.
- [39] O. I. Corrigan. *Thermochemica Acta*, 248:245–258, 1995.
- [40] M. Descamps, J. F. Willart, E. Dudognon, and V. Caron. *Journal of Pharmaceutical Sciences*, 96:1398–1407, 2007.
- [41] Y. Li, J. Han, G. G. Z. Zhang, D. J. W. Grant, and R. Suryanarayanan. *Pharmaceutical Development and Technology*, 5:257–266, 2000.
- [42] *The Collected Works of J. Willard Gibbs*. Longmas, Green and Co, New York, London, Toronto, 1928.
- [43] M. Volmer and A. Weber. *Zeitschrift für Physikalische Chemie*, 119:227, 1926.
- [44] A. Bruger and R. Ramberger. *Mickrochimica Acta*, II:259–271, 1979.
- [45] M. Sacchetti. *Journal of Thermal Analysis and Calorimetry*, 63:345–350, 2001.
- [46] T. Threlfall. *Organic Process Resaerch & Development*, 7:1017–1027, 2003.
- [47] J. Schmelzer, J. Möller, and V. V. Slezov. *Journal of Physics and Chemistry of Solids*, 56:1013–1022, 1995.

- [48] L. Granasy and D. W. Oxtoby. *Journal of Chemical Physics*, 112:2410–2419, 2000.
- [49] L. Yu. *Journal of Pharmaceutical Science*, 84:966–974, 1995.
- [50] M. Haisa, S. Kashino, and H. Maeda. *Acta Crystallographica - Section B: Structural Crystallography and Crystal Chemistry*, 30:2510–2512, 1974.
- [51] C. L. Jackson and G. B. McKenna. *Journal of Chemical Physics*, 93:9002–9011, 1990.
- [52] C. Alba-Simionesco, G. Dosseh, E. Dumont, B. Frick, B. Geil, D. Morineau, V. Teboul, and Y. Xia. *The European Physical Journal E*, 12:19–28, 2003.
- [53] D. C. Bassett and R. Davitt. *Polymer*, 15:721–728, 1974.
- [54] S. Z. D. Cheng, Z. Q. Wu, and B. Wunderlich. *Macromolecules*, 20:2802–2810, 1987.
- [55] P. H. Buffat and J-P Borel. *Physical Review A*, 13:1050–2947, 1976.
- [56] P. R. Couchman and W. A. Jesser. *Nature*, 269:481–483, 1977.
- [57] C. L. Jackson and G. B. McKenna. *Chemistry of Materials*, 8:2128–2137, 1996.
- [58] M. Arnt, R. Stannarius, H. Groothues, E. Hempel, and F. Kremer. *Physical Review Letters*, 79:2077–2080, 1997.
- [59] W. Masierak, T. Emmler, E. Gedat, A. Schreiber, G. H. Findenegg, and G. Buntkowsky. *Journal of Chemical Physics B*, 108:18890–18896, 2004.
- [60] F. Rittig, A. Huwe, G. Fleisher, J. Kärger, and F. Kremer. *Physical Chemistry Chemical Physics*, 1:519–523, 1998.
- [61] W. Gorbatschow, M. Arndt, R. Stannarius, and F. Kremer. *Europhysics Letters*, 35:239–242, 1996.
- [62] A. Sargsyan, A. Tonoyan, S. Davtyan, and C. Schick. *European Polymer Journal*, 43:3113–3127, 2007.
- [63] W. Zheng and S. L. Simon. *The Journal of Chemical Physics*, 127:194501–194511, 2007.
- [64] W.F. Hemminger and H.K. Cammenga. *Methoden der Thermischen Analyse*. Springer-Verlag, 1989.

- [65] G. Höhne and W. Hemminger. *Thermochemica Acta*, 151:295–304, 1989.
- [66] G. Höhne, W. Hemminger, and H.-J. Flammersheim. *Differential Scanning Calorimetry*. Springer, 1995.
- [67] W. F. Hemminger and S. M. Sarge. *Journal of Thermal Analysis*, 37:1455–1477, 1991.
- [68] F. Kremer and A. Schönhal. *Broadband Dielectric Spectroscopy*. Springer, Berlin, 2000.
- [69] C. J. F. Böttcher. *Theory of Dielectric Polarization*. Elsevier, Amsterdam, 1973.
- [70] N. G. McCrum, B. E. Read, and G. Williams. *Anelastic and Dielectric Effects in Polymeric Solids*. Dover, New York, 1991.
- [71] G. Nichols and C. S. Frampton. *Journal of Pharmaceutical Sciences*, 87:684–693, 1998.
- [72] M. Szelagiewicz, C. Marcolli, S. Cianferani, A. Hard, A. Vit, A. Burkhard, M. Raumer, U. Hofmeier, A. Zilian, E. Francotte, and R. Schenker. *Journal of Thermal Analysis and Calorimetry*, 57:23–43, 1999.
- [73] M. L. Peterson, S. L. Morissette, C. McNulty, A. Goldsweig, P. Shaw, M. LeQuesne, J. Mongale, N. Encina, J. Marchionna, A. Johnson, J. Gonzalez Zugasti, A. V. Lemmo, S. J. Ellis, M. J. Cima, and O. J. Almarsson. *Journal of American Chemical Society*, 124:10958, 2002.
- [74] A. Burger and R. Ramberger. *Mikrochimica Acta*, II:273–316, 1979.
- [75] D. Enke, F. Janowski, and W. Schwieger. *Microporous and Mesoporous Materials*, 60:19–30, 2003.
- [76] S. Pankaj. Master's thesis, Martin-Luther-University Halle-Wittenberg, 2006.
- [77] H. Masuda and K. Fukuda. *Science*, 268:1466–1468, 1995.
- [78] H. Masuda, Y. Kouichi, and A. Osaka. *Japanese Journal of Applied Physics*, 37:L1340–1342, 1998.
- [79] A. P. Li, F. Müller, A. Birner, K. Nielsch, and U. Gösele. *Journal of Applied Physics*, 84:6023–6026, 1998.

- [80] H. Masuda, F. Hasegawa, and S. Ono. *Journal of The Electrochemical Society*, 144:L127–130, 1997.
- [81] B. C. Hancock and M. Parks. *Pharmaceutical Research*, 17:397–404, 2000.
- [82] G. P. Johari, S. Kim, and D. Shanker. *Journal of Pharmaceutical Sciences*, 94:2207–2223.
- [83] G. P. Johari and D. Pyke. *Physical Chemistry Chemical Physics*, 2:5479 – 5484, 2000.
- [84] G. B. McKenna. *Journal of research of the National Institute of Standards and Technology*, 99:169, 1994.
- [85] L. C. E. Struik. *Physical Aging in Amorphous Polymers and Other Materials*. Elsevier, Amsterdam, 1978.
- [86] A. J. Kovacs, J. M. Hutchison, and J. J. Alklonis. *The Structure of Non-Crystalline Materials*. Gaskell P. H. (ED), Cambridge, 1977.
- [87] S. Vyazovkin and I. Dranca. *The Journal of Physical Chemistry B*, 109:18637–18644, 2005.
- [88] M. Hanaya T. Hikima and M. Oguni. *Bulletin of the Chemical Society of Japan*, 69:1863–1868, 1996.
- [89] M. Hatase, M. Hanaya, T. Hikima, and M. Oguni. *Journal of Non-Crystalline Solids*, 257:307–310, 2002.
- [90] L. Gránásy, T. Pusztai, G. Tegze, J. A. Warren, and J. F. Douglas. *Physical Review E*, 72:11605, 2005.
- [91] G. P. Johari and M. Goldstein. *The Journal of Chemical Physics*, 53:2372–2388, 1970.
- [92] H. Wagner and R. Richert. *The Journal of Chemical Physics*, 110:11660–11663, 1999.
- [93] W. Hesse G. Tammann. *Zeitschrift für anorganische und allgemeine Chemie*, 156:245–257, 1926.
- [94] E. Donth. *The Glass Transition. Relaxation Dynamics in Liquids and Disordered Materials*. Springer, Berlin, 2001.
- [95] M. Beiner, H. Huth, and K. Schröter. *Journal of Non-Crystalline Solids*, 279:126–135, 2001.

- [96] K. L. Ngai. *Physical Review E*, 57:7346 – 7349, 1998.
- [97] C. Schick, A. Wurm, and A. Mohamed. *Colloid and Polymer Science*, 279:800–806, 2001.
- [98] J. Pak, M. Pyda, and B. Wunderlich. *Macromolecules*, 36:495–499, 2003.
- [99] L. Mandelkern. *In Physical Properties of Polymers*. Cambridge University Press, Cambridge, 1997.
- [100] A. Schreiber, I. Ketelsen, and G. H. Findenegg. *Physical Chemistry Chemical Physics*, 3:1185–1195, 2001.
- [101] P. Di Martino, P. Conflant, M. Darche, J. P. Huvenne, and A. M. Guyot-Hermann. *Journal of Thermal Analysis*, 48:447–458, 1997.
- [102] P. Espeau, R. Ceolin, J. L. Tamarit, M. A. Perrin, J. P. Gauchi, and F. J. Leveiller. *Journal of Pharmaceutical Science*, 94:524–539, 2005.
- [103] F. Giordano, A. Rossi, R. Bettini, A. Savioli, A. Gazzaniga, and C. Norvak. *Journal of Thermal Analysis and Calorimetry*, 68:575, 2002.
- [104] M. Beiner, G. T. Rengarajan, S. Pankaj, D. Enke, and M. Steinhart. *Nano Letters*, 7:1381–1385, 2007.
- [105] S-L. Wang, S-Y. Lin, and Y-S. Wei. *Chemical and Pharmaceutical Bulletin*, 2:153–156, 2002.
- [106] R. Prasad and S. Lele. *Philosophical Magazine Letters*, 70:357–361, 1994.
- [107] G. T. Rengarajan, D. Enke, M. Steinhart, and M. Beiner. *Journal of Materials Chemistry*, 18:2537–2539, 2008.
- [108] M. Beiner. *Journal of Polymer Science: Part B: Polymer Physics*, 46:1556–1561, 2008.
- [109] G. Strobl. *Progress in Polymer Science*, 31:398–442, 2006.
- [110] E. B. Sirota. *Macromolecules*, 40:1043–1048, 2007.
- [111] S Y. Chung, Y M. Kim, J G. Kim, and Y J. Kim. *Nature Physics*, 23:68–73, 2008.

Publications

Parts of this work have been published in:

1. G. T. Rengarajan, D. Enke, M. Steinhart and M. Beiner, *Journal of Materials Chemistry*, 18:2537-2539, 2008.
2. Gopalakrishnan T. Rengarajan, D. Enke and M. Beiner, *The Open Physical Chemistry Journal*, 1: 18-24, 2007.
3. M. Beiner, G. T. Rengarajan, S. Pankaj, D. Enke and M. Steinhart, *Nano Letters*, 7:1381-1385, 2007.
4. Gopalakrishnan T. Rengarajan, D. Enke and M. Beiner, *Letters in Drug Design & Discovery*, 3:723-730, 2006.

Other works have been published in

5. K. L. Ngai, Gopalakrishnan. T. Rengarajan and M. Beiner, *Polymer*, 47:7222- 7230, 2006.
6. Gopalakrishnan. T. Rengarajan and M. Beiner, *Journal of Physics Conference Series*, 40:67-75, 2006.

Patents

1. M. Beiner, G. T. Rengarajan, S. Pankaj, M. Steinhart, Verfahren zur Herstellung langzeitstabiler amorpher Arzneimittel, *DE 10 2007 048 217 A1*, 2007.
2. M. Beiner, G. T. Rengarajan, Verfahren zur Herstellung langzeitstabiler amorpher Arzneimittel, *DE 10 2006 044 199 A1*, 2006.

Acknowledgements

This thesis work arose in part out of years of research that has been done since I came to Dr. Beiner's group. By that time, I have worked with number of people whose contributions in assorted ways to the research and the making of the thesis deserved special mention. It is a pleasure to convey my gratitude to them all in my humble acknowledgement.

In the first place I would like to record to Dr. Beiner for his supervision, advice, and guidance from the very early stage of this research work as well as giving me extraordinary experiences though out this work. Above all he provided me unflinching encouragement and support in various ways. I am indebted to him more than he knows.

I gratefully acknowledge Prof. Thurn-Albrecht for the fruitful discussions at different stages of this thesis work.

I gratefully acknowledge Dr. Hempel for introducing me to Calorimetry and her support during the course of this work. Many thanks to Dr. Schröter and Ms. K. Herfurt for all the technical support during my stay in Halle.

Many thanks go in particular to I. Gunkel and P. Kohn for their extended help with the my Theoretical Physics course which was a requirement for awarding the doctoral degree. I would also like to thank S. Pankaj for the measurements on porous alumina. I would also like to extend my thanks to N. Shingne, T. Henze and A. Petzold for their timely favours at different stages of this thesis work.

It is a pleasure to pay tribute to sample collaborators. To Dr. Enke for providing ample number of CPG substrates and Prof. Steinhart for the porous alumina templates. I would like to thank for their high quality samples. Prof. Steinhart, I am grateful in every possible way and hope to keep up our collaboration in the future.

My deepest gratitude goes to my family for their unflagging love and support throughout my life; this dissertation is simply impossible without them.

Eidesstattliche Erklärung

Ich erkläre hiermit, dass ich keine anderen als die von mir angegebenen Quellen und Hilfsmittel zur Erstellung meiner Dissertation verwendet habe. Den benutzten Werken wörtlich oder inhaltlich entnommene Stellen sind als solche gekennzeichnet.

Gopalakrishnan Trichy Rengarajan

Halle (Saale), Oktober 2009

Curriculum vitae

First Name	Gopalakrishnan
Family Name	Trichy Rengarajan
Date of Birth	September 19, 1978
Place of Birth	Trichirapalli, India
Nationality	Indian
E-mail	gopalyajur@gmail.com

EDUCATION

Aug. 1997 - Aug. 2001	Bachelor of Technology (B.Tech) in Polymer Technology University of Madras (Chennai, India) Awarded Gold Medal for academic excellence
Dec. 2001 - Feb. 2001	Trainee in Blow Film Process Esvee Polymers Pvt. Ltd (Chennai, India)
Apr. 2002 - Aug. 2002	Engineer at Injection Molding Unit Supreme Industries Ltd (Pondicherry, India)
Oct. 2002 - Feb. 2005	Master of Science (M.Sc) in Applied Polymer Science Martin-Luther-University Halle-Wittenberg (Germany)
May. 2005 - Aug. 2009	Ph. D student in Experimental Polymer Physics Group Martin-Luther-University Halle-Wittenberg (Germany) (Supervised by PD. Dr. Mario Beiner)
